Rock magnetic and geochemical signals of late Quaternary climate variability over Western Africa

Dissertation
zur Erlangung des
Doktorgrades der Naturwissenschaften
am Fachbereich Geowissenschaften
der Universität Bremen

Vorgelegt von

Achakie Cletus ITAMBI

Bremen, 2008

Tag des Kolloquiums:

10 October 2008

Gutachter:

Prof. Dr. Tilo von Dobeneck
(Universität Bremen)

Dr. Mark J. Dekkers
(Utrecht University)

Prüfer:

Prof. Dr. Kai-Uwe Hinrichs
(Universität Bremen)

Prof. Dr. Wolfgang Bach
(Universität Bremen)

This work is dedicated to my dad

Mr. ITAMBI Simon A.(late) and my mum Mrs Esther Ndi Itambi

For their love, care and sacrifices they made in order to educate us.

Table of contents

Summary

This thesis investigates the paleo- climatic and environmental changes over northwest Africa by focusing on the Senegal region and the Gulf of Guinea. Emphasis was placed on the timing of past climate changes, the frequency of occurrence, and regional impact. Possible shifts in the position of the intertropical conversion zone (ITCZ) were also investigated. A multi proxy approach integrating rock and environmental magnetic parameters, diffuse reflectance spectrophotometry, scanning electron microscopy, color reflectance, grain size analysis and climate modeling experiments was employed.

Environmental magnetic results, X-ray fluorescence and end member modeling of diffuse reflectance spectroscopy from three sediment cores along a N-S transect at the Senegal continental margin (GeoB 9506-1 at 15°36'N 18°21'W, GeoB 9516-5 at 13°40'N 18°25'W and GeoB 9527-5 at 12°26'N 18°13W) revealed climatic signatures synchronous with north Atlantic Heinrich events (Chapter 2). The signals occurring during extreme glacial periods within the North African continent are characterized by high concentration of magnetic minerals as depicted by the high magnetic susceptibility compared to the warmer periods. Typical signatures for Saharan dust contribution (i.e. pigmented magnetic minerals hematite, goethite and Ti content) were abundant confirming that these sediments were wind derived. Therefore, during the Heinrich events, severe droughts persisted over North Africa. Coupled with the stronger wind strengths, Saharan dust enriched in magnetic particles was eroded and deposited into the ocean. Fluvial transported sediments comprising of clays with less magnetic mineral contents were deposited at warmer periods which indicates persistence of more humid conditions.

Millennial-scale climate oscillations occurring at times scales synchronous with shorter so-called Dansgaard-Oeschger cycles were also identified for the first time at this location Chapter 2). While the Heinrich signal was pronounced at the two northern most locations (15°36'N and 13°40'N), the D-O signals were most pronounced at the southern location (12°26'N), where the Heinrich events appeared suppressed. This latitudinal difference leads to the conclusion that a climate boundary (which certainly reflects the southward shift of the northern limit of summer position of the ITCZ) existed between 13 and 12°N during the last glacial. This shift might have been driven by the stronger NE trades at this period. The D-O synchronous events in the southern core reflect variations in the West African monsoon

demonstrating that arid/drier conditions occured further south of the Sahel than previously reported.

An understanding of the driving force behind the changes in West African hydrology was performed by means of a fresh water hosing experiment using coupled climate model (Chapter 3). The experiment suggested that the North Atlantic sea surface temperature and West African climate are linked by shifts in the position of the monsoon trough and the mid tropospheric African Easterly jet. The cooling of the North Atlantic sea surface is directly linked to the weakening of the Atlantic Meridional Overturing Circulation.

A detailed investigation of the magnetic mineral assemblages of the Senegalese sediments shows a wide range of magnetic minerals representing different sources, morphologies and characteristics (Chapter 4). This demonstrates the complexity of the depositional environment. Wind blown detrital (titano-)magnetite dominated the glacial sediments where euhedral particles, spherules and amorphous grains dominate the magnetic fraction. The particles showed erosion, dissolution features and shrinkage cracks indicating low temperature oxidation (maghemitization). Grains of hemoilmenite lamellae with titanomagnetite intergrowth which suggest high temperatures oxidation of the original titanomagnetite were also identified. Hematite and goethite were more dominant at these intervals as a result of the increase input of Saharan dust.

The interglacial sediments showed lower concentrations of magnetic particles, with the bulk of the heavy liquid separates dominated by euhedral and framboidal pyrite. This pyrite domination, together with the dissolution surfaces identified in the grains confirms that reducing conditions persisted during warmer climate, driven by high marine productivity.

Iron oxide rich framboids originating from the oxidation of pyrite and “possible” pyrrhotite oxidation showed that secondary magnetization occurred in this region. However, their effects on the paleo- magnetic and climatic signals are considered negligible since such particles occur in very low concentrations (<< 1%) in the extracts.

Sediment cores from off Cameroon and Gabon revealed three zones depicting degree of reductive dissolution of the magnetic particles (chapter 5). They showed that dissolution had occurred at some intervals but with the most part of the core dominated by primary magnetic signals. Fined grained magnetite dominates the mineral assemblage and representing variations in terrigenous input.

The Holocene showed significant variation in the climate, which implies other forces other than orbital changes in summer insolation drive climate change in this region. These millennial-scale events correlate with lake level records from the African continent. This shows that aridity periods indicated by low lake levels were always recorded in marine sediments, with high Ti enriched dust being deposited into the ocean.

1. Introduction

Motivation and objectives

The history of climate change dates back to the 19th century when Joseph Fourier, a French Physicist in 1824, first described the green house effect. Between then and 1960 scientists such as Svante Arrehnius, Stewart Callendar and Charles Keeling embarked on studies to investigate evidence of global warming. They showed that the atmospheric CO_2 level was rising, driven by human activities, which could lead to increasing atmospheric temperatures. The next decades saw a growing scientific, political and public interest in climate research which provided increasingly substantial evidence for ongoing and future changes in the world's climate. In an organized effort of governments and scientists, the Intergovernmental Panel of Climate Change presents yearly updated reports predicting the state of the climate system and the various forms of human impact. To understand the interaction of natural and man-made climate variability and the response of vegetation and local climate, it is imperative that past climate changes be studied.

The Earths climate has been changing for over 4 billion years before human existence, driven by natural phenomena such as volcanic activity, atmospheric chemistry, orbital variations of insolation and solar activity. Past climate change occurred at different time scales, ranging from few years to thousands and millions of years, driven by different factors whose effects could be at regional or global scales. Studying and understanding the causes, extent, and frequency of these changes is vital in order to be able to isolate anthropogenic impact from climate change driven by natural phenomena.

The African continent makes up about 21 % of the earth's surface, which makes it an important element in any climate model. As recent as the last century (1960 – 70s), the Sahel region of North Africa experienced a sharp drop in the annual rainfall (~25 %) which led to severe droughts. This had a devastating effect on the population, resulting in famine, starvation and death. There was also mass migration to areas less affected leading to over population in some areas. Such occurrences will be more common and severe in the future if current climate trends persist. Changes affecting the African continent are therefore important in any global climate reconstruction model. This paleo -climatic and -environmental study is undertaken in order to contribute to our understanding of the climate system of this region, hoping it will aid in developing reliable models that can predict future climate change.

The first part is to reconstruct past climate changes over northwest Africa from sediment cores obtained at the Senegal continental margin. Attention is focused on the frequency of climate variations during the last glacial cycle. This region is situated around the present day northern limit of the summer position of the ITCZ, a climatic boundary that separates humid conditions to the south from arid conditions to the north. Seasonal migration of this boundary determines the latitudinal extent of rainfall, and the amount of precipitation received in the Sahel. By studying cores from latitudes between 12 and 16 °N, it was hoped that past shifts in the position of this boundary could be identified. A good understanding of the positioning of the ITCZ in the past and present is important to forecast aridity changes in this climatically sensitive part of Africa. The degree of variability in precipitation in central Africa during the Holocene is also investigated.

Experimental paleoclimatic reconstructions are performed by applying so-called proxy methods to natural climate achieves such as paleosols, ice records, lake and marine sediments and tree rings. Next to a wide range of isotopic, biostratigraphic and geochemical methods, rock magnetic parameters have shown (Thompson and Oldfield, 1986; Frederichs et al., 1999; Evans and Heller, 2003) to provide suitable parameters for paleoclimate reconstruction. The concentration, grain-size and mineralogy of the magnetic assemblage mirror weathering, erosion and particle transport by air and water, hence climate-sensitive geological processes. Investigating the variations of the above mentioned factors and relating them to climate change forms the basis of environmental magnetism. However, other factors other than climate change might mask or destroy the magnetic signals. These include post depositional diagenesis (Berner, 1984; Canfield and Berner 1987; Karlin 1990) and biomineralization (Petersen et al., 1986; von Dobeneck et al., 1987). It is therefore important that a detailed understanding of the magnetic assemblage be understood for a reliable interpretation of results. For this reason and the fact that there are many potential sources for the magnetic minerals deposited at the Senegal continental margin, this study also attempts to identify and characterize the magnetic minerals as well as their potential alteration.

2. Millennial-scale North West African droughts relates to H Events and D-O Cycles: Evidence in marine sediments from off-shore Senegal

Itambi[1] A. C., T. von Dobeneck[1, 2], S. Mulitza[2], T. Bickert[2], D. Heslop[1, 2]

1) Geosciences Department, University of Bremen, Klagenfurter Strasse, D-28359 Bremen, Germany
2) Research Center Ocean Margins, University of Bremen, Leobener Strasse, D-28359 Bremen, Germany

Abstract

We present a suite of new high resolution records (0-135 ka) representing pulses of aeolian, fluvial and biogenic sedimentation along the Senegalese continental margin. A multi-proxy approach based on rock magnetic, element and color data was applied on three cores enclosing the present day northern limit of the ITCZ. A strong episodic aeolian contribution driven by stronger winds, dry conditions and characterized by high hematite and goethite input was revealed north of 13°N. These millennial-scale dust fluxes are synchronous with North Atlantic Heinrich stadials. Fluvial clay input driven by the West African Monsoon predominates at 12°N and varies at Dansgaard-Oeschger Cycles while marine productivity is strongly enhanced during the African Humid Periods and Marine Isotope Stage 5. From latitudinal signal variations, we deduce that the last glacial ITCZ summer position was located between core positions at 12°26' and 13°40'N. Furthermore, this work also shows that sub-millennial periods of aridity over northwest Africa occurred more frequently and further south than previously thought.

This manuscript is in press in Paleoceanography

2.1 Introduction

Since the discovery of rapid millennial-scale glacial fluctuations known as Heinrich Events and Dansgaard-Oeschger Cycles (Heinrich, 1988; Johnsen et al., 1992; Dansgaard et al., 1993; Bond et al., 1992, 1993 and 1995), numerous climate researchers have embarked on studies to better understand the regional expression of these rapid climate variations around the world (e.g., Kennett and Ingram,1995, in the Santa Barbara Basin; Schulz et al., 1998, the Arabian sea; Wang et al., 2001, in China). Climatic signals that are synchronous with Heinrich Events and Dansgaard-Oeschger Cycles have been identified at several low latitude subtropical and tropical locations (e.g., Kennett and Ingram,1995; Arz et al., 1998; Schulz et al., 1998; Wang et al., 2001; Adegbie et al., 2003; Weldeab et al., 2007). A fundamental question is the driving force behind such a global imprint of the high latitude climate system. Broeker et al. (1994), Ganopolski and Rahmstorf (2001), and Hemming (2004) suggested a change in deep sea circulation as the positive feedback mechanism while others such as Arz et al. (1998), Schulz et al. (1998), and Wang et al. (2001) proposed a more atmosphere linked mechanism.

North African climate has been quite unstable recently with numerous drought episodes that have seen the rapid southward encroachment of the Saharan desert. The quantity of terrigenous sedimentation into the northwest African continental margin reflects the degree of continental aridity and humidity (deMenocal et al., 2000b). Aerosol samples from as far as the Caribbean have shown that dust reaching this region comes from the Saharan desert and is directly linked to African drought (Prospero and Nees, 1977; Middleton, 1985; Arimoto et al, 1995; Prospero and Lamb, 2003).

In this study we investigate variations in fluvial and aeolian input into the continental margin of northwest Africa which may be interpreted as indicating humid and dry periods over the North African continent during the late Quaternary. We also demonstrate the latitudinal dependence of these millennial-scale climate fluctuations, in particular, the southward shifts in the position of the summer northern limit of the Intertropical Convergence Zone (ITCZ) during the last glacial.

We chose three sediment cores at ~3000 m water depth forming an N-S transect along the Senegalese continental margin. These sediments show a systematic alternation between reddish brown and dark green layers that are synchronous with stadial and interstadial cyclicity of the climate system. The region under investigation is ideal for such studies as it lies along the northern summer limit of the ITCZ which serves as the transition zone between tropical conditions in the south and Saharan desert to the north. The core locations are also in

close proximity to major river mouths and are thus expected to register changes in fluvial input.

A multi-proxy approach involving reflectance and magnetic techniques was employed. Diffuse Reflectance Spectrophotometry provided a rapid method suitable to identify iron oxides and other pigmented mineral components of the sediments (Balsam et al., 1995; Heslop et al., 2007). Rock magnetic parameters characterized sediment sources as well as depositional environments (Thompson and Oldfield, 1986; Robinson, 1986; Bloemendal et al., 1992; Frederichs et al., 1999). Elemental records from high resolution XRF scanning provided ratios representing climatically driven flux variations of terrigenous and biogenic sources (e.g., Arz et al., 1998; Jansen et al., 1998).

2.1.2 Geographic setting and material

The Senegal continental margin is located between 12 and 16°N. This stretch also includes Gambia which is surrounded by Senegal. The geographic position of the entire margin is very significant in understanding climate variability within the N African continent because of its sensitivity to the West African Monsoon system which determines the amount and distribution of precipitation. A low pressure cell known as the Intertropical Convergence Zone (ITCZ) where the Northeast Trade Winds (NET) converge with the Southeast Trade Winds (SET) near the equator plays a very important role within this region. This band is characterized by high precipitation, whose intensity and northward limit is determined by solar insolation (Kutzbach, 1981; deMenocal et al., 1993) and the strength of NE and SE trades. Its present day summer position is ~20°N and it acts as the major climatic boundary separating arid conditions to the north from humid conditions to the south.

Saharan dust flux into this region has been documented by numerous studies (e.g., Prospero et al., 1981; Tiedemann et al., 1994; Balsam et al., 1995, Stuut et al., 2005). The aeolian fraction is mostly transported by Harmattan winds which also control surface ocean circulation and hence the generation of the Canary Current. The Saharan Air Layer (SAL) is another major component of the atmospheric circulation, running at higher altitudes (Sarnthein and Koopmann, 1980).

Because of the strong interaction between atmospheric circulation and the sea surface, upwelling cells develop along this margin, enriching the waters in nutrients thus stimulating productivity (Hagen and Schemainda, 1984; Fischer et al., 1996; deMenocal, 2000a; Adkins et al., 2006).

Suspended and dissolved matter is transported into the ocean via the Senegal, Gambia, and some smaller rivers (Gac and Kane, 1986a; 1986b; Meybeck et al., 1987; Kattan et al., 1987; Koopman 1981; Sarnthein et al., 1981). Odin (1975) pointed out that iron is precipitated at the mixing zone between marine water and iron rich fluvial water. The precipitated iron is then available for synsedimentary mineral formation such as the green marine clays that are present in our samples.

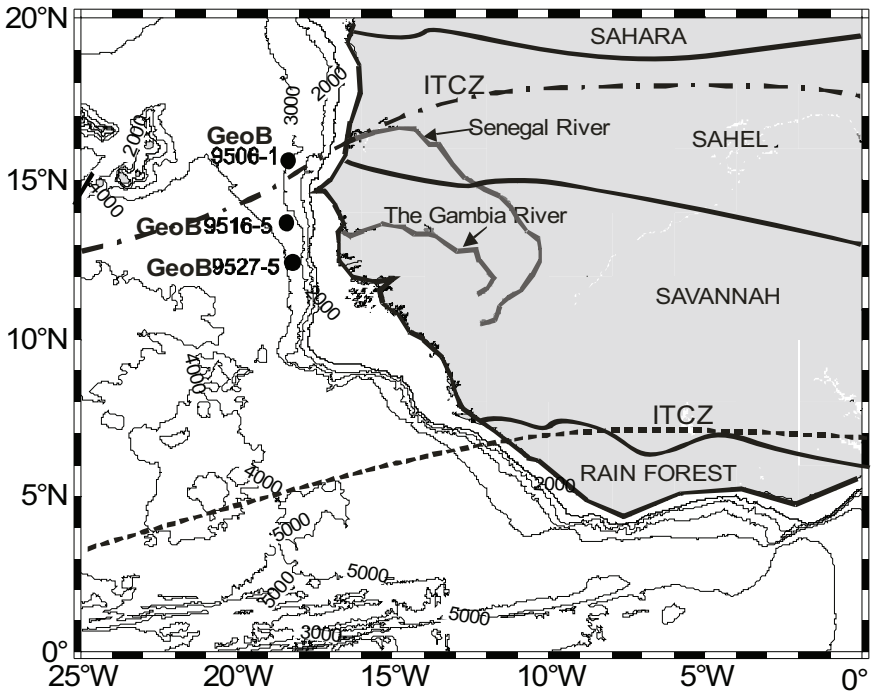

Figure 1. Study area and core locations. The dash lines indicate the present day boreal summer (dash-dotted line) and boreal winter (dash line) positions of the Intertropical Convergence Zone (ITCZ).

The Late Quaternary sediments investigated were obtained during RV Meteor cruise M65 along the NW African continental margin (Mulitza et al., 2006). The three gravity cores GeoB 9506-1 (15°36'N/18°21'W; 2956 m), GeoB 9516-5 (13°40'N/18°25'W; 3504 m) and GeoB 9527-5 (12°26'N/18°13W; 3679 m) were the deepest of three W-E oriented core transects off-shore Senegal (Fig. 1). As with the cores from shallower water depths collected during this cruise, the selected cores show systematic sequences of alternating reddish brown and dark green layers which can be correlated over a wide area. The cores were also selected based on their location between humid conditions in the south and arid conditions to the north. Smear slide analysis identified mud as the dominant terrigenous material. Some sandy mud layers were observed in the northern-most core (GeoB 9506-1). The only evidence of

bioturbation was in the deepest part of GeoB 9527-5 (~9.5 m) were pyrite precipitation was also identified. The color ranges between light brown to dark green, with the degree of lightness increasing from south to north.

2.2 Methods

2.2.1 Magnetic parameters

Low field magnetic susceptibility (κ) was measured on archive halves of the sediment cores at a resolution of 1 cm using an automatic core scanner with a *Bartington Instruments MS2 F* Spot Sensor. Background measurements were taken after each point to correct for instrumental drift. Magnetic susceptibility provides an integral measure of magnetic mineral concentration (Thompson et al., 1980; Verosub and Roberts, 1995).

A range of mineral and grain-size specific rock magnetic measurements were performed on discrete samples taken at 5 cm intervals in 6.2 cm^3 cubes: A dual frequency (low (χ_{lf}) at 470 Hz, high (χ_{hf}) at 4700 Hz) *Bartington* susceptibility meter was used to quantify the contribution of ultra-fine superparamagnetic (SP) particles to the susceptibility signal using the diagnostic parameter frequency dependence of magnetic susceptibility $\kappa_{fd\%}$ (Dearing et al., 1996).

Anhysteretic remanent magnetization (ARM) was imparted using a 100 mT alternating peak field and a 40 μT DC biasing field in an automated *2G Enterprises 755R DC SQUID* pass-through magnetometer. The ARM was subsequently AF demagnetized at increments of 5 mT from 5-50 mT and increments of 10 mT from 60-100 mT. ARM is used as an indicator of grain-size and concentration of sub-micron magnetite (Thomson and Oldfield, 1986; King et al., 1982; Oldfield and Yu, 1994).

Isothermal remanent magnetization (IRM) was imparted at 23 incremental steps up to a field of 700 mT. The IRM at this maximum field was considered as the saturation isothermal remanent magnetization (SIRM) which together with the IRM measured at 300 mT was used in calculating the hard isothermal remanent magnetization (HIRM) representing the proportion of the high coercivity materials (antiferromagnets hematite and goethite). However, only the hematite and not the goethite fraction could be inferred in this study due to the limitation of the saturation field used.

The S-ratio given by the equation;

$$S_{0.3T} = \frac{IRM_{0.3T}}{SIRM}$$

represents the relative contribution of low coercive minerals, essentially (Ti-) magnetite, to SIRM (King and Channel, 1991; Maher and Thompson, 1999). The ratio ranges between 0 and 1. Pure ferrimagnetic minerals have S-ratios close to 1 and the ratio decreases with increasing content of antiferromagnetic minerals.

2.2.2 Diffuse Reflectance Spectrophotometry (DRS)

Color reflectance spectra were determined with a hand-held *Minolta-CM2600d/2500d* camera on the archive halves. The core surface was first cleaned to remove oxidized material that might have been formed during storage, covered with a thin transparent film and then measured at 3 cm intervals.

A non-Negative Matrix Factorization (NMF) algorithm developed by Lee and Seung (1999) and adapted to this purpose by Heslop et al. (2007) was used to analyze the DRS data to obtain end-member spectra and relative abundances of pigmented mineral components.

2.2.3 X-ray fluorescence (XRF)

Elemental abundances were obtained at 2 cm resolution using a *CORTEX* X-ray flourescence scanner at the Bremen IODP core repository center. The acquired XRF spectra were processed using *Kevex* software, giving the resulting element abundances in counts per second (cps). Jansen et al. (1998) and Röhl and Abrams (2000) provide a detailed description of the instrument and measurement procedure.

2.2.4 Cluster analysis

To differentiate the sources of the sediments in our study area, we performed a fuzzy c-means cluster analysis of the combined magnetic and elemental data with the MATLAB fuzzy math toolbox. The data were pretreated, involving the transformation of each variable to a normal distribution based on a data adaptive lookup table. The clustering itself employed a fuzzy exponent of 1.5 and a similarity measured based upon Euclidean distances. Finally, membership values of each point to the cluster centers were calculated and the positions of the determined cluster centers converted back to the measurement space using the inverse of the transform applied during the data pretreatment.

2.3 Results

2.3.1 Chronostratigraphic correlation

The age-depth relationship for core GeoB 9516-5 was established by correlating the benthic $\delta^{18}O$ with the benthic $\delta^{18}O$ record of MD95-2042 (Shackleton et al., 2004), SPECMAP (Imbrie et al., 1984) and the $\delta^{18}O$ record from nearby ODP site 659 (Tiedemann et al., 1994) as shown in Figure 2a. GeoB 9516-5 was chosen for the initial chronostratigraphy because test results for post-depositional processes indicated it had been least affected by diagenesis as will be shown later.

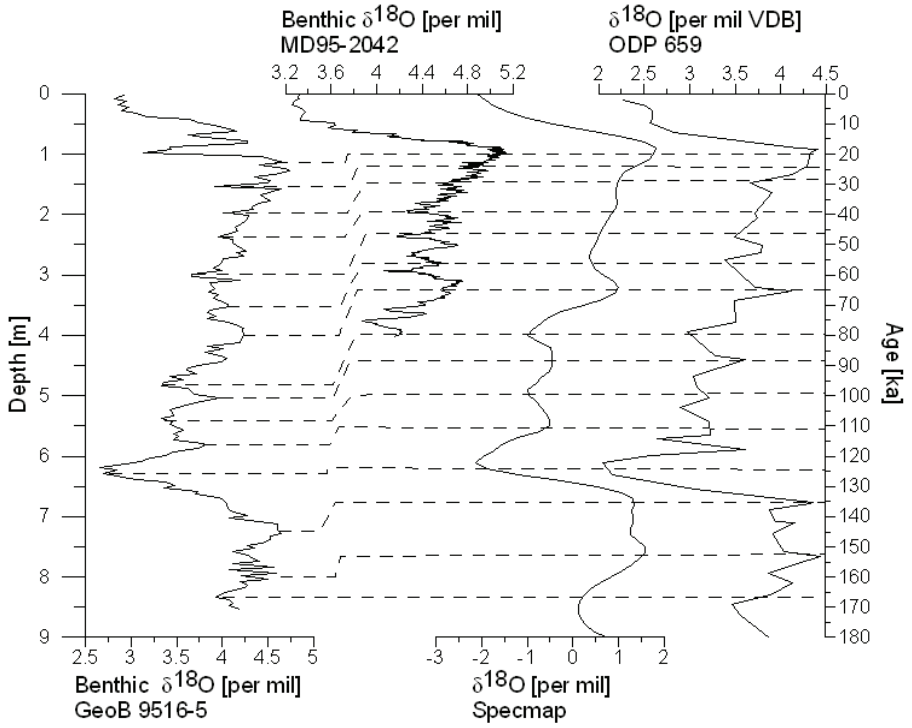

Figure 2a. Correlation of the benthic $\delta^{18}O$ of core GeoB 9516-5 with established age models; benthic $\delta^{18}O$ of core MD95-2042 (Shackleton et al., 2004); SPECMAP (Imbrie et al., 1984) and near by core ODP 659 (Tiedemann et al., 1994)

Thus, we were able to assign 15 tie points (Figure 2a). The top 20-70 ka was correlated using the benthic $\delta^{18}O$ of core MD95-2042 (Shackleton et al., 2004), while older ages were derived by correlating to SPECMAP (Imbrie et al., 1984) and the higher resolution $\delta^{18}O$ based age record for ODP hole 659 (Tiedemann et al., 1994) (Figure 2a).

Two correlation tools programmed by Thomas Frederichs and Karl Fabian of the Marine Geophysics section, University of Bremen were used for the correlation and the ages

between tie points were obtained by linear interpolation. The oxygen isotope record for our core displays two large minima between 0.5 and 1.0 m core depths. The smaller minimum at 0.68 m represents the Bolling/Allerod interstadial while we cannot readily give a good explanation for large minimum at 0.98 m. We also could not identify such large drops in other records (e.g., Bloemendal et al., 1988, core V22-197), from the same area.

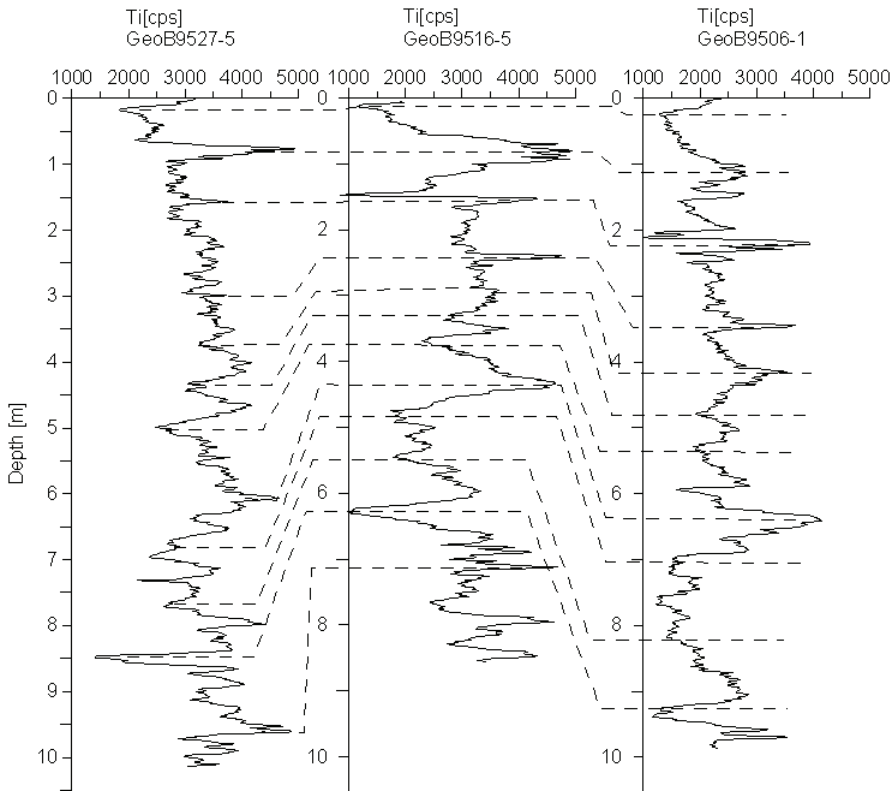

Figure 2b. Correlation between the Ti records of GeoB 9516-5 to those of cores GeoB 9506-1 GeoB 9527-5, used in the establishment of age-depth relationships for the latter two.

Most magnetic and geochemical records of the three cores exhibit very similar patterns thus enabling us to establish age control for cores GeoB 9506-1 and GeoB 9527-5 by first correlating some magnetic and geochemical (ARM/IRM, HIRM, and Ti) depth records of these cores to those of GeoB 9516-5 (Figure 2b). This relationship was subsequently used to establish their age-depth profiles. Ti was chosen as a tool for correlating the three cores because of its chemical stability and resistance to post depositional diagenesis. Saharan dust is enriched in Ti and the signals are well imprinted in all three cores. The ages determined were

cross checked with ^{14}C ages of a nearby core (Mulitza et al., 2008) and show a very good coincidence.

All three cores seem to be continuous in time and reach ages of 178 ka (GeoB 9516-5), 127 ka (GeoB 9506-1) and 138 ka (GeoB 9527-5). The northern-most core has the highest average sedimentation rates (7.76 cm/kyr), the central core has the least (4.76 cm/kyr) and the southernmost value is 7.31 cm/kyr, (Figure 2c). However, all three cores show higher sedimentation during the glacial. In the following, only the commonly reached age of ~135 ka is considered.

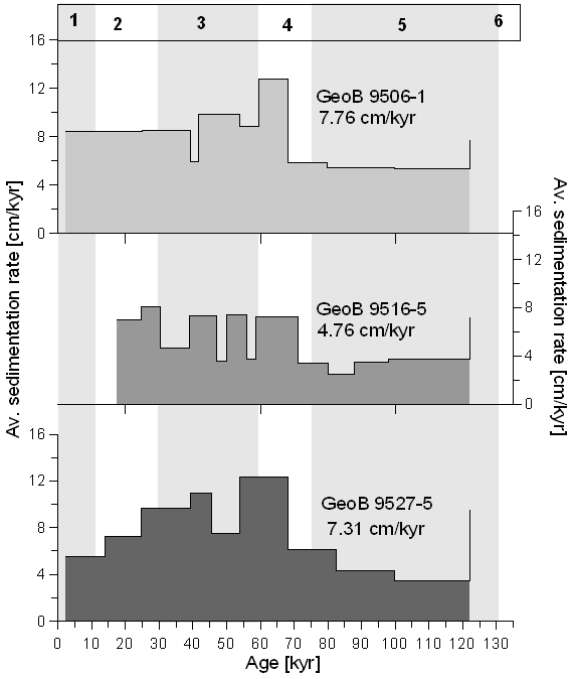

Figure 2c. Average sedimentation rates. All three cores show the highest sedimentation during the Last Glacial.

2.3.2 Diffuse reflectance spectrophotometry

This method was employed because individual minerals have a specific color spectrum which can readily be identified using end-member analysis. We only present data of core GeoB 9516-5 since the two others showed similar but less intense variation in color. We identified three end-member (EM) spectra (Figure 3a). Their first derivative curves (Figure 3b) show peaks that can be used for mineralogical identification. In EM 1, three prominent peaks are observed at wave lengths which are typical for hematite and goethite (Balsam et al., 1995). This end-member is thought to represent aeolian derived sediments from the Saharan desert. EM 2 has highest reflectance values and is typical for carbonates. In the third end-member EM 3, the absolute reflectance values are very low (less than 3%) and

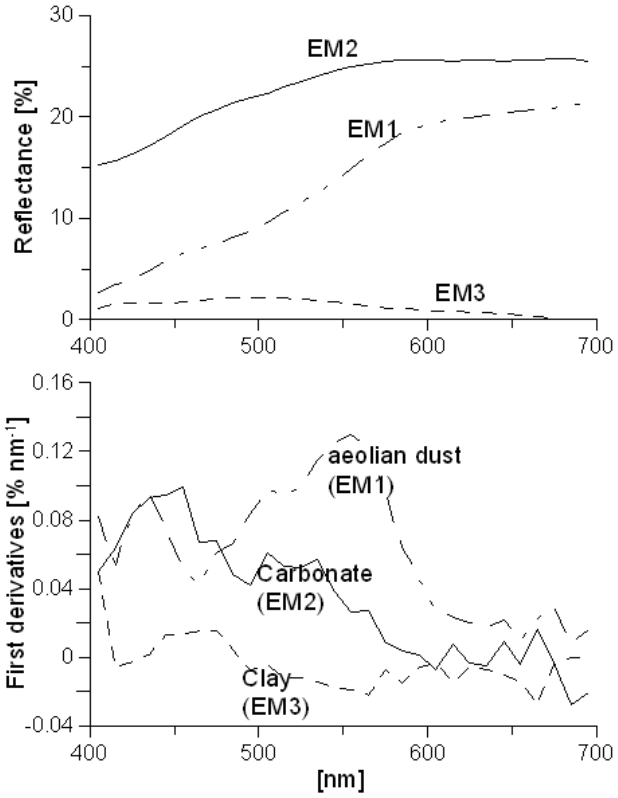

Figure 3. (a), three spectra of end-member components revealed using the NMF algorithm (Heslop et al., 2007). (b) The first derivatives of the reflectance spectra show the main end-member components. The main iron oxides contributing to the reflectance are goethite and hematite (EM 1) while there is a strong carbonate (EM 2) and clay (EM 3) signature. These end-members are obtained from core GeoB 9516-5.

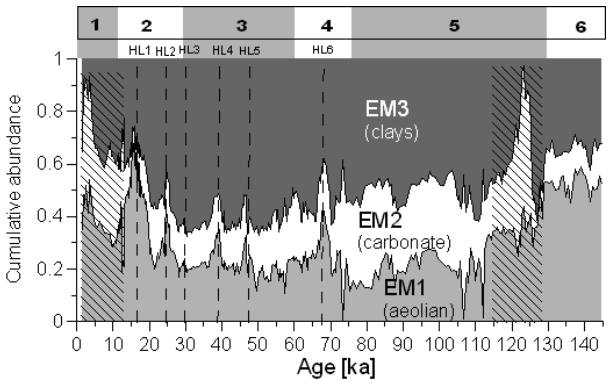

Figure 3c. Down-hole cumulative abundances for the three end-members of core GeoB 9516-5. EM 1 is the aeolian fraction, EM 2 carbonate and EM 3 clays. Dash lines represent time intervals corresponding to north Atlantic Heinrich Events (HL 1-HL 6). Here, we refer to these signals as Heinrich-like Events (HL). Note the high concentration of hematite and goethite at these intervals especially the broad peak incorporating the Last Glacial Maxima and HL 1. Two episodes of the African Humid Period (AHP) are designated by hatched shading. The horizontal bar shows the Marine Isotope Stages (MIS, 1-6)

the derivative curve shows a prominent broad peak between 435 and 475 nm. It represents the clay fraction which in this case is dominated by fluvially derived green marine clays.

Down-core variations in the abundances of the three end members are illustrated in Figure 3c. EM 1 is synchronous with glacial maxima and Heinrich stadials.
Carbonate enriched sediment represented by EM 2 is prominent during warmer conditions (interglacial) as well as intervals corresponding to the African Humid Period. The clay component (EM 3) is relatively abundant throughout the entire profile. However, it is significantly reduced during extremely dry conditions and is diluted and modulated by varying carbonate sedimentation.

2.3.3 Environmental magnetism

2.3.3.1 Concentration of magnetic minerals

Concentration dependent parameters (Figure 4a) show a wide range of magnetic mineral concentrations. Magnetic susceptibility (κ) varies tremendously in all three cores, with values ranging between 60 x 10^{-6} SI and 800 x 10^{-6} SI and is much higher in the reddish-brown layers. The dark-green layers in GeoB 9516-5 have a fairly constant κ of ~200 x 10^{-6} SI, less than half the values of the reddish-brown layers. Such κ represents magnetic minerals enrichment and corresponds to Heinrich stadials as well as the glacial maxima (GM). Core GeoB 9516-5 displays the highest κ values of ~800 x 10^{-6} SI in a broad peak that covers the Last Glacial Maximum (LGM) and Heinrich-like Event 1. An interesting observation here is the anti-correlation between the total concentration of magnetic minerals (IRM) and the concentration of fine grained ferrimagnetic minerals (ARM). While the ARM peaks in the green clay layers, IRM is at maximum in the reddish brown layers and shows a strong positive correlation to κ clearly delineating the grain-size distinction of aeolian and fluvial fractions.

Similar patterns are observed in GeoB 9506-1 and GeoB 9527-5 for which we draw analogue conclusions. However, the concentration of magnetic minerals varies tremendously. In core GeoB 9506-1, the amplitude variation in κ is restricted between 100 and 300 x 10^{-6} SI. In GeoB 9527-5, high κ values (~800 x 10^{-6} SI) are observed during the LGM with the rest of the core remaining below 200 x 10^{-6} SI. In cores GeoB 9506-1 and GeoB 9527-5, the ARM drops abruptly to values as low as 0.04 A/m between 70 and 120 ka.

2.3.3.2 Magnetic mineralogy

Figure 4b shows down core changes in magnetic mineralogy. High values in the S-ratio (>0.95) corresponding to maxima in the ARM (Figure 4a) within the dark-green layers indicate that the mineralogy is dominated by fine-grained magnetite. On the other hand, the reddish-brown layers show evidence of a hematite dominated magnetic mineralogy. The S-ratio is at minimum at these intervals and correlates with the hard isothermal remenant magnetization (HIRM).

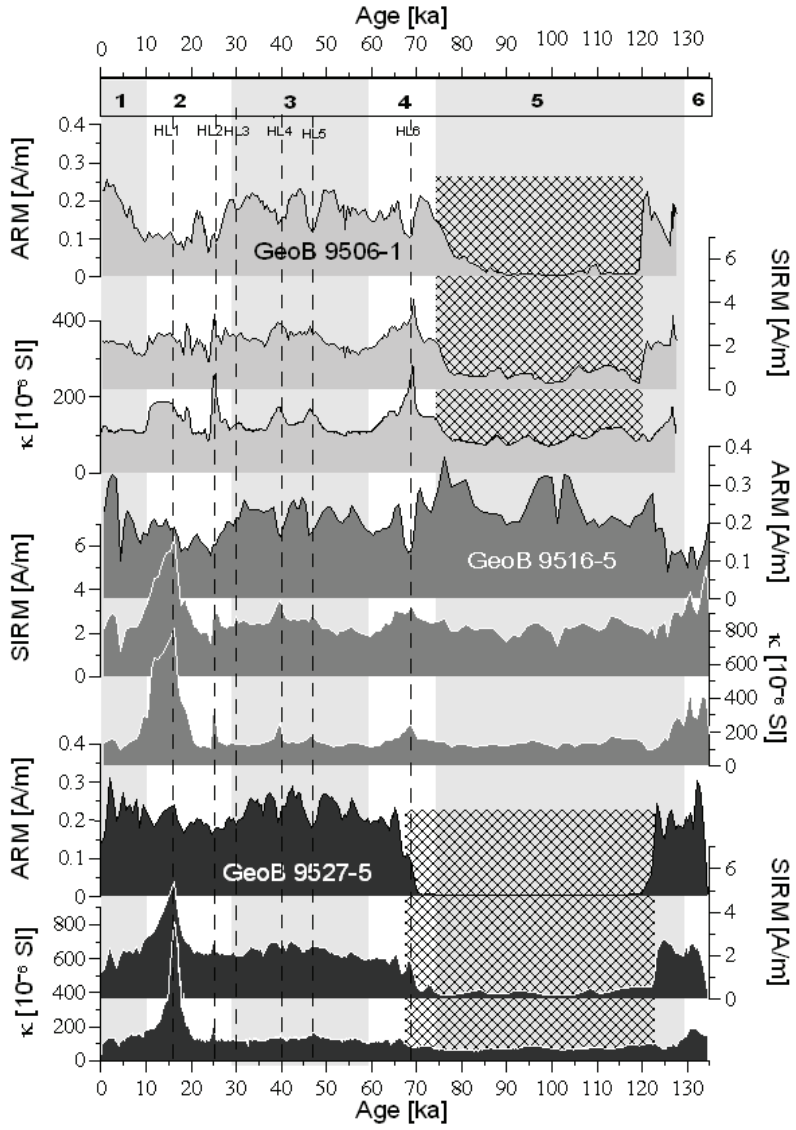

Figure 4a. Concentration dependent parameters κ, ARM and SIRM. Note the anticorrelation between ARM and IRM and the high concentration of magnetic minerals during Heinrich-like events. The drastic drop in concentration parameters in cores GeoB 9506-1 and GeoB 9527-5 (cross hatching) marks diagenetic overprint.

The HIRM indicates high coercivity minerals such as hematite and goethite. The magnetic mineralogy shows fluctuations between hematite and magnetite dominance similar to variations observed in other magnetic parameters thus suggesting that hematite is dominant during extreme cold periods while interglacials are marked by larger input of magnetically soft magnetite. The down-hole profiles of GeoB 9516-5 remain relatively stable while there is a significant drop in the S-ratio in GeoB 9527-5 and GeoB 9506-1 during MIS 5, corresponding to the observed drop in ARM.

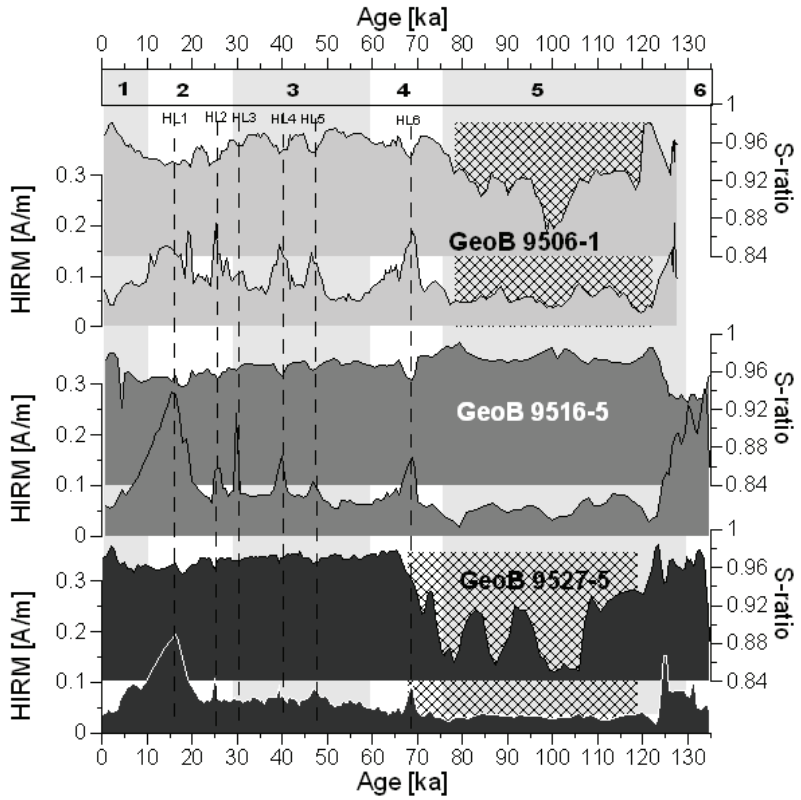

Figure 4b. Magnetic mineralogy changes illustrated by S-ratio and HIRM. The two parameters point to the dominance of high coercivity hematite at the reddish brown layers while dark green layers contain magnetically soft minerals such as magnetite (S-ratio closer to 1). Cross hatching indicates diagenesis.

2.3.3.3 Magnetic grain-size

The various applied magnetogranulometric parameters $\kappa_{fd\%}$, ARM/IRM and SIRM/κ all show similar trends. As significant contribution from ultra-fine superparamagnetic material has the potential to bias our interpretation of susceptibility related grain-size ratios towards coarser values, we present ARM/IRM (Figure 4c) which is unaffected by this effect. High

values of ARM/IRM indicate the presence of SD (Ti-) magnetite which in this case points to fining at interglacial intervals while coarser material dominates glacial periods.

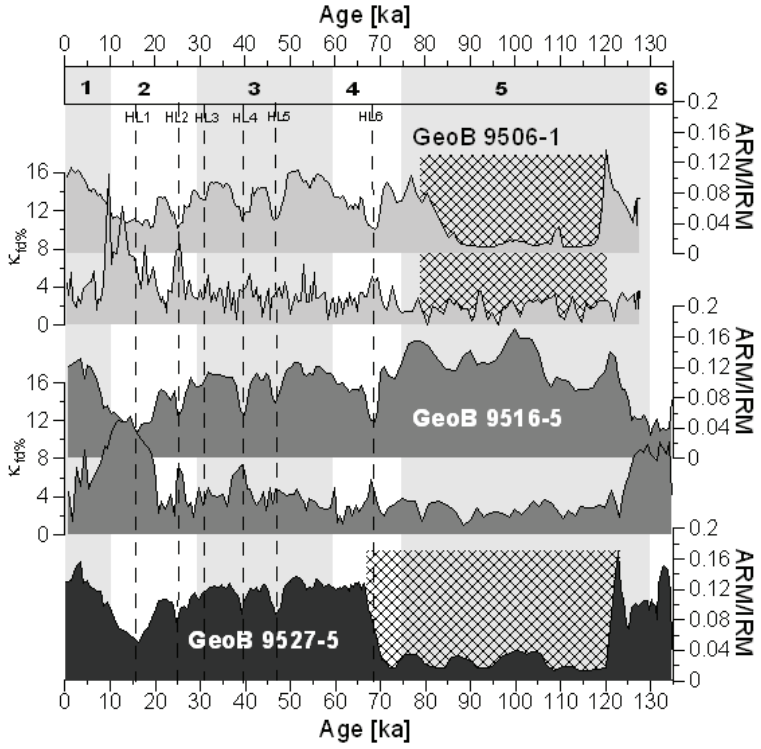

Figure 4c. Down-hole variation in magnetic grain-sizes. Variations in ARM/IRM indicate coarsening at the cold events while fine SD particles that contribute more to ARM dominate the warmer intervals. High $\kappa_{fd\%}$ also suggests a strong contribution of superparamagnetic minerals during cold periods. Cross hatching indicates diagenesis

The relative contribution of superparamagnetic (SP) grains to the magnetic susceptibility determined by the frequency dependence susceptibility ($\kappa_{fd\%}$) is strongly enhanced at glacial and Heinrich-like Events (Figure 4c). It reaches high values (12%) in GeoB 9516-5 and positively correlates to κ which implies a dominant contribution of these particles to the magnetic signals. Two prominent peaks occur between 14-19 ka and 130-150 ka and can be observed in κ, $\kappa_{fd\%}$, and HIRM. These mark the last two glacial maxima. For reasons of instrumental sensitivity, $\kappa_{fd\%}$ is much noisier in GeoB 9506-1, with values between 0 and 16%. The signal is less pronounced than in GeoB 9516-5. Maximum values lie between 13 and 20 ka, covering the LGM and Heinrich-like event 1.

2.3.4 Elemental abundances (XRF)

Elemental abundances (Figure 5) also show sub-Milankovitch variations. Ti, Al, Si and Fe are considered to indicate terrigenous input while Ca represents the biogenic fraction.

Since Si and Al have signatures similar to Ti suggesting supply from terrigenous source, only the profiles for Ti, Fe, and Ca are included in our plots. Ti and Fe anticorrelate with Ca, but Fe variation is of much lower amplitude. It remains fairly constant, ranging between 10 000 to 35 000 cps. The relative supply of Fe is high at all periods with a minimum value >10000 cps whereas Ca ranges from values as low down as 2000 to maximum of ~60000 cps.

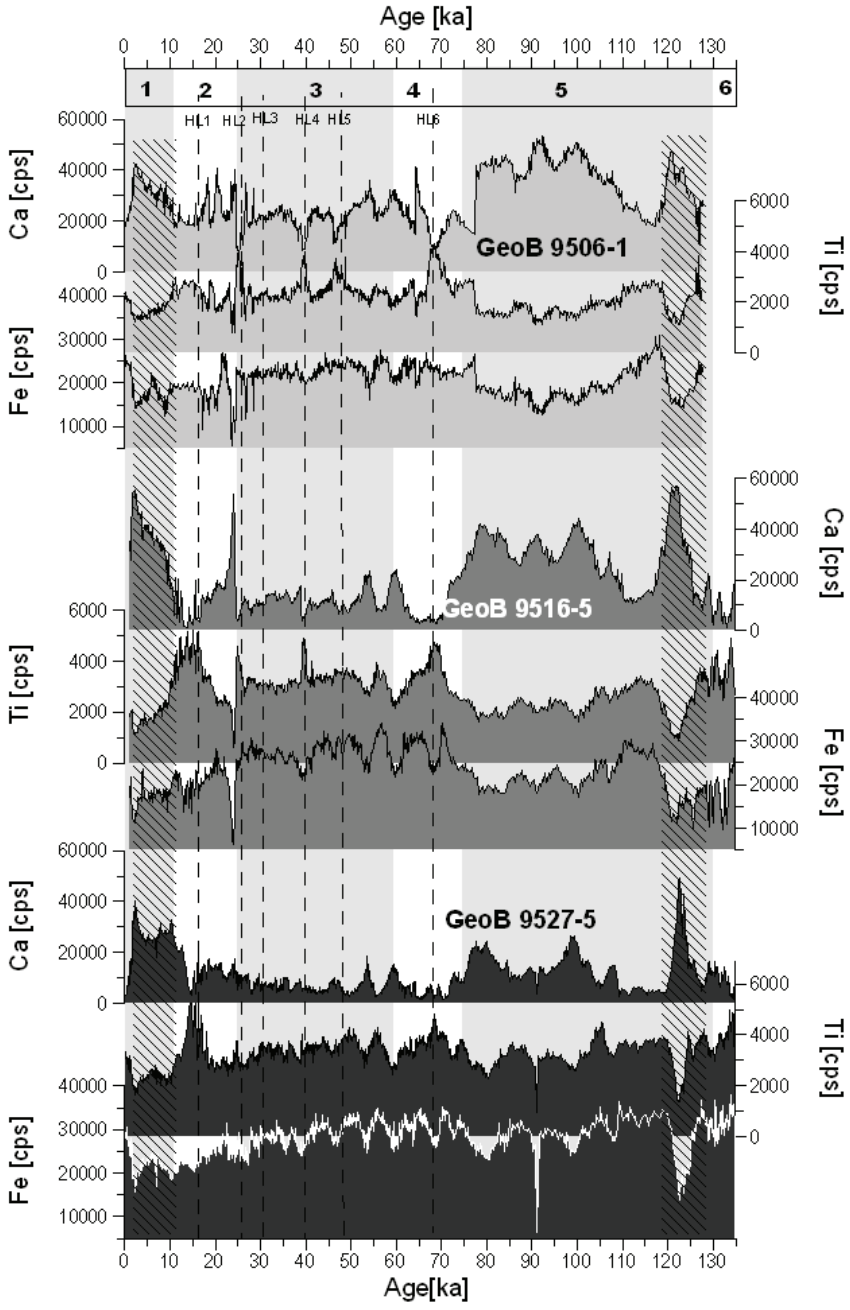

Figure 5. Elemental abundances. The pattern of these signals strongly mirror those observed in the magnetic as well as the reflectance profiles. Ti signals are stronger than those of Fe at cold periods (extremely dry events). Note the high Ca content at the AHP (hatching).

Climatic signals similar to those observed in magnetic profiles are also imprinted in the elemental records. However, these tend to be more evident in the Ti than in the Fe records. All the major and minor peaks corresponding to glacial termination and Heinrich-like events are absent in Fe. Aeolian sediments are enriched in Ti (Glaccum 1978) while fluvial sediment deposited in this region carry high Fe (e.g., Gac et al., 1986a). There has been a relatively constant decrease in terrigenous input since the beginning of the last glacial cycle. Heinrich-like signals marked by peaks in Ti are less strongly imprinted in the southernmost core (GeoB 9527-5) though it shows a major peak between ~14 and 19 ka, similar in amplitude to that observed in core GeoB 9516-5. Some additional peaks in Ti are observed in GeoB 9516-5 and GeoB 9506-1 and are of much lower amplitude. Heinrich signals are characterized by much higher content of Ti. The additional peaks fall within the background values and are therefore strongly imprinted as a result of much higher productivity before and after these signals.

The abrupt onset and termination of the African Humid Period (AHP) occurs between 12 – 3 ka in all three cores (Figure 5). It is worth noting here that the age constraints of the humid period as observed in our profiles cannot be confirmed with certainty since the top part of the core (~15-0 ka) is only assigned ages by linear interpolation. We therefore look at the characteristics of the AHP rather than its onset and termination. It is marked by very high Ca sedimentation as well as corresponding drop in terrigenous input (Ti and Fe). A similar peak in Ca occurs between 130-118 ka and has been described (deMenocal et al., 2000) as an earlier episode of the AHP. Ca increases substantially during MIS 5. Interestingly, pronounced humid periods tend to occur immediately after the glacial maxima.

2.4 Discussion

2.4.1 Sediment sources and fluxes

The magnetic parameters provide an insight into the mineralogy, grain-size and source of sediment into this region. Looking at the relationship between IRM and ARM as well as the κ, S-ratio, HIRM and ARM/IRM, the prominence of two terrigenous sources each with a distinct magnetic mineralogy, grain-size, and source can be seen. Biplots of Fe vs. κ (Figure 6a) clearly demonstrate such groupings. Group A comprises samples that are highly enriched in magnetic iron minerals. Thus, magnetic susceptibility varies whereas the predominantly paramagnetic iron content remains constant or decreases accordingly. This group is well documented in core GeoB 9516-5 and GeoB 9525-5 and represents sediments deposited under drier conditions through aeolian transport whereas the B group which shows variation in

weakly magnetic iron content along a line of nearly constant susceptibility indicating fluvially derived Fe-rich clay sediments supplied by the monsoon affected region south of the Sahara (Odin 1975). In the southern- and northern-most cores, an additional group (C) of interglacial samples showing similar trends in Fe but lower susceptibility values. As will be shown later, this group corresponds to samples which have been affected by diagenetic reduction of iron.

This observation also conforms to the work of Bloemendal et al. (1992) which demonstrated similar results in this region. However, our result also contrasts earlier work by Bloemendal (1988) which suggested that interglacials were characterized by ultra-fine grained minerals. Evidence from the proxy parameters $\kappa_{fd\%}$ and ARM/IRM suggest there is significant contribution of ultra-fine grain minerals during glacial or cold periods whereas interglacials comprised almost entirely of fine SD magnetite. These ultra fine minerals may occur as coatings on quartz grains. Low ARM/IRM during glacials also indicate the presence of coarse particles, which can be attributed to the stronger winds that have been reported during such periods.

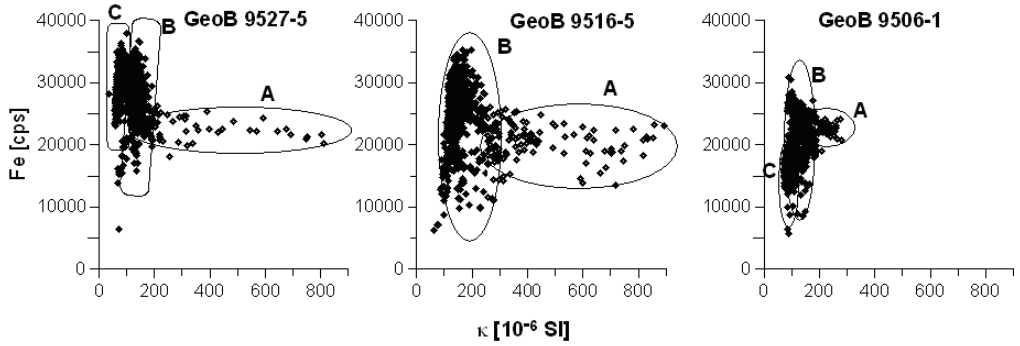

Figure 6a. Biplots of Fe vs. κ. Group A comprises aeolian sediments deposited under extremely dry conditions. Group B sediments are mostly riverine. The third group C exists only in the southern-most and northern-most cores and comprise of samples that have been severely affected by diagenesis.

The mineralogy indicators: HIRM and S-ratio point to the dominance of high coercivity hematite within the reddish brown layers. This is further confirmed by the reflectance data which clearly identify peaks representative of hematite and goethite from the spectra, confirming earlier documentation of the joint occurrence of these minerals in northwest African dust by Balsam et al. (1995). Downcore variation of fractional abundance of the hematite/goethite end-member corresponds positively to those of κ and HIRM, implying that these minerals are the dominant magnetic carriers. Correlation of peaks in κ and $\kappa_{fd\%}$ which also coincides with prevalence of high coercivity minerals (lows in S-ratio) suggests the presence of fine high coercive and partly superparamagnetic (SP) hematite and/or goethite.

Magnetically soft magnetite dominates sediments deposited during warmer periods and is evident in the high S-ratio and ARM at these intervals (e.g. Bloemendal et al., 1992). These minerals are of much finer SD-PSD grain-size, corresponding to grain-sizes of less than 1 µm.

Relative variations in total terrigenous vs. biogenic input are represented by the Fe/Ca ratio (Figure 6b). High amplitudes oscillations similar to Heinrich layers observed in the IRD belt of the Northern Atlantic (Heinrich 1988; Bond et al., 1993) are clearly imprinted in the two northern cores. The records show a general northward increase in the biogenic fraction (low Fe/Ca).

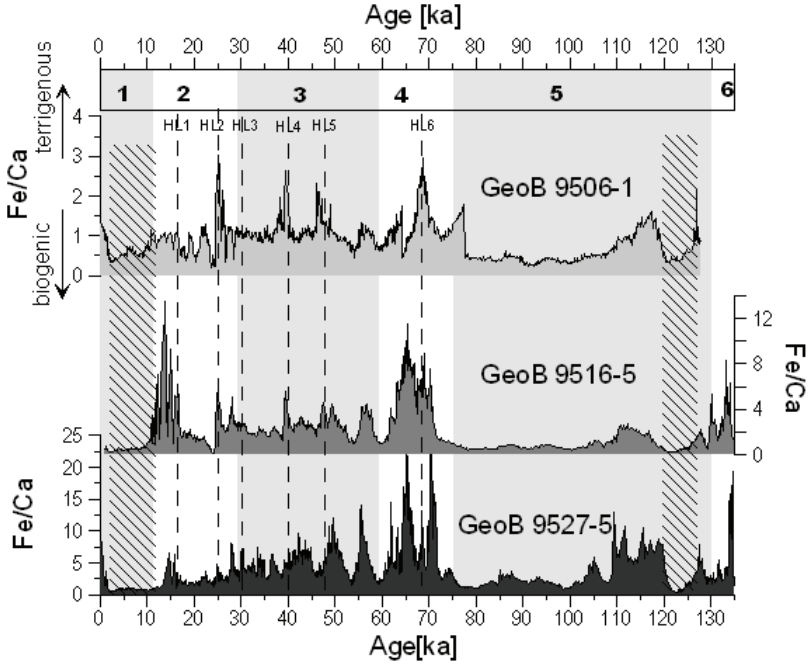

Figure 6b. Variations in terrigenous vs. biogenic input indicated by Fe/Ca. Increased terrigenous input at Heinrich-like Events and glacial maxima. These signals are most strongly visible in the two northern most cores. Note that the plots are on different scales on the y-axis due to their huge differences which can be attributed to a southward increase in the Fe content (see the biplots above) and the northward increase in the Ca.

For a joint interpretation of rock magnetic and element data, a fuzzy cluster analysis was applied on normalized data sets of ARM, HIRM, κ, Ti, Fe, Ca, Al, and K. Figure 6c shows the four identified clusters: Cluster 1 is characterized by peaks in the magnetic properties HIRM and κ as well as the terrigenous signals K and Ti. The hematite/goethite and Ti rich sediments represented by these parameters are a typical signature for Saharan dust (Balsam et al, 1995; Larrasoaña et al., 2003). This observation is further strengthened by the good correlation between this cluster and the end-member representing aeolian dust (hematite/goethite) obtained from the DRS data. Schütz and Rahn (1982) showed that Saharan dust is rich in Ti while Glaccum (1978) identified the presence of a rich Ti phase

(Rutile) in Saharan derived dust collected in the Caribbean. Cluster 1 therefore represents the aeolian fraction with the source area being the southern Sahara. Using back trajectory for present day aeolian transport, Stuut et al. (2005) traced the source region of aerosols deposited in this area to Algeria.

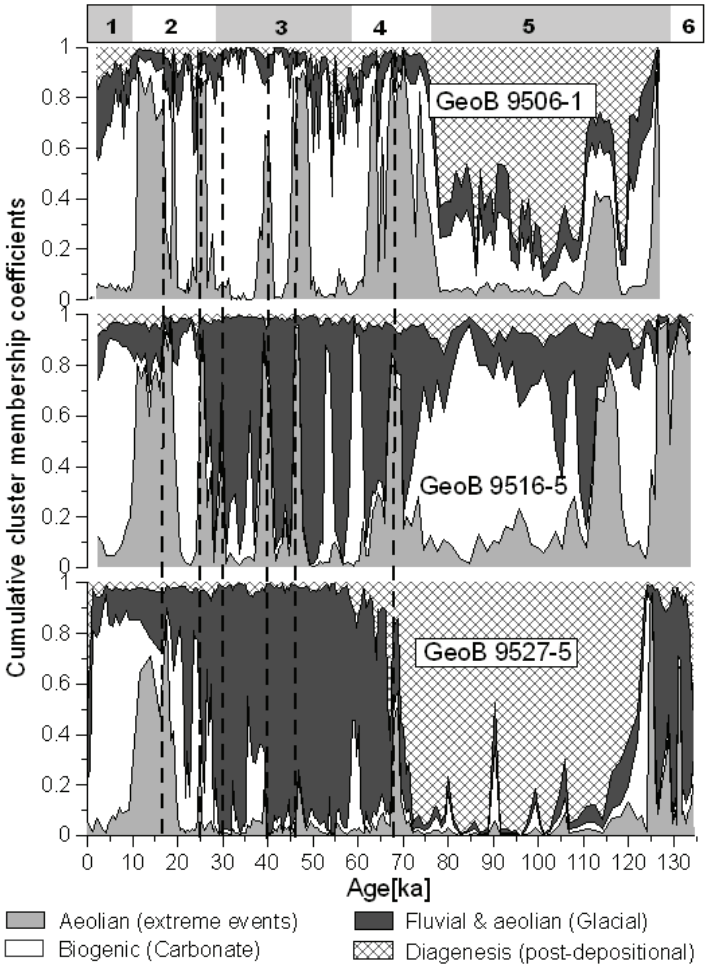

Figure 6c. Cumulative plot of down-hole profiles of the four clusters representing sediment sources. Cross hatching indicates diagenesis while the Heinrich signals are indicated by the dash lines.

High concentration in the terrigenous elements Fe and Al coupled with very low values in the magnetic parameters are typical characteristics of the second cluster. The high Fe content and drop in remanence is evidence of reductive dissolution of the magnetic mineral magnetite which leaves behind less magnetic Fe phases (e.g., Karlin et al., 1987). The drop in the HIRM implies even more resistant antiferromagnetic phases have been affected. This cluster represents the post-depositional process, reductive diagenesis.

Cluster 3 shows highest value in the Ca content and the terrigenous signals are lowest. We classify this as the biogenic fraction, representing marine bioproductivity.

The fourth cluster is dominated by high ARM and intermediate values in the terrigenous signals. The Fe content is relatively high which is typical for fluvial sediments in this region as well as high Ti indicating aeolian deposits. We therefore recognize this cluster as fluvial input as well as significant contributions from aeolian source.

Of the four clusters identified, three represent primary sediment sources while one identifies sediments severely overprinted by post-depositional processes. The variation of cluster membership through time in the three cores is illustrated in Figure 6c. Aeolian sediments (C1) are deposited during extremely dry conditions corresponding to glacial maxima and Heinrich stadials. Sarnthein et al. (1982) and Thiede et al. (1982) showed that increased aridity and stronger winds during glacials results in an increased deposition of aeolian sediments into the ocean.

Reductive diagenesis (C2) is observed during MIS 5 in GeoB 9506-1 and GeoB 9527-5. According to Berner (1980), the degree of iron mineral diagenesis is determined by the organic matter content and sedimentation rates. Mienert et al. (1988) suggested that warmer climatic conditions lead to increased productivity and deposition of carbonates in the ocean at interglacials. The northern-most core which shows the highest Ca lies in close proximity to the upwelling cells off northwest Africa. The high influx of organic matter thus creates reducing conditions that may lead to the dissolution of magnetic iron phases (Karlin and Levi, 1983; Canfield and Berner, 1987). High Fe content in intervals with very low magnetic susceptibility indicates this dissolution of magnetite. Although there is high Ca in all the cores at the reduced interval, their sedimentation rates differ significantly, with the southern and northern cores having a >40% higher average sedimentation rate than the relatively unaffected central location.

In core GeoB 9516-5 which is largely unaffected by diagenesis, the carbonate (C3) is the dominant source of sediment during interglacial. Detrital input is drastically reduced during humid periods due to increased vegetation cover while influx of biogenic carbonate which could be due dilution effect or enhanced productivity increases. Adkins et al. (2006) demonstrated by normalizing the terrigenous and carbonate fluxes that the terrigenous fraction dilute the carbonate record and is also a good indicator for climate change in this region. However, in the northern-most core, this biogenic signal tends to dominate the last glacial cycle as well, with the exception of Heinrich-like Events (Figure 6c). A possible argument for the trend in the carbonate record where there is a northward increase could as well be attributed to calcite dissolution, which is controlled by calcite lysocline depth (Bickert and Wefer 1996) and $C_{org}/CaCO_3$ rain rate (Martin and Sayles 1996), both of which seem to

be relevant in the region (Funk et al., 2004b). It has been shown that glacial periods were characterized by the northern encroachment of the Antarctic Bottom Water (AABW) as a result of weakening in North Atlantic Bottom Water (NABW) formation (Oppo and Fairbanks, 1987; Duplessy et al., 1988; Sarnthein et al., 1994; Beveridge et al., 1995). However, Curry and Lohmann (1986, 1990) found that the water produced by mixing of the two water masses in the eastern Atlantic was insufficiently corrosive to have had a major impact on the dissolution of carbonate. They concluded that there was no evidence of carbonate dissolution in the Sierra Leone rise sediments from cores recovered above 3750 m water depths, while high dissolution (~50%) only occurred below 4900 m. The deepest of our cores is 3679 m thus we rule out depth related dissolution and influx of corrosive AABW as being responsible for the differences in calcite content. Carbonate concentration is therefore most likely related to the carbonate accumulation rate due to productivity and its northward increase can therefore be associated with the stronger upwelling to the north. Hagen (2001), Adkins et al. (2006) demonstrated that more intense NE trade winds intensify upwelling in this region during glacials when there is greater aridity. This, together with the year round upwelling cells around 20°N, could be responsible for the high productivity at the northern most location.

Cluster 4 represents predominantly terrigenous input and is most strongly evident during the last glacial, dominating cores GeoB 9516-5 and GeoB 9527-5. It is a joint fluvial and aeolian signal for sediments that are deposited under “normal” glacial conditions. In the northern-most core, this signal is suppressed by the dominant productivity signal.

2.4.2 Prominence of millennial-scale climate signals

Heinrich-like Events (Heinrich, 1988) are the most pronounced abrupt millennial-scale climate signals observed in our study area, occurring at between 5-10 ka intervals during the last glacial. Imposed between these are low amplitude rapid millennial-scale climate oscillations that occur at time-scales similar to Dansgaard-Oeschger Cycles. These millennial signals are absent or are of very low amplitude in the two northern-most cores while they are more pronounced in the southern core, with amplitude similar to or greater than at Heinrich-like Events. At the southern-most location where the two types of signals are much visible, the Heinrich signals are most strongly imprinted in the magnetic parameters while the millennial signals are more visible in the elemental records. This discrepancy in the prevalence of Heinrich and Dansgaard-Oeschger related signals can be explained by the relative positioning of the three cores with respect to the position of the ITCZ and hence the

influence of the West African Monsoon. The ratios Ti/Al and Si/Al (Figure 6d) are indicators for continental precipitation and wind strength respectively. High values point to pronounced aeolian contribution whereas low values indicate enhanced continental precipitation. Interestingly, the two northern-most cores only show strong signals at the extremely dry events corresponding to Heinrich stadials, with the Ti/Al being synchronous with Si/Al.

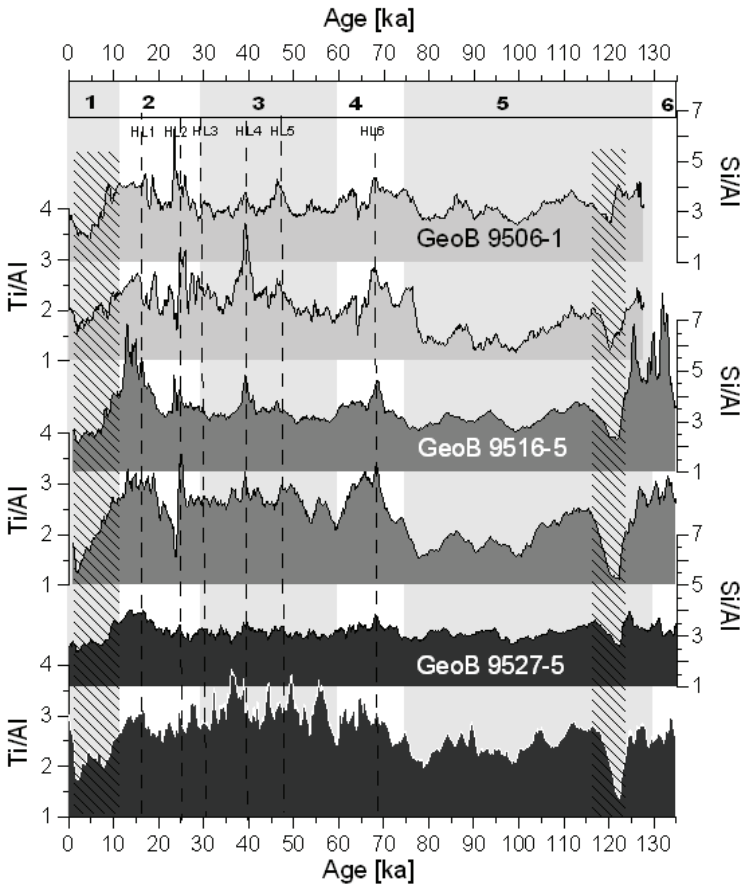

Figure 6d. Aeolian vs. fluvial sediment input into the Senegalese continental margin illustrated by the Ti/Al ratio. Si/Al indicates the wind strength which correlates positively with aeolian input in the two northern most cores but anti-correlates in the southern core (see next figure). Note the periods of the aeolian signature in the two northern-most cores which ranges between 5 and 10 kyr. The southern-most core shows a more frequent oscillation in the climate system (1-3 kyr) synchronous with D-O stadials.

This implies that these sediments were generated and transported by strong NE trade winds. In the southern-most core (GeoB 9527-5), the Ti/Al ratio varies frequently and is synchronous with periods of minima (D-O stadials) in the North Atlantic ice core oxygen isotope records. Ti/Al and Si/Al anti-correlate at this location. The occurrence of imprints of millennial scale climatic signals in our study area is a further testament to the wide impact of these events and the teleconnection of the Earth's climate system. Two hypotheses have been suggested to be

responsible for abrupt climate change: Shutting down of the ocean conveyor belt (Ganopolski and Rahmstorf, 2001; Broecker, 1994, 2000; Broecker, 2003) and interaction of the ocean and atmosphere within the tropics (Cane and Clement, 1999) and are both linked to climate change within our study area.

We believe that climate in our study area is controlled by two factors based on the latitudinal positions of the cores. The first factor has a global imprint and is associated with the Thermohaline Circulation (THC) and related changes in the wind system over North Africa. The shutting down or weakening of the THC due to fresh water input in the north Atlantic resulted in an increase in sea surface temperatures within the tropics and cooling in the north Atlantic.

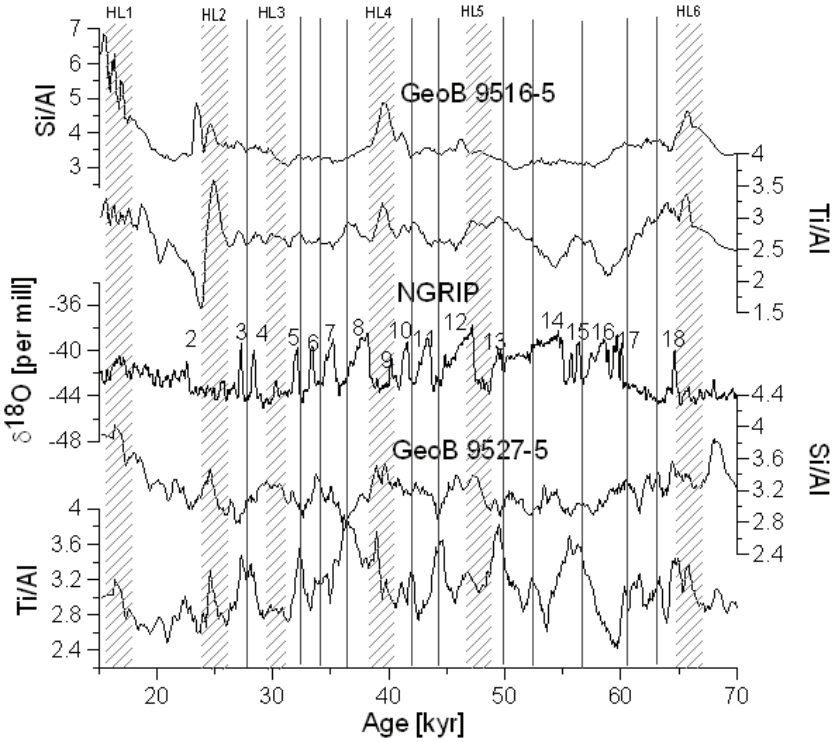

Figure 6e. Millennial-scale oscillations synchronous with D-O stadials of d18O of the North Atlantic Greenland Project (NGRIP), observed in core GeoB 9527-5 (12°26'N) during the last glacial cycle. Climate signals of longer time intervals (Heinrich-Like) are observed in GeoB 9516-5 (13°40'N) Note the anti-correlation between the aeolian signature (Ti/Al) and the wind strength indicator (Si/Al) in GeoB 9527-5 while being positively correlated in GeoB 9516-5.

This discrepancy in temperature reorganized atmospheric circulation over North Africa. The likely scenario is weakening of the SE trades and at the same time, strengthening of the NE trade and Harmattan winds which are responsible for aeolian sediment transport. These changes are recorded at intervals corresponding to N Atlantic Heinrich Events (Figure 6b, d and e) and are strongly imprinted in cores GeoB 9506-1 and GeoB 9516-5. Because of their

latitudinal positions, the two cores can only register significant changes in aeolian input at extremely dry conditions when the wind strengths are higher.

This is consistent with published results from different parts of the world which indicate that Heinrich-like Events are caused by stronger winds (e.g., Arz et al., 1998; Wang et al., 2001; Schulz et al., 1998). Cacho et al. (1999); Bard et al. (2000) and Abreu et al. (2003) showed that the Eastern North Atlantic was marked by colder and drier glacial conditions.

The second factor is related to glacial millennial-scale oscillations of drought and precipitation over North West Africa. The amount of precipitation received over this region is directly controlled by the West African Monsoon. During weak monsoon, the decrease in rain fall results in droughts which are felt further south of the Sahel. Under such a situation, the aeolian derived sediments are deposited further south and their signature is more enhanced. Such events occur more frequently than the Heinrich signals.

Core GeoB 9527-5 (Figure 6e), which is mostly under the influence of the northern summer limit of the ITCZ varies at these sub-millennial time scale and show, with the Ti/Al anti-correlating with Si/Al.

We believe the aridity signals observed in this core location is due to drier conditions in the Sahel region as a consequence of weakening in the summer monsoon.

It records rather the precipitation changes and shows less dependence on the wind strength. These signals are largely synchronous with D-O stadials and consistent with studies by Adegbie et al., (2003) and Weldeab et al. (2007) which document evidence for the variation of West African monsoon at millennial time-scales synchronous with D-O cycles in eastern tropical Atlantic.

Tada et al. (1999), Schulz et al. (1998), Fang et al. (2000) and Rohling et al. (2003) showed that stadials are characterized by dry, dusty and windy conditions, and higher concentration of atmospheric dust. These studies also show that there is a reorganization of the main atmospheric circulation features in the northern Hemisphere, from the pole to the tropics at D-O cycles. The West African monsoon tend to weaken at intervals corresponding to D-O stadials as a result of the weakening of the SE trades and resulting in drier and dusty conditions in the Sahel region.

During insolation maxima when the summer monsoon penetrates further north, there is decrease in the dust input. This evidence is consistent with Larrasoaña et al. (2003) who identified a strong relation between Saharan dust input into the Mediterranean to changes in the West African monsoon.

2.5 Conclusions

We have established a new high resolution timescale for this region that dates to the last 135 ka. Analyses of the various magnetic, geochemical and diffuse reflectance profiles indicate that terrigenous input into the Senegalese continental margin clearly registers the climatic conditions over NW Africa at different timescales. These climatic changes also demonstrate a latitudinal effect that can be attributed to variation in the position of the ITCZ.

Terrigenous input increases significantly during glacial periods. However, even within the glacial, abrupt changes characterized by high coercivity magnetic minerals hematite and goethite which are the typical magnetic minerals for Saharan dust are dominant. These events occurring at 16, 25, 30, 40, 48 and 67 ka are well correlated to the north Atlantic Heinrich Events and we refer to them here as Heinrich-like Events. The grain-size parameter ARM/IRM indicates a coarsening of the grain-size which together with the ratios Ti/Al and Si/Al shows the prevalence of stronger winds at these intervals brought about by the reorganization of the atmospheric circulation which enhanced aeolian transport.

We also observe that the dominant source of sediment varies latitudinally, with a northward increase in the productivity signal (Ca) during glacials due to the proximity to upwelling cells. Carbonate sedimentation is higher at interglacials and the AHP. Aeolian sediments which indicate continental aridity are deposited at glacial maxima and Heinrich-like Events and dominant at the two northern most locations. The southern core is more controlled by fluvial input.

The abrupt change in the climatic signals from Heinrich-like Events at the northern-most locations (13°40'N) to D-O stadials at site GeoB 9527-5 (12°26'N) prompts us to conclude that a climatic boundary existed during the last glacial period between 13°40'N and 12°26'N. Atmospheric reorganization shifted the position of the ITCZ during this period to between 12 and 13°N, creating a wind modulated system north of this boundary. South of this shifted position of the ITCZ was characterized by enhanced precipitation from the West African monsoon as a result of warmer sea surface temperatures. Precipitation changes related to weakening of the monsoon strength were then registered at our southern most location (12°26'N).

The identification of these drought and humid conditions at D-O timescale further south over West Africa stresses the importance to better understand the underlying forcing mechanism responsible in order to fully prepare for future climate changes.

Acknowledgements

We thank Monika Segl for help with stable isotope ($\delta^{18}O$) measurements; captain and crew of RV METEOR cruise M65 who played a vital part in the recovery of the investigated sediment cores. This study was enabled by A.C. Itambi's funding within the Deutsche Forschungsgemeinschaft (DFG) International Graduate Program "Proxies in Earth History". This publication contributes to research projects A8 and C1 of the DFG Research Center Ocean Margins (MARUM) at the University of Bremen, Germany.

3. Sahel mega droughts triggered by glacial slowdowns of Atlantic meridional overturning

Stefan Mulitza, Matthias Prange, Jan-Berend Stuut, Matthias Zabel, Tilo von Dobeneck, Achakie C. Itambi, Jean Nizou, Michael Schulz and Gerold Wefer

MARUM and Department of Geosciences, University of Bremen,
Leobener Strasse, D-28359 Bremen

Abstract

The influence of the large-scale ocean circulation on Sahel rainfall is elusive due to the shortness of the observational record. We reconstructed the history of eolian and fluvial sedimentation on the continental slope off Senegal during the past 57,000 years. Our data show that abrupt onsets of arid conditions in the West African Sahel were linked to cold North Atlantic sea surface temperatures during times of reduced meridional overturning circulation associated with Heinrich Stadials. Climate modelling suggests that this drying is induced by a southward shift of the West African monsoon trough in conjunction with an intensification and southward expansion of the mid-tropospheric African Easterly Jet.

This manuscript is in press in Paleoceanography

3.1 Introduction

Life in the semiarid Sahel belt of tropical North Africa strongly depends on the availability of water and has been frequently affected by shifts to more arid climate, at least since the Pliocene [*deMenocal, 1995*]. The most recent drought occurred in the early 70s and 80s of the last century with partial recovery during the late 90s [e.g., *Nicholson, 2000*]. Historical records suggest that Sahel droughts result from changes in the large scale distribution of sea surface temperature [e.g., *Lamb, 1978; Folland et al., 1986*] which – amongst other factors – is influenced by the heat transport due to the Atlantic meridional overturning circulation (AMOC) [*Newell and Hsiung, 1987*]. The contribution of the AMOC to the long-term variability of Sahel precipitation has not yet been demonstrated. Since the AMOC underwent substantial variations during the late Quaternary [*McManus et al., 2004*], high-resolution sediment records from ocean margin settings offer the opportunity to study the response of continental climate to changes in ocean circulation.

The continental slope off Northern Senegal is an ideal site to study the history of Sahel drought, because it records the varying input of eolian dust and fluvial sediments from the adjacent African continent [*Koopmann, 1981; Sarnthein et al., 1981*] (Figure 1). Dust with particle sizes up to 200µm [*Stuut et al., 2005*] is mobilized in the Sahel and the western Sahara [*Grousset et al., 1998; Jullien et al., 2007*] and transported offshore mainly by continental trade winds and the Saharan Air Layer [*Prospero and Carlson, 1981*]. Recent ship based dust samples collected off Senegal and Mauritania between 13 and 20°N indicate that 44-83% of the dust is deposited at grain sizes larger than 10 µm [*Stuut et al., 2005*]. By contrast, 95% of the terrigenous sediments delivered by the Senegal River have grain sizes below 10 µm [*Gac and Kane, 1986*].

The material transported with the Senegal River also has a very distinct geochemical signature. Compared to the chemical composition of atmospheric dust in the Sahel [*Orange et al., 1993*], suspended sediments in the Senegal River are significantly more aluminous and less siliceous [*Gac and Kane, 1986*]; suspended matter from the Senegal River mouth at St. Louis in the period from August 1981 to November 1982 shows a mean Al/Si ratio of 0.55 (n = 10, s.d. = 0.03) [*Gac and Kane, 1986*] compared to the much lower mean Al/Si ratio of 42 atmospheric dust samples in Dakar of 0.18 from 1984 to 1987 (n = 4 annual means, s.d. = 0.03) [*Orange et al., 1993*].

Sediment input from the Senegal River is highly dependent on the total water discharge and mainly occurs during the rainy summer season [*Kattan et al., 1987*]. Both dust

mobilisation and fluvial input are controlled by the background climate; the most recent multi-decadal Sahel drought has been associated with an increase in dust mobilisation and export over the Atlantic [*Prospero and Lamb, 2003*] and a decrease in Senegal River discharge by more than 50% with respect to the long-term mean [*Kattan et al., 1987*].

Here we present a 57 kyr-long record of terrigenous sedimentation from the continental slope off Senegal, westward of the Senegal River mouth. Variations in the composition of the terrigenous material indicate that Sahel megadroughts occurred during Heinrich Stadials and were associated with cold North Atlantic sea surface temperatures during times of reduced meridional overturning circulation. We study the physics behind the changes in West African hydrology be means of a freshwater-hosing experiment using a fully coupled climate model. Our model results suggest that North Atlantic sea surface temperature and West African rainfall are linked through shifts in the positions of the monsoon trough and the mid-tropospheric African Easterly Jet.

3.2 Material and Methods

3.2.1 Measurements on Core GeoB9508-5

Our 965 cm long gravity core GeoB9508-5 was retrieved from the continental slope off Senegal at about 15°29.90N/17°56.88W from 2384 m water depth (Figure 1). Bulk sediment samples were taken every 2.5 cm downcore, washed over 150 and 63 µm sieves and dried in an oven at 60°C. From the size fraction >250 µm of each sample, 1-10 specimens of *Cibicidoides wuellerstorfi* were picked for isotope analyses. The isotopic composition of the foraminiferal shells was measured using a Finnigan MAT 252 mass spectrometer equipped with an automatic carbonate preparation device. The working standard gas (Burgbrohl CO_2) was calibrated against VPDB by using the NBS 18, 19 and 20 standards. Internal precision, based on replicates of an internal limestone standard, was better than 0.07‰. From the total of 391 measurements, 10 outliers were rejected.

The age model of core GeoB9508-5 is based on 12 radiocarbon ages on mixed samples of planktonic foraminifera picked from the >150 µm fraction. All dates were measured at the Leibniz-Laboratory for Radiometric Dating and Stable Isotope Research in Kiel. Raw ages were corrected for a reservoir age of 400 years; they were then converted to calendar ages using the 'Fairbanks0107' calibration curve [*Fairbanks et al., 2005*] for ages smaller than 40,000 yr (Table 1). 7 additional age points were introduced between the fixed radiocarbon

ages by alignment to the benthic $\delta^{18}O$ record of core MD95-2042 [*Shackleton et al., 2004*] (Figure 2).

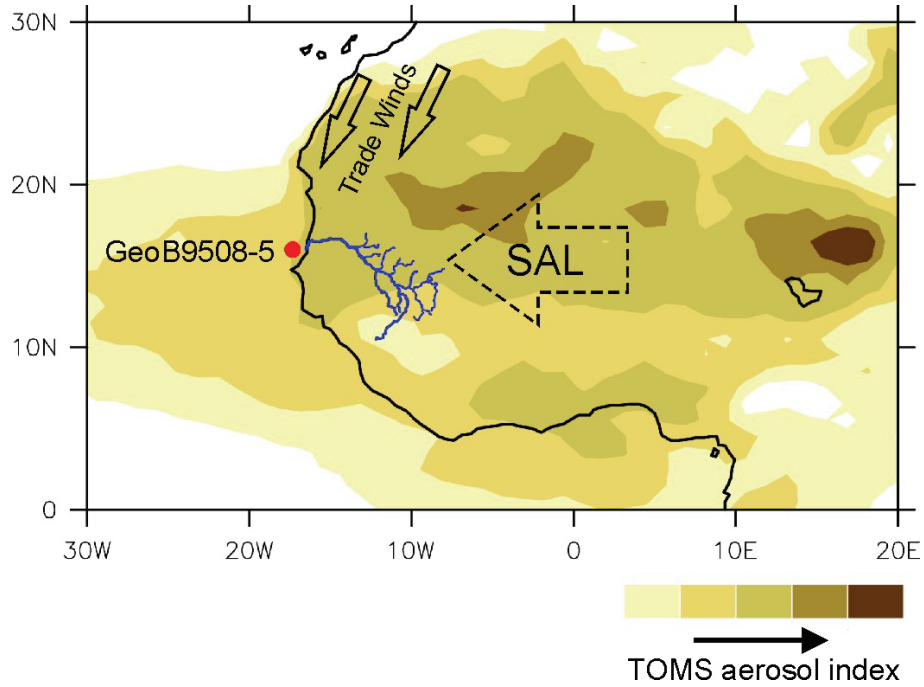

Figure 1. Position of gravity core GeoB9508-5 (red dot) close to the mouth of the Senegal River (blue) and Total Ozone Mapping Spectrometer (TOMS) averaged aerosol concentrations for the years 1997-2005 highlighting the Sahara–Sahel Dust Corridor. Data were obtained from http://toms.gsfc.nasa.gov/. Arrows indicate principal wind directions of trade winds and Saharan Air Layer (SAL).

Samples for grain size analyses were taken every 5 cm downcore. In order to isolate the terrigenous fraction from the deep-marine sediments, several pre-treatment steps were undertaken to remove different biogenic constituents. Organic carbon was removed by adding 10 ml H_2O_2 (35%) to approximately 750 mg of bulk sediment. Reaction was sped up by boiling the mixture. Boiling was continued until reaction stopped and excess H_2O_2 was decomposed into H_2O and O_2. Subsequently, $CaCO_3$ was removed by boiling the sediment sample in 100 ml demineralised water for 1 minute with 10 ml HCl (10%). The sample was diluted with demineralised water until pH=7. Subsequently, biogenic opal was removed by adding 6 gram NaOH to the sample in 100 ml water, and boiled for 10 minutes. The sample was diluted again with demineralised water until pH=7. As a last step before the analysis, the sediment sample in 100 ml was boiled shortly with 300 mg of the dispersing agent $Na_4P_2O_7*10H_2O$. All samples were measured with a Coulter laser particle sizer LS200, resulting in 92 size classes from 0.4 - 2000 µm at a 5cm (~250yr) downcore sampling interval.

Table 1. Radiocarbon dates and age model of core GeoB9508-5. AMS ages were corrected by a reservoir age of 400 years and then converted to calendar ages using the 'Fairbanks0107' calibration curve [*Fairbanks, et al., 2005*]. Ages for the depth intervals in italics were derived by correlation to the benthic $\delta^{18}O$ record of core MD95-2042 [*Shackleton, et al., 2004*].

Sample Code	Core depth (cm)	Species	^{14}C AMS age (-400) (kyrs BP)	Error (yrs)	Calendar Age (kyrs BP)
KIA 31283	3		520	30/30	531
KIA 31282	68		5745	50/50	6533
KIA 33724	98		8830	60/60	9900
KIA 33725	123		10160	80/80	11830
KIA 33726	163		11080	80/80	12940
	172				14600
	236				15800
KIA 31770	308		16250	90/90	19373
KIA 31769	343		19190	120/120	22789
KIA 31768	388		21630	120/120	26021
KIA 31766	483		26410	210/200	31674
	513				33370
KIA 31765	583		31690	350/340	37069
	603				38680
KIA 31764	663		36600	640/590	41785
	753				47470
KIA 31281	778		42940	1660/1370	-
	923				56070

Samples for geochemical measurements were taken at 4 cm intervals. The sediment material was dried at 200°C, powdered and homogenised. Single element concentrations were determined on 4g of dry subsamples by energy-dispersive polarisation X-ray fluorescence (EDP-XRF) spectroscopy using a Spectro Xepos instrument [*Wien et al., 2005*]. The instrument was operated by means of the software Spectro X-Lab Pro, Version 2.4, using the Turboquant method [*Schramm and Heckel, 1998*]. Analytical quality was assessed by repeated analyses of the certified standard reference material MAG-1 [*Govindaraju, 1994*]. The measured values were within 2% of the accepted value for Si, Al, K, Ca, and Fe and within 5% for Ti. The standard deviation of replicates was less than 2%.

3.2.2 Setup of Model Experiments

Numerical experiments were performed with an adjusted version of the 'paleo release' of the NCAR (National Center for Atmospheric Research) Community Climate System Model CCSM2.0.1. The global climate model is composed of four components representing atmosphere, ocean, land, and sea ice. The resolution of the atmospheric component is given by T31 (3.75° by 3.75° transform grid) spectral truncation for 26 layers, while the ocean has a mean resolution of 3.6° by 1.6° with 25 levels. The latitudinal resolution of the oceanic model grid is variable, with finer resolution near the equator (~0.9°). This version of CCSM2.0.1 is referred to as CCSM2/T31x3a [*Prange, 2008*].

A control run was performed in which we adopted the atmospheric composition of 1990 AD and initialized the model with modern observational data sets. An asynchronous integration technique was used to achieve a statistical equilibrium of the climate system within 300 years of model integration [*Prange, 2008*]. This spinup phase was followed by a 200-year long synchronous integration, the second half of which serves for model-data analysis of the control climate in the present study.

The present-day control run was perturbed by a freshwater flux of 0.1 Sv into high northern seas. The surface freshwater forcing was applied to the Labrador Sea, the Nordic Seas, the Arctic Ocean as well as the Hudson and Baffin bays. The continuously perturbed model was integrated (synchronously) for almost 450 years. Averages over the last 100 years of the water-hosing experiment were used for further analysis.

3.3 Results

3.3.1 Downcore variability of benthic $\delta^{18}O$, grain size and Al/Si ratios

The age model of the core indicates an age at the base of the core of about 57 kyrs and mean sedimentation rates of about 17 cm/kyr. Between about 57 and 15 kyrs B.P., the benthic $\delta^{18}O$ record is characterized by a series of events with relatively low benthic $\delta^{18}O$ values (Figure 2). It has been previously shown [*Shackleton et al., 2000*] that these events coincide with warm temperatures over Antarctica, the so called Antarctic Isotope Maxima (AIM) [*EPICA, 2006*] (Fig 3D, E), and are probably due to a combination of ice volume and deep-water temperature changes that occur synchronously with temperature changes over Antarctica.

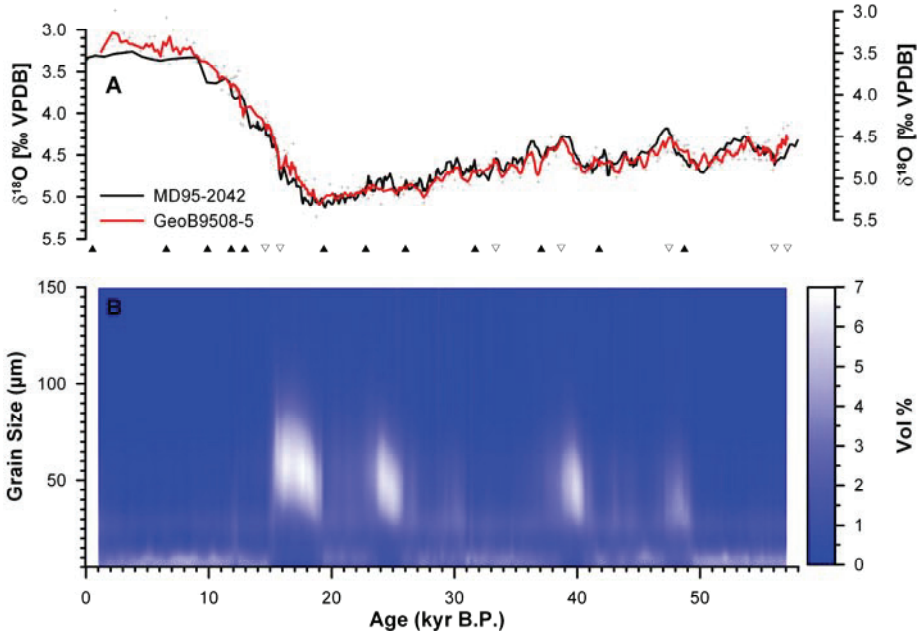

Figure 2. (A) Benthic $\delta^{18}O$ records versus age for the cores GeoB9508-5 (this work) and MD95-2042 (*S2)* and **(B)** grain size distribution in core GeoB9508-5. Filled triangles indicate AMS radiocarbon datings, open triangles indicate age points derived by correlation with the benthic $\delta^{18}O$ record of core MD95-2042.

The Holocene section of this core contains only small amounts of coarse-grained dust (Figure 2) and is characterized by mean Al/Si ratios of about 0.45 (n = 26, s.d. = 0.01, Figures 2B, 3B). This value lies between the present day end member values for atmospheric dust (0.18) and Senegal River suspension (0.55) and suggests that the most recent period of sedimentation on the continental slope off northern Senegal was dominated by both the input

of fluvial material and atmospheric dust. The glacial section of the downcore record of GeoB9508-5 is characterized by a series of abrupt increases in grain size associated with decreases of Al/Si ratios starting at about 49, 41, 31, 26, 19 and 13 kyrs B.P (Figures 2, 3). These events coincide with the most prominent Antarctic Isotope Maxima (AIMs 1, 2, 8, 12) and their Northern Hemisphere counterparts, the Heinrich Stadials 1-5 and the Younger Dryas.

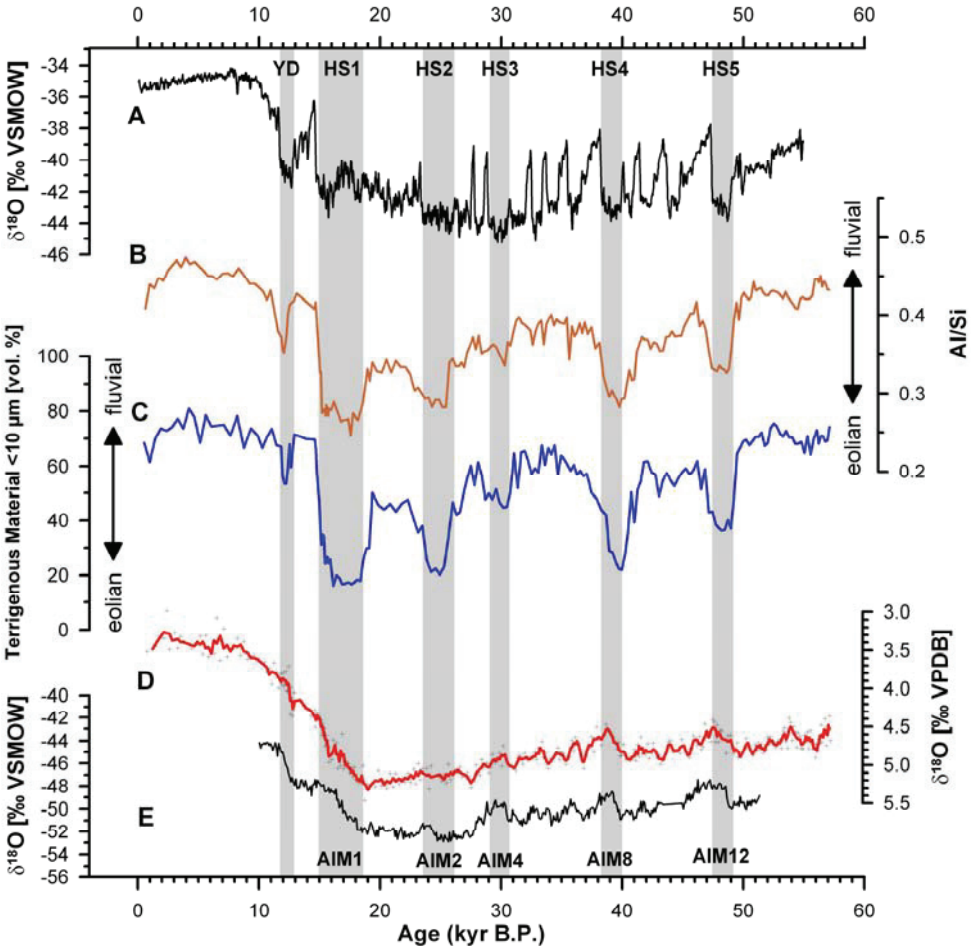

Figure 3. Comparison of sedimentary records of Core GeoB9508-5 with **(A)** ^{18}O of Greenland (NGRIP) and (E) Antarctic (EDML, bottom) ice cores [*EPICA, 2006*]. **(B)** Bulk Al/Si ratios, **(C)** relative abundance of terrigenous sediments with grain size < 10µm and **(D)** oxygen isotope record of benthic foraminifera in core GeoB9508-5. Grey bars indicate the approximate occurrence of Dansgaard-Oeschger Stadials associated with Heinrich Events (i.e., Heinrich Stadials, HS) and the Younger Dryas (YD) in the Northern Hemisphere, and the corresponding Antarctic Isotope Maxima (AIM) in the Southern Hemisphere. Arrows indicate dominant mode of terrigenous sediment transport.

During the Heinrich Stadials both low Al/Si ratios (<0.3) and the low amount of fine material (<20%) are consistent with the deposition of atmospheric dust and indicate a reduced contribution from Senegal River suspension. Generally, the amount of fine material (<10μm) is highly correlated ($R^2 = 0.9$ when interpolated to 500-year intervals) with Al/Si ratios.

3.3.2 Modern atmospheric circulation in CCSM2/T31x3a

CCSM2/T31x3a simulates a robust Atlantic overturning circulation. Approximately 10 Sv of deepwater formed in the North Atlantic are exported to the Southern Ocean. A detailed description of the overall model performance in simulating the global climatology and ocean circulation can be found elsewhere [*Prange, 2008*].

For the present study, the model's skill in simulating the West African monsoon circulation is of paramount importance. Recently, a comprehensive analysis of coupled general circulation models (CGCMs) revealed that many global state-of-the-art models failed to capture the major features of the West African monsoon circulation under modern boundary conditions [*Cook and Vizy, 2006*]. Eight of the 18 examined CGCMs did not even reproduce the summer migration of the tropical rain belt onto the West African continent. Figure 4A shows climatological near-surface winds and precipitation over West Africa for the summer season July–September as derived from reanalysis [*Kalnay et al., 1996*] and observational [*Legates and Willmott, 1990*] data, respectively. Transporting moisture onto the continent across the Guinean coast, the northward low-level monsoon flow penetrates as far north as 20°N, where it converges with dry northerly winds at the monsoon trough. Summer precipitation over West Africa has two distinct regional maxima. One is centered on the west coast between ~5°N and ~12° N; another is near the Cameroon highlands in the eastern Guinea coastal region. Both the wind and precipitation patterns are rather well captured by CCSM2/T31x3a (Figure 4B). Even though the winds over the Sahara are somewhat stronger than in the reanalysis, their flow direction is satisfactorily simulated. Convergence with the southerly monsoon winds takes place at ~20°N. Summer precipitation maxima reside on the African continent. The location of the west coast maximum is fairly well reproduced, albeit the amount of rainfall is underestimated by the model. The Cameroon maximum is also too weak and too far inland.

In winter (January–March) the northerly dry Harmattan winds penetrate as far south as ~10°N in the reanalysis data (Figure 4C). In the Sahel, observed rainfall approaches zero, while the zonal band of maximum rainfall is located over the Gulf of Guinea. Even though the

Harmattan winds are stronger and penetrate farther south in the CCSM2/T31x3a control run, the overall patterns of low-level winds and rainfall are well simulated (Figure 4D).

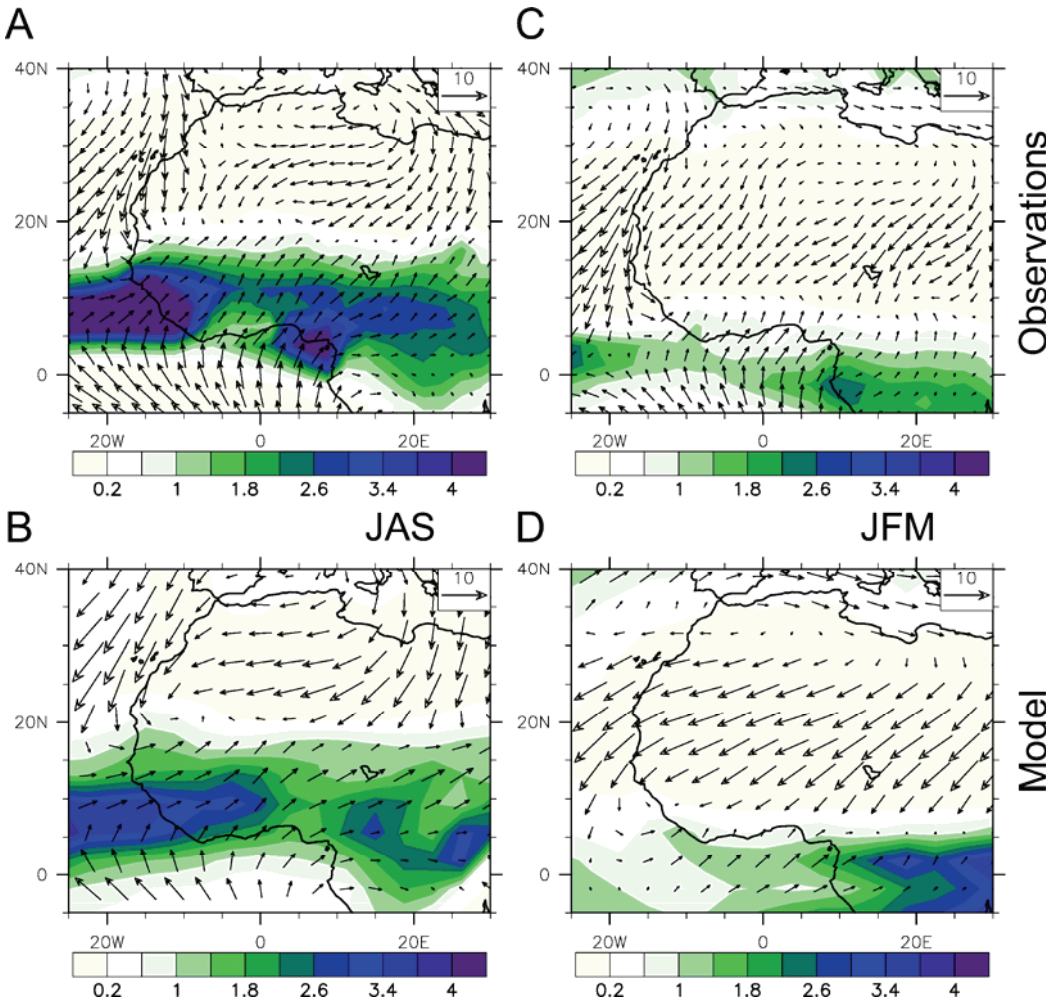

Figure 4. Mean precipitation ($m \cdot yr^{-1}$) and near-surface winds ($m \cdot s^{-1}$) over West Africa for July–September (**A**, **B**) and January–March (**C**, **D**) as calculated from observational/reanalysis data (**A**, **C**) and the CCSM2/T31x3a control run (**B**, **D**). The land data for the precipitation climatology are based on historical rain gauge measurements [*Legates and Willmott, 1990*]. Winds are taken from the NCEP/NCAR reanalysis data set [*Kalnay et al., 1996*] and averaged over the entire reanalysis period (1948–2006). The model results represent averages over the last 100 years of the control run.

The atmospheric circulation at higher tropospheric levels is also well captured by CCSM2/T31x3a. Figure 5 shows a cross section of the mean zonal wind velocity on the Greenwich meridian from reanalysis data and model output for the summer season. The West African monsoon is depicted as a low-level westerly flow. Above the low-level westerlies is the African Easterly Jet (AEJ) with maximum wind speeds between 700 and 500 hPa. The African Easterly Jet is the equatorward portion of the Saharan High, the divergence center that

overlays the near-surface continental thermal low in both the model and the reanalysis data. In the upper troposphere (higher than 300 hPa) the lowermost part of the Tropical Easterly Jet (TEJ) is visible in both the model and reanalysis data.

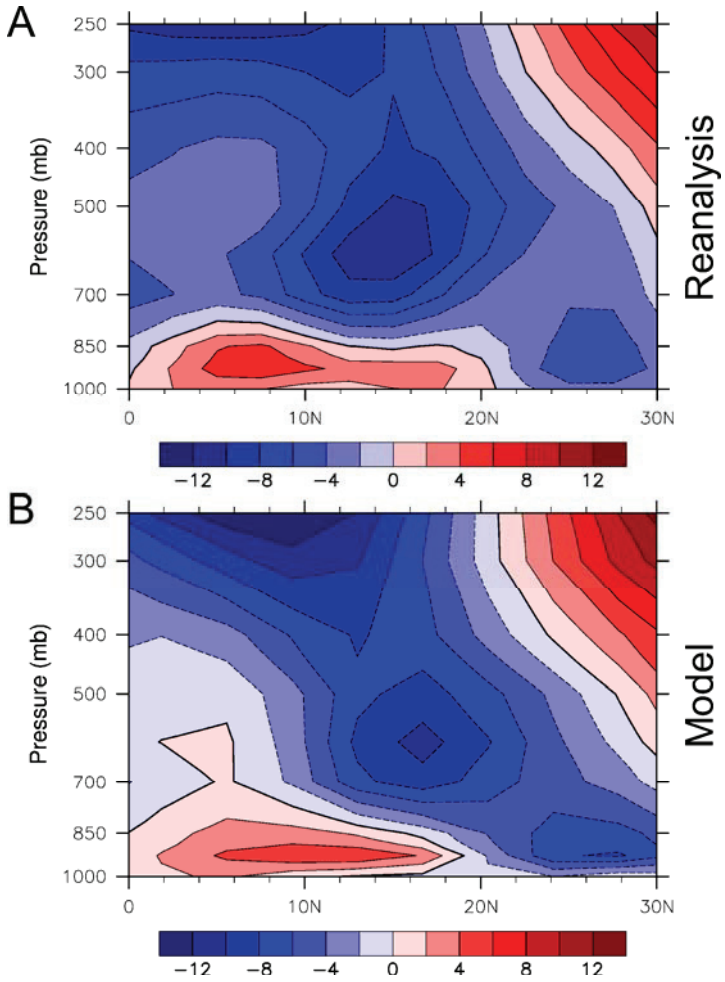

Figure 5. Latitude-height cross sections of July–September mean zonal wind velocity ($m \cdot s^{-1}$) over West Africa along the Greenwich meridian from the NCEP/NCAR reanalysis (**A**) and the CCSM2/T31x3a control run (**B**). NCEP/NCAR winds are averaged over the entire reanalysis period (1948–2006), while the model result represents an average over the last 100 years of the control run. Positive (negative) values indicate westerly (easterly) flow.

Compared to climatological data, summer rainfall is undersimulated south of ~15°N and somewhat too high to the north of it. In CCSM2/T31x3a, 65% of the annual rainfall in the West African Sahel (i.e., west of 10°E in the latitude belt 10°N–20°N) occurs during the summer months July–September, while only 1.5% takes place during January–March. The precipitation climatology [*Legates and Willmott, 1990*] suggests that about 70% (1%) of the annual West African Sahel rainfall occurs during July–September (January–March). In

summary, CCSM2/T31x3a simulates a realistic West African monsoon circulation and captures the major features of the West African precipitation climatology.

3.3.3 Response of the atmospheric circulation to AMOC slowdown

The continuous but small (0.1 Sv = $0.1 \cdot 10^6$ m^3 s^{-1}) freshwater input to the northern North Atlantic and Arctic Oceans induces a gradual decline of the AMOC. Deepwater formation in the North Atlantic slowly decreases and eventually drops below 2 Sv after ~300 years of integration. Summer precipitation and runoff over the West African Sahel parallels the decrease of the AMOC, suggesting an almost linear relationship between overturning strength and Sahel rainfall (Figure 6). The simulated drying is not restricted to the Sahel.

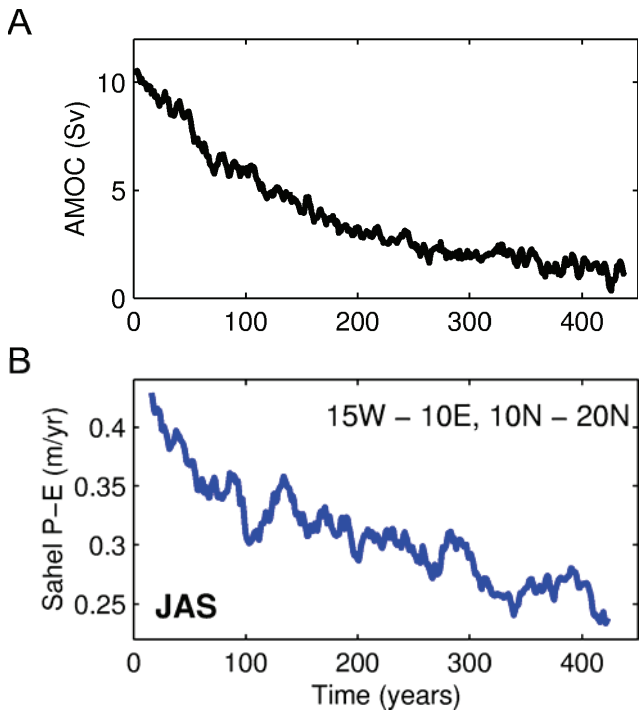

Figure 6. Results from the CGCM water-hosing simulation where the high northern seas are perturbed by a continuous freshwater input of 0.1 Sv. **(A)** Temporal evolution of the Atlantic meridional overturning circulation (AMOC), starting from the equilibrium climate of the control run. Shown is the maximum of the overturning streamfunction north of 40°N smoothed with a 5-year boxcar average. **(B)** Summer, i.e. July/August/September (JAS), net precipitation (total precipitation minus evapotranspiration) averaged over the West African Sahel (15°W–10°E, 10°N–20°N) smoothed with a 30-year boxcar average.

Rather, it affects the entire West African region including the Guinea coast (Figure 7A). The slowing of the AMOC reduces the northward oceanic heat transport and induces surface cooling in the North Atlantic realm which extends far over Europe, the Mediterranean, and

northern North Africa (Figure 8). During summer (July–September), the associated positive sea-level pressure anomaly results in a southward shift of the West African monsoon trough (also referred to as the Intertropical Convergence Zone) by about 3-4° latitude (Figure 7B). As a result, monsoonal rainfall retreats over the northern portion of the West African Sahel.

Reduced evapotranspiration from the drier land surface (a reduction of ~10 W m^{-2} in averaged summer surface latent heat flux over the West African Sahel) and less cloudiness (plus ~15 W m^{-2} of averaged summer net solar flux at the surface) amplify the Sahel surface warming which is initiated by the anomalous southward low-level transport of warm Saharan air (note that reduced latent heat and enhanced shortwave fluxes at the surface are essentially balanced by increased sensible heat and net longwave fluxes). This warming results in a steepening of the meridional surface temperature gradient between the Sahel and the relatively cool Guinean coast. According to the thermal wind balance, the zonal mid-level circulation intensifies at the altitude of the African Easterly Jet (Figures 7C and 9). Near 15°N, where the surface wind anomaly converges (Figure 7B), an anomalous ascent of air occurs below the level of condensation. This upward flow supplies the anomalous easterly mid-level jet with relatively dry air from the north, while over southern West Africa, the accelerated mid-level easterly flow enhances the export of moisture from the continent to the Atlantic Ocean (Figure 7D). The enhanced moisture divergence is associated with a further reduction in rainfall over West Africa.

3.4. Discussion

Today's terrigenous sediments deposited on the continental slope of Senegal mainly stem from atmospheric dust and river input. These transport processes signify two different precipitation regimes: dust input mainly occurs during dry conditions whereas river input occurs when precipitation is high in the drainage basin of the Senegal River. Since our core is located at the boundary between both regimes it reflects the relative proportions of fluviatile and eolian sediments and should be a sensitive recorder of Sahel precipitation.

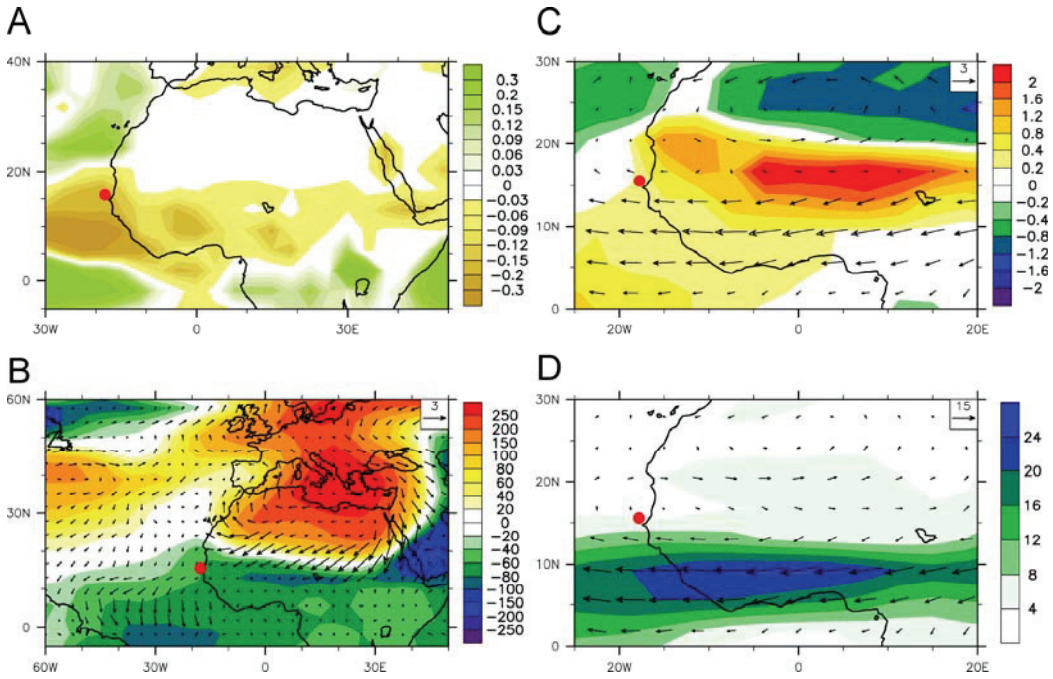

Figure 7. African climate response to a substantial weakening of the AMOC in a CGCM water-hosing experiment. Shown are differences between the climate state with weak AMOC (averages over the last 100 years of the water-hosing experiment) and the state with strong AMOC (100-year averages from the control run; supporting online text). The red dot indicates the position of core GeoB9508-5. **(A)** Annual net precipitation (total precipitation minus evapotranspiration in $m \cdot yr^{-1}$); **(B)** Summer (July/August/September; JAS) sea-level pressure (Pa) and near-surface winds ($m \cdot s^{-1}$); **(C)** Summer (JAS) surface temperature (°C) and winds at 700 hPa ($m \cdot s^{-1}$); **(D)** Summer (JAS) moisture transport at 700 hPa (contours indicate the magnitude of the moisture transport in $g \cdot kg^{-1} \cdot m \cdot s^{-1}$).

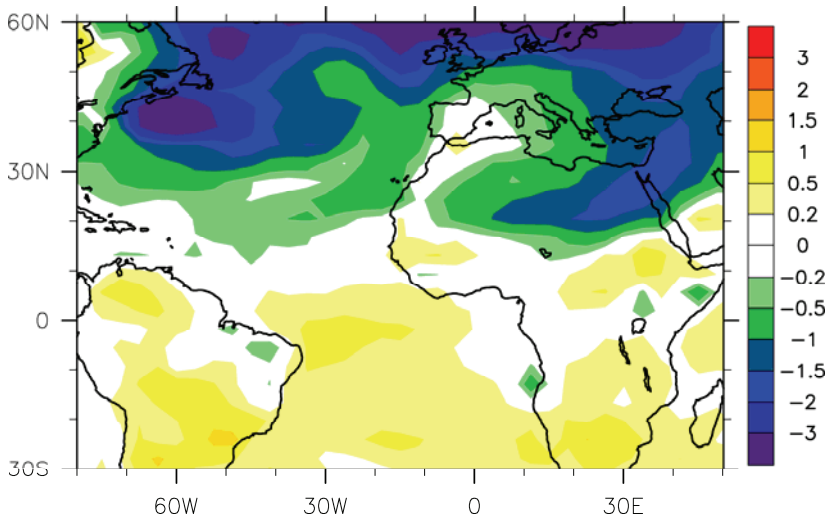

Figure 8. Response of the annual mean surface temperature (°C) to a substantial weakening of the AMOC in the water-hosing experiment. Shown is the difference between the climate state with weak AMOC (average over the last 100 years of the hosing experiment) and the state with strong AMOC (100-year average from the CCSM2/T31x3a control run).

The salient feature in gravity core GeoB9508-1 is a series of abrupt increases in grain size associated with decreased Al/Si ratios. These events must be interpreted as periods with much lower sediment discharge from the Senegal River together with an increase in atmospheric dust input as a consequence of drought. Geomorphological evidence for a much drier climate in much of northern Senegal is given for the most recent multi-millennial period of drought, occurring between about 19 and 15 kyrs B.P at the onset of the last deglaciation. During this time much of Senegal was covered by the so called Ogolian Dunes [*Michel, 1973*]. The presence of these dunes as far south as 14°N suggests a southward shift of the corresponding climate zone by 4-5° and provides additional evidence for aridity in the West African Sahel. Further evidence for aridity in the Sahel, at least during the Younger Dryas, comes from several lake records [*Gasse and Van Campo, 1994; Gasse, 2000*].

Within the accuracy of the age model, the repeated and abrupt initiation of dry Sahel climates occurs synchronously with the coldest sea surface temperatures in the northeastern Atlantic during the past 60 kyrs [*de Abreu et al., 2003*]. These extremely cold sea surface temperatures only occur during Dansgaard-Oeschger Stadials associated with ice rafting (Heinrich) Events in the Northern Hemisphere. The longest drought with an approximate duration of about 4 kyrs occurs at the onset of the last deglaciation together with Heinrich Stadial (HS) 1 in the North Atlantic [*Sarnthein et al., 2000*] and a pronounced warming (AIM 1) of the same duration over Antarctica [*EPICA, 2006*] (Figure 2E). It is generally accepted [*EPICA, 2006*] that the antiphasing of temperatures over Greenland and Antarctica is due to reductions in the AMOC with a decrease of the heat export from the South Atlantic to the North Atlantic and a subsequent cooling of much of the North Atlantic surface. Hence, our data strongly suggest a relation between the strength of the AMOC and sea surface temperature in the North Atlantic on the one hand and Sahel precipitation on the other hand.

Previous studies [e.g., *Street-Perrott and Perrott, 1990; Mulitza and Rühlemann, 2000; Chiang and Koutavas, 2004; Dahl et al., 2005; Itambi et al., 2008*] interpreted drought in the tropics by a southward shift of the Intertropical Convergence Zone (ITCZ). Our experiments indeed suggest a southward shift of the ITCZ (i.e. monsoon trough) during AMOC slowdown by a few degrees latitude over West Africa. It is however problematic to explain the widespread nature of drought exclusively with an ITCZ shift. Today, the ITCZ seems to be effectively independent of the system that produces most of the rainfall. The tropical rainbelt – which is often confused with the ITCZ – is in fact produced by a deep core of ascent lying between the axes of the AEJ and the TEJ, some ten degrees of latitude south of the ITCZ [*Nicholson and Grist, 2003*]. Interestingly, a southward shift of the ITCZ has been rejected as

a cause of the multi-decadal Sahel drought during the second part of the last century [*Citeau et al., 1989*].

Also, a southward shift of the ITCZ as the sole reason for drought would require increased precipitation to the south of the present-day ITCZ. Such a pattern would be in disagreement with late Quaternary paleolimnological records from Lake Bosumtwi (~6°N), Ghana, which indicate dry conditions at the Guinean coast during millennial-scale periods of reduced AMOC [*Peck et al., 2004; Shanahan et al., 2006*]. Likewise, paleoceanographic records off Nigeria (~3°N) [*Weldeab et al. 2007*], Congo (~6°S) [*Schefuß et al., 2005*] and Angola (~12°S) [*Dupont et al., 2008*] do not show indications of increased precipitation during Heinrich Stadials. The simulated drying in our water hosing experiment is not restricted to the Sahel. Rather, it affects the entire West African region including the Guinea coast (Figure 3A) in agreement with the paleoclimatic evidence, but in contrast to the simulation of *Dahl et al.* [*2005*]. For this reason, the proposed mechanism which involves an intensified moisture export by the mid-level African Easterly Jet is a reasonable explanation for the observed precipitation pattern.

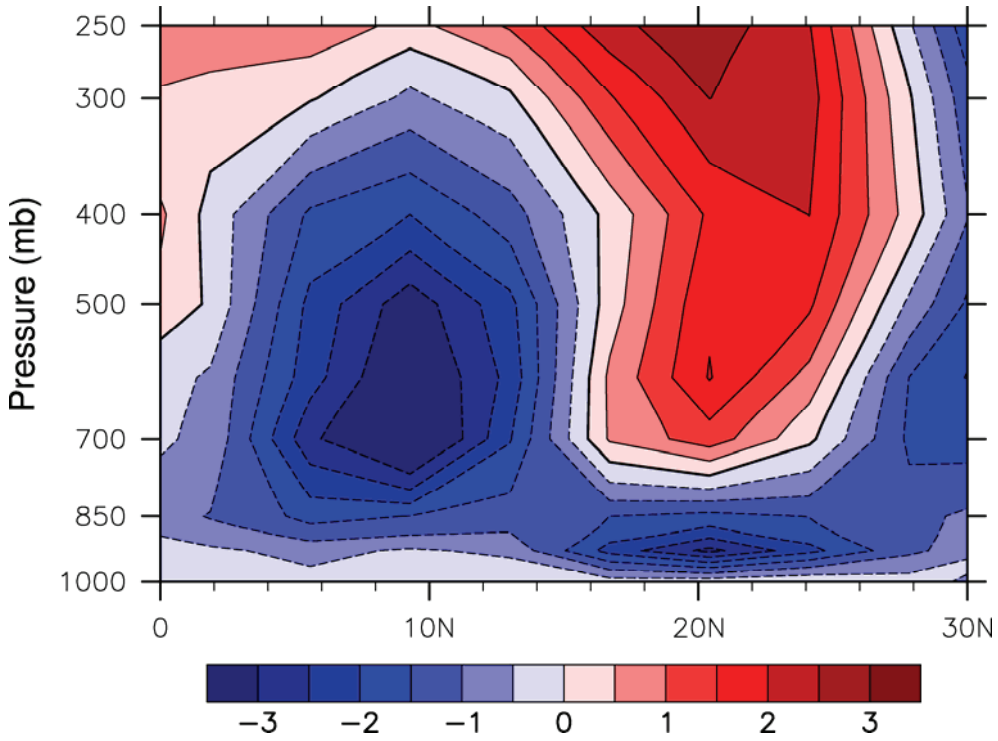

Figure 9. Response of the July–September mean zonal wind velocity ($m \cdot s^{-1}$) to a substantial weakening of the AMOC, plotted as a latitude-height cross section along the Greenwich meridian. Shown is the difference between the climate state with weak AMOC (average over the last 100 years of the water-hosing experiment) and the state with strong AMOC (100-year average from

the CCSM2/T31x3a control run). Positive (negative) values indicate westerly (easterly) wind anomalies.

It must be noted that our model setup includes a comprehensive land surface component with sophisticated soil-vegetation biogeophysics and hydrology [*Bonan et al., 2002; Oleson et al., 2004*], but fixed vegetation. An interactive vegetation cover would likely worsen the simulation of the present monsoon climatology. Prescribing the vegetation provides for a more reliable simulation of the climatology, although potentially important feedbacks are excluded in the water-hosing experiment. Even though vegetation-climate feedbacks could conceivably act to amplify the response of Sahel precipitation to a remotely forced perturbation [*Charney, 1975; Zeng et al., 1999*], there is no obvious reason why the basic dynamical mechanisms of Sahel drying deduced from our CGCM water-hosing experiment should be affected fundamentally by vegetation dynamics [*cf. Hales et al., 2006*]. We also note that the assumption of a strong positive vegetation-precipitation feedback over northern Africa has recently been challenged [*Levis et al., 2004; Liu et al., 2007; Liu et al., 2006; Wang et al., 2008*]. Essentially, the same holds for dust radiative feedbacks [*Yoshioka et al., 2007*]. Excluding vegetation and dust feedbacks, our approach can be considered as a 'maximum simplicity model' to simulate a physically consistent mechanism of Sahel drying in response to a weakening of the AMOC.

In the present study, no attempts have been made to simulate and perturb a glacial climate state. Simulations of glacial West African climate can hardly be validated. Moreover, it has recently been shown that the simulation of glacial African rainfall is mostly model dependent [*Braconnot et al., 2007*]. Within the framework of the Paleoclimate Modeling Intercomparison Project PMIP-2, simulations of the Last Glacial Maximum with five different CGCMs yielded summer Sahelian rainfall anomalies ranging between –42% and +16% depending on the model. We therefore suspect that trustworthy simulations of the glacial West African monsoon dynamics are currently not available. We suppose, however, that the basic dynamical mechanisms of Sahel drying in response to a slackening of the AMOC, as found in our CGCM water-hosing experiment, are largely independent of the climatic background state. This is consistent with the GeoB9508-5 proxy records which suggest similar responses of Sahel rainfall to AMOC perturbations for all Heinrich events (Figure 3) despite varying boundary conditions (i.e. ice-sheet distribution, orbital parameters and atmospheric composition) in the course of Marine Isotope Stages 2 and 3.

3.5 Conclusions

Our study suggests a close relation between AMOC, North Atlantic sea surface temperature and Sahel precipitation. Predictions of the future rainfall in the Sahel are highly uncertain and range from wetter conditions to much drier conditions [*Douville et al., 2006; Solomon et al., 2007*]. However, climate projections show that the thermohaline overturning will probably slow down in response to anthropogenic-induced warming [*Solomon et al., 2007*]. From the results of this study, it seems likely that the future of precipitation in the Sahel will strongly depend on the behaviour of the AMOC and its influence on the spatial structure of global warming.

Acknowledgements Thanks to Monika Segl and her team for help with isotope analyses. AMS ^{14}C datings were done by the staff of the Leibniz-Laboratory for Radiometric Dating and Stable Isotope Research in Kiel. The climate model experiments were performed on the IBM pSeries 690 Supercomputer of the Norddeutscher Verbund für Hoch- und Höchstleistungsrechnen (HLRN). This work was supported by the Deutsche Forschungsgemeinschaft through MARUM at Bremen University.

4. Magnetic mineral inventory of equatorial Atlantic Ocean marine sediments off Senegal – glacial and interglacial contrast

Itambi A.C. [1], von Dobeneck T. [1, 2], Dekkers M.J. [3], Heslop D. [1, 2] and Frederichs T. [1]

1) Geosciences Department, University of Bremen, Klagenfurter Strasse, D-28359 Bremen, Germany
2) Research Center Ocean Margins, University of Bremen, Leobener Strasse, D-28359 Bremen, Germany
3) Paleomagnetic Laboratory Fort Hoofddijk, Utrecht University, Budapestlaan 17, 3584 *CD Utrecht, The Netherlands*

Abstract

Variations in climate regulate the concentration, grain size and mineralogy of magnetic particles in sediments. In some regions, other non climate related factors such as volcanic and cosmic sources may significantly contribute to the signals. In addition, post-depositional diagenesis and biomineralization may mask or destroy the primary magnetic signals. In complex sedimentary environments with many potential sources, it is therefore vital that all factors contributing to, and affecting the magnetic signals be well understood. This will enable a better constrained interpretation of paleomagnetic and climate results. Rock magnetic methods and electron microscopy provide suitable means to characterize magnetic assemblages on Senegal continental margin. Iron oxides, iron titanium oxides and iron sulphides are the dominant phases deposited in this region. Glacial samples show magnetic mineral enrichment comprising of larger grain size (1-30 μm) as well as superparamagnetic particles. The bulk of the materials are primary minerals of detrital origin that have undergone little in situ alteration. Magnetic spherules of volcanic origin and iron oxides of secondary origin were identified but these minerals have little impact on the primary signals because of their low concentrations. In contrast, the interglacial samples appeared to have been severely affected by diagenesis, with pyrite (framboidal and euhedral) making up over 50 % of the iron phases. Grain size of the primary minerals ranges between 1 and 10 μm. Pyrite formation tend to be climate related, possibly by diagensis resulting from bio-productivity during warmer periods.

This manuscript will be submitted to the Geophysical Journal International

4.1 Introduction

Rock magnetic properties of marine and lake sediments have been widely used in climate reconstruction since the discovery of the correlation of the magnetic susceptibility of sediments to past climate change (Thompson et al., 1975). The analysis has grown into the field of environmental magnetism (Thompson and Oldfield, 1986; Evans and Heller, 2003). At present many magnetic parameters other than susceptibility and their ratios are incorporated to delineate subtle variation in the magnetic mineralogy that can be interpreted in terms of paleoenvironment and paleoclimate. These parameters include remanent magnetization based mineral magnetic parameters such as anhysteretic and isothermal remanent magnetizations (ARM and IRM respectively) and their acquisition curves, as well as measurements as function of temperature below and above room temperature which show magnetic transitions that are mineral specific. Magnetic grain size can be analyzed by means of hysteresis loop parameters, and through determination of so called first order reversal curve (FORC) diagrams that enable an estimate of the magnetic interaction as well. These diagnostic parameters are capable of characterizing magnetic particles by their concentrations, grain-sizes and mineralogy. Examples of useful recent reviews, data compilations and textbooks of environmental magnetic parameters are Verosub and Roberts (1995), Dekkers (1997), Frederichs et al. (1999), Maher and Thompson (1999), Evans and Heller (2003), Peters and Dekkers (2003), and Dekkers (2007).

The suitability of these parameters for paleoenvironmental and paleoclimate reconstruction is due to: 1) all Earth's materials possess some form of magnetism, with magnetite magnetically being the most prominent magnetic mineral. 2) The formation of some widely distributed iron oxide minerals is climatically driven e.g., hematite is produced under arid conditions and transported to the ocean by an eolian pathway whereas goethite is formed under more humid conditions and transported more via riverine systems (Schwertmann, 1985, 1988; Cornell and Schwertmann, 1996).

Marine sedimentary environments are often complex because of the variable potential sources of magnetic minerals. Presumably climatically regulated sources not only include detrital minerals that reflect weathering and erosion on land, but also post-depositional processes like diagenesis, authigenesis and biomineralization are in a sense climatically driven via the amount of organic matter (Karlin & Levi, 1985; von Dobeneck et al., 1987; Suk et al., 1990). Volcanic material (Freeman, 1986) and cosmic particles (Brownlow, 1966; Brownlee, 1981) are other potential sources of magnetic minerals which may contribute

significantly to, and in some cases be, the dominant carriers of the magnetic signature in the sediments. Therefore, the interpretation of rock and paleomagnetic results is not always straightforward. Possible ambiguity is reduced by extensive mineral magnetic research at high fields and at low and high temperature and by utilizing (electron) microscopy to visualize the magnetic particles that are responsible for the measured magnetic properties. The present study involves this type of analysis on a core off-coast Senegal (figure 1).

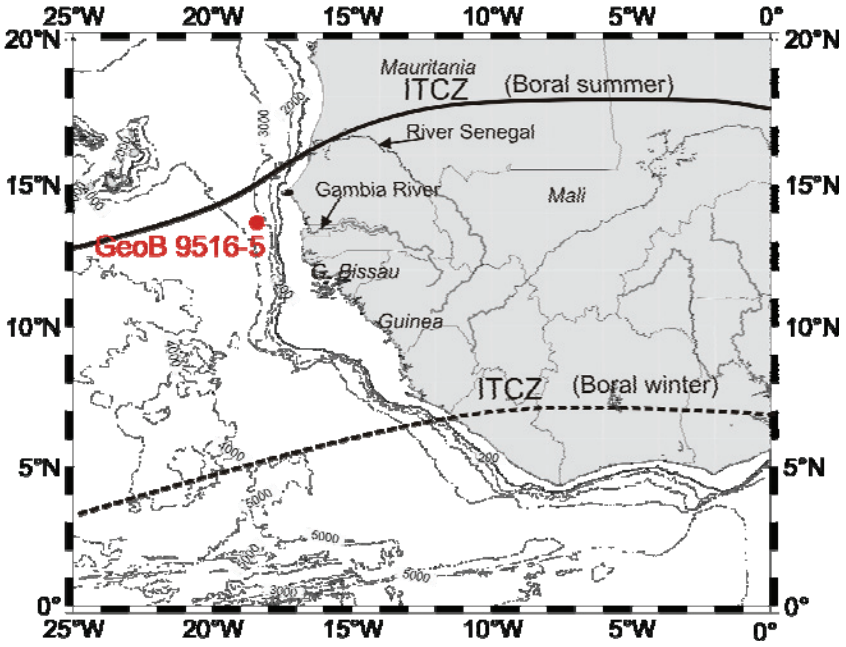

Fig. 1. Location of core GeoB 9516-5 off Senegal. The solid line indicate the present day summer northern limit of the tropical rain belt (ITCZ) while the dash lines show the winter position.

The Senegal continental margin is situated at the northern summer limit of the Intertropical Convergence Zone, i.e. the boundary between humid and arid North Africa. It receives detrital sediments via fluvial (Gac and Kane, 1986a & b) and aeolian pathways (Balsam et al., 1995; Bloemendal et al., 1988). Odin (1975) documented the precipitation of specific iron phase goethite, in the so called green marine clays, close to the Senegal River mouth. The northwest African margin is also characterized by high marine productivity and average sedimentation rates of ~ 8 cm/kyr (for three cores including the one studied in this paper, Itambi et al. (2008)). This may create microphylic conditions suitable for reductive diagenesis and biomineralization. A magnetically complex sedimentary environment may well be the overall result.

Bloemendal et al. (1988) were amongst the first to show climate driven variations in magnetic mineral fluxes in this region. They documented that glacials were marked by a higher concentration of magnetic minerals, mostly dominated by single domain (SD) and pseudo-single-domain (PSD) magnetite as well as a significant proportion of hematite and goethite whereas the warmer interglacials were characterized by enhanced input of superparamagnetic (SP) magnetite. This conflict with our recent findings (Itambi et al., 2008) which tend to identify a very high concentration of SP particles (frequency dependence of susceptibility > 12%) during extreme glacial events (Heinrich-like events) and a SD magnetite dominated interglacial. The SP particles correlate to the "hard" isothermal remanent magnetization (HIRM) and low-field susceptibility. Moreover intervals identified from diffuse reflectance spectrophotometry as enriched in hematite and goethite have a larger amount of SP particles. This prompted Itambi et al. (2008) to suggest the presence of ultra fine grained hematite and goethite as coatings on quartz grains.

It is therefore imperative that studies be carried out in this seemingly complex sedimentary environment with several potential sources for the magnetic mineral assemblage, in order to identify the magnetic mineral phases, distinguish the contribution that each mineral and grain-size class may make to the magnetic properties, for a better constrained interpretation of paleomagnetic, environmental and climatic results. To achieve this, we perform several more advanced rock magnetic measurements capable of distinguishing between magnetic mineral phases. These include determination of the remanence behaviour at low temperature, acquisition of thermomagnetic data with a Curie balance, and determination of FORC diagrams and IRM acquisition curves. Since no single technique is able to fully characterize the sediment, we also applied scanning electron microscopy in addition to the mineral magnetic analysis. The results show a magnetic mineral assemblage consisting of the full range of detrital, authigenic, diagenetic and possible cosmic provenance. Pyrite which indicates a reducing anoxic environment was abundant. Some re-oxidized particles of secondary origin were also detected.

4.2 Materials and methods

During the research cruise M61 (Mulitza et al., 2006) over northwest Africa, sediment cores showing an alternating sequence of reddish brown and dark green layers were recovered. Itambi et al. (in revision) analysed the climate records of some of these cores, i.e. GeoB 9506-1; GeoB 9516-5 and GeoB 9527-5 (Fig. 1) and reported magnetic signals that follow glacial and interglacial patterns synchronous with the color changes. The glacial

intervals were reddish brown and demonstrated a higher concentration of magnetic minerals, as was reflected in the magnetic susceptibility ($150 \leq \kappa \leq 800 \times 10^{-6}$ SI), and SIRM. On the other hand the interglacial were dark green, with lower concentration of magnetic minerals ($100 \leq \kappa \leq 150 \times 10^{-6}$ SI). The SIRM was equally lower. For this reason, several samples were selected from these two lithological units from core GeoB 9516-5 and studied here in more detail. Since the samples tend to be representative of the two climatic periods, we focus our analysis and discussion in this paper on two samples, one from each lithology. The glacial sample was recovered at 85 cm core depth while the interglacial sample was taken at 836 cm depth.

4.2.1 Magnetic and heavy liquid extraction

The magnetic minerals were extracted for Scanning electron microscopy (SEM) and magnetic properties measuring system (MPMS) analysis. Two extraction methods were used, magnetic extraction described by Petersen et al. (1986) and von Dobeneck et al. (1987), and heavy liquid separation (HLS) proposed by Franke et al. (2007a). As demonstrated by Franke et al. (2007a), magnetic extraction has the potential to extract larger quantities of magnetic minerals but tends to be biased with respect to the coarser particles. HLS also includes non-magnetic phases such as iron sulphides since the separation is dependent on the density of the particles. To enhance the concentration of magnetic minerals from the HLS, a portion of the extract was dispersed again with demineralised water in a small glass vial and a “magnetic finger” (cf. Petersen et al. (1986)) was used to attract the magnetic component. After separation, the separates were stored in glass vials filled with ethanol until further processing (usually between 2 and 4 days).

4.2.2 Magnetic measurements at room temperature

These meausrements involved determination of acquisition curves of the isothermal remanent magnetization (IRM) in fields up to 7 Tesla and determination of first order reversal curves (FORCs) (Pike et al., 1999, Roberts et al., 2000). The IRM was measured using the Quantum Design Magnetic Properties Measuring System (MPMS-2) SQUID magnetometer at the marine geophysics department of the University of Bremen (Germany). IRM acquisition curves were processed with the software described by Kruiver et al. (2001) that is based on fitting of lognormal coercivity distributions. FORC diagrams were acquired with an Alternating Gradient Magnetometer Model 2900 (MicroMag, Princeton USA), to determine the domain-state of the particles. Bulk sediments of about 25 mg were put into a 0.5 mm

straw, sealed with non magnetic glue and were mounted on a P1 parallel silica probe for measurements. A total of 200 FORCs were measured per sample at a field increment of 0.984 mT; the saturation field was 2 Tesla. The averaging time was 0.1s.

Since both samples demonstrated low coercivities, a maximum field of 120 mT was used. The data was processed using Harrison-Feinberg algorithm - FORCINEL (Harrison and Feinberg, 2008.

4.2.3 Magnetic measurements below and above room temperature

Low temperature remanence was performed on bulk samples as well as separates using the MPMS. The samples were weighted (20-35 mg) and then put into a gelatine capsule which was inserted and firmly held in a straw. The samples were cooled in the absence of a field (zero-field-cooled, ZFC) to 5 K where an isothermal remanent magnetization was imparted at a field of 7 T. The remanent magnetization was measured during zero field warming from 5 K to room temperature (300 K) at 2 K increments. The samples were again cooled but this time in an applied field of 7 T (field-cooled, FC) which was switched off at 5 K before warming to 300 K.

Further an (S)IRM was cycled by cooling through 300-5 K and then gradually warmed back through the same temperature range. The remanence was continually measured at ~ 2 K intervals during the entire cycling. The susceptibility measurements were performed before the ZFC at four frequencies (1, 10, 100 and 1000 Hz), and warming through a temperature range 5 to 300 K and a field or 0.04 mT.

High temperature heating and cooling curves were measured on a modified horizontal translation Curie balance at the paleomagnetic laboratory ‘Fort Hoofddijk’, Utrecht University (The Netherlands) (Mullender et al., 1993). Samples were heated in air in a cycling field between 150 and 300 mT to a maximum temperature of 700 °C and at a heating rate of 10 °C/min. After heating at 700 °C, the sample was cooled back to room temperature at a rate of -10 °C/min. In order to investigate chemical alteration, we employed the incremental heating and cooling segment protocol. This involved heating the samples to a certain temperature, cooling it down to a chosen value (typically 80-100°C lower), and then heating and cooling repeatedly to increasingly higher temperatures until the maximum temperature of 700 °C is attained. The temperature segments used are stated in the caption of figure 6.

4.2.4 Scanning Electron Microscopy

Portions of the HLS concentrate (up to ~ 15 mg) were allowed to dry in air and the samples were spread on a carbon sticker. This was sputtered with carbon for SEM and accompanying Energy Dispersive EDS X-ray spectroscopy analysis. The SEM instrument used is the SUPRA^{TM} 40 high resolution FESEM based on the 3rd generation GEMINI column by Carl Zeiss SMT. Secondary electron (SE) imaging was used at energy levels between 5 and 15 kV. For elemental composition, the EDS attached to the instrument was used and the applied energy for this analysis was 15 kV. The elemental spectra were normalized by their oxygen.

4.3 Results

4.3.1 Rock magnetic results

4.3.1.1 IRM acquisition at room temperature:

IRM acquisition was done on bulk material. The glacial sample (Fig. 2a) acquires about 65 % of its remanence at 200 mT and continues to acquire IRM at 7 T. The interglacial sample (Fig. 2b) shows that up to 90 % of its 7 Tesla IRM has been acquired at 200 mT yet IRM acquisition continues at 7 T. In order to assess the mineral phases contributing to the IRM, IRM component analysis (Kruiver et al., 2001) was done (Fig. 2 and Table 1). A total of three components were identified for the glacial sample (Fig. 2a, c and e). Component 1 with a remanent acquisition coercive force ($B_{1/2}$) of ~40 mT and a dispersion parameter (DP) of 0.35 log mT shows the highest contribution to the IRM, with an SIRM of 3.6 x 10^{-2} Am^2/kg (Table 1). This soft component is interpreted as magnetite. In the second component, the $B_{1/2}$ is ~400 mT, indicating hematite. This component has the smallest contribution to the acquisition curve, with an SIRM of 1.5 x 10^{-2} Am^2/kg. For the third component the $B_{1/2}$ is very high (~11.5 Tesla), a strong indication that it is goethite. This component contributes up to 42.4 % of the remanence. Since the IRM was only acquired up to a 7 T field, the high $B_{1/2}$ for component three is an extrapolation based on the log-Gaussian curve shape forced to each component.

The interglacial sample yielded 4 components (Fig. 2b, d and f) with marked differences to the glacial sample. Component one which contributes 73.1 % to the remanence and is

interpreted as magnetite, has a harder coercivity ($B_{1/2}$ ~49 mT) and a narrower DP (0.29) compared to the same component in the glacial sample. The harder magnetite could be indicative of low temperature oxidation (partial maghemitization; e.g. Petersen and Vali, 1987; Van Velzen and Dekkers, 1999).

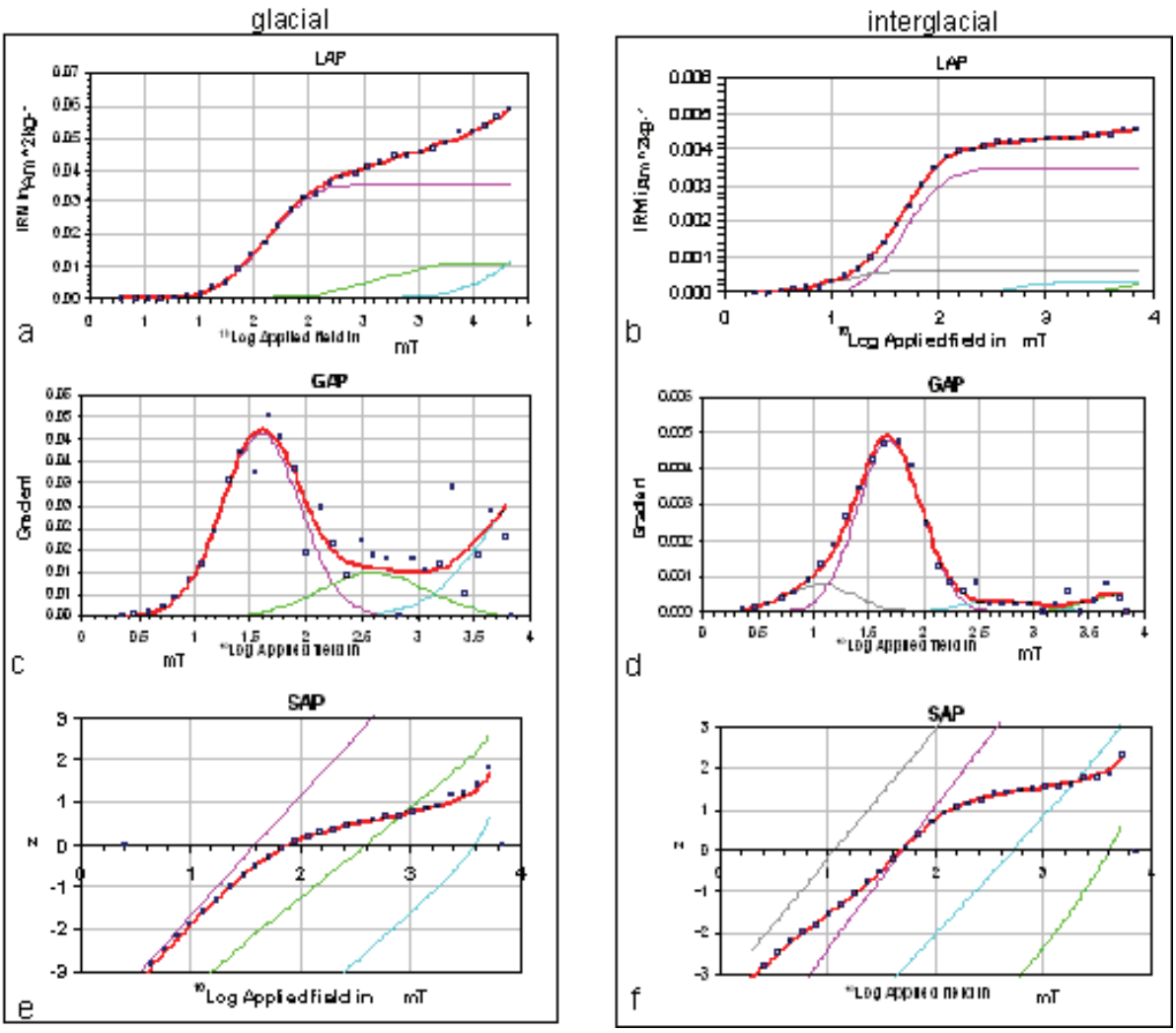

Fig. 2. IRM acquisition curves with the result of component analysis. LAP = linear acquisition plots, GAP = gradient acquisition plots and SAP is the standardized acquisition plot. Dots are data points while the red line show best fit. In the glacial sample, the colours purple, green and blue represent magnetite, hematite and goethite respectively. In the interglacial sample, the same colour represent magnetite, goethite and hematite respectively while the grey line shows "soft" magnetite. Contribution of hematite and goethite is stronger at glacial intervals, reflecting influx of aeolian dust while magnetite dominates the interglacial.

The second component is interpreted as hematite, with a $B_{1/2}$ ~500 mT and a DP of 0.35 mT and contributes 5.9 %. Component 3 which has a $B_{1/2}$ representative of goethite (~6.3 T) and DP of 0.32 is the second dominant component with an 8.4 % contribution to the remanence.

Component 4 is a very soft component with a $B_{1/2}$ of 11.5 and DP of 0.32. This component is a consequence of the symmetric base function that is mandatory. Small grains show skew-to-the-left distribution (Heslop et al., 2004; Egli, 2004) which cannot be fitted, proper fitting requires a second distribution, which has no physical meaning. As often, magnetite is the dominant contributor in all samples, but its dominance is much greater in the interglacial sample where it contributes about 2/3 of the SIRM. High coercivity minerals hematite and goethite make up a more significant proportion of the glacial sample. In general, the glacial sediments are more strongly enriched in magnetic minerals than the interglacial.

4.3.1.2 FORC measurements

FORC distributions for the two climatic periods show distinct features (Fig. 3). Glacial sediments are characterized by two maxima in the FORC density (Fig. 3a) while the interglacial sample shows only one. The central contours around the most prominent density maximum centered at Bc, Bu of ~12, 0 mT (glacial) and ~26, 0 mT (interglacial) are mostly closed which complies with single domain magnetite. Both samples also show very little contour spreading on the Bu axis indicating that magnetic interaction is not important (Pike et al., 1999; Roberts et al., 2000).

Table 1, Results of the IRM component analysis

Glacial				
Component	SIRM (Am2/kg)	Log (B1/2)	B1/2 mT	DP mT
1	0.036	1.6	39.8	0.35
2	0.0115	2.6	398	0.47
3	0.035	4.06	1118	0.50

Interglacial				
Component	SIRM (Am2/kg)	Log (B1/2)	B1/2 mT	DP mT
1	3.47×10^{-3}	1.69	49	0.29
2	4.0×10^{-4}	3.8	6309	0.32
3	2.8×10^{-4}	2.7	501	0.35
4	6.0×10^{-4}	1.06	11	0.32

In the glacial sample the FORC diagram is characterized by diverging contours indicative of fine particles. The second, very low field density maximum is centered on Bu and Bc = 0. This has been described by Roberts et al. (2000) as being distinctive of particles which lose their coercivity i.e., superparamagnetic particles (Pike et al., 2001). The identification of SP particles in these samples further confirms the work of Itambi et al. (in revision) where values of up to 16 % were measured for the frequency dependence of susceptibility at extreme glacial events and < 4 % at interglacial periods.

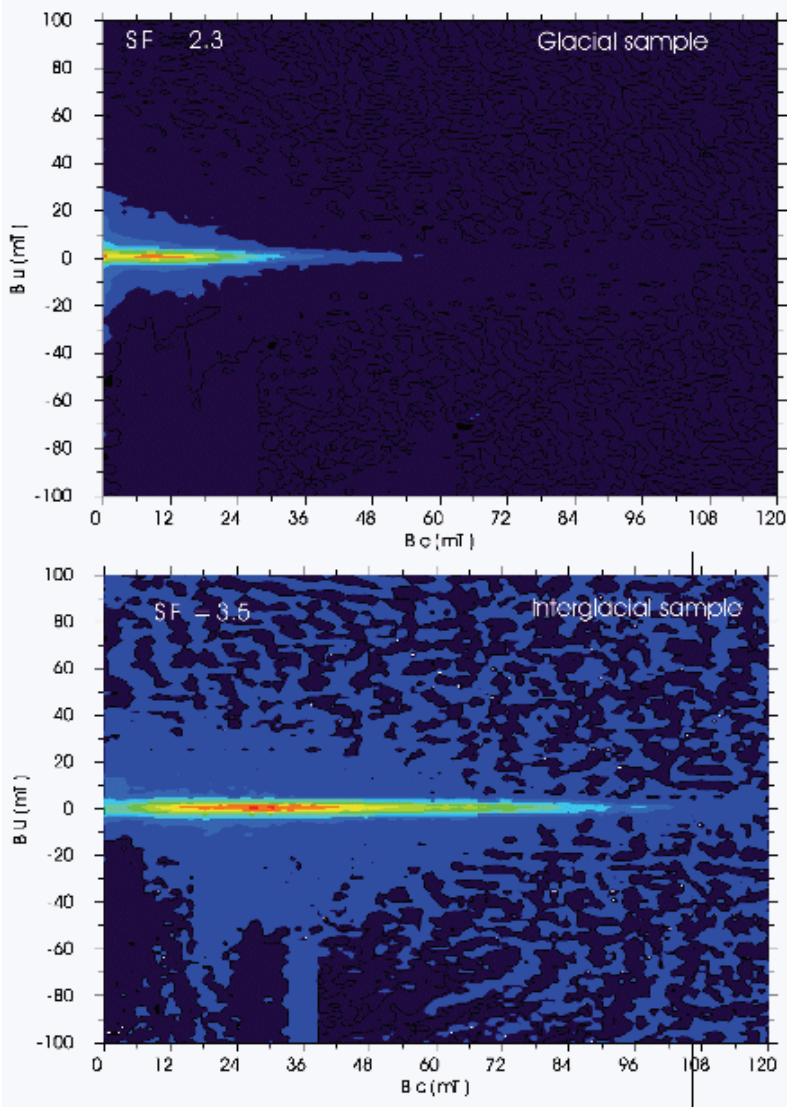

Fig. 3. FORC diagrams illustrating the main magnetic behaviour. Two regions of maximum FORC density are observed in the glacial sediment at Bc = 0, and Bc = 12 mT. The peak at Bc and Bu = 0 indicate presence of SP particles. The interglacial samples show maximum density at 26 mT. The absence of hematite and goethite features may be related to the maximum field of 2 T used. The distributions in both samples are centered at Bu= 0, with no vertical spreading. This implies that magnetic interaction is not important.

In the interglacial samples, the FORC distributions display maxima at about 26 mT which are centered at Bu = 0 (Fig. 3b) with elongated contours that go up to high coercivities close to 90 mT. Despite the identification of hematite and goethite in the IRM component analysis, their diagnostic characteristics are absent in the FORC diagrams. The lack of visualization can be attributed to the maximum field of 2 Tesla in which the FORCs were generated.

4.3.1.3 Low temperature results

Zero-field-cooled and field-cooled warming curves: On warming the remanence of both samples shows a drastic drop between 5 and 25 K, with ~50 % of the remanence lost at 25 K (Fig. 4a & b). The remanence decay is stronger in the glacial sample, with over half of the remanence lost before 30 K while in the interglacial sample, only about one third is lost. Several reasons have been put forward as an explanation. It may be attributed to the presence of an ultrafine-grained superparamagnetic phase which has very low unblocking temperatures. Equally, paramagnetic iron bearing minerals that become magnetically ordered at low temperatures have also been related to the rapid drop at this low temperature (Coey, 1988; France and Oldfield, 2000). Further the presence of the magnetic iron sulphide pyrrhotite, which shows a magnetic transition temperature between 30 and 40 K that can be used for its identification (Dekkers et al. 1989; Rochette et al., 1990), cannot be ruled out beforehand as the cause for the decay. The same applies to siderite which has a Néel temperature of 38 K (Jacobs, 1963; Frederichs et al., 2003).

From about 40 K upward, the remanence gradually decays to minima at room temperature in the glacial sample (Fig. 4a), and only 4 % of the initial remanence generated at 5 K is retained at 300 K. In the interglacial sample (Fig. 4b) a second notable decrease occurs between 100 and 120 K, interpreted as the Verwey transition of magnetite. This represents a first order crystallographic phase transition from an inverse cubic spinel to a monoclinic structure, and occurs in stoichiometric magnetite at 117 K (Verwey 1939). The shifted Verwey transition to lower temperatures can be resulting from non-stoichiometric magnetite. Partial oxidation of magnetite (maghemitization) is put forward as a reason (e.g., Özdemir et al., 1993; Dunlop and Özdemir, 1997; Smirnov and Tarduno, 2000). Also substitution of Ti for Fe is a plausible cause (e.g., Kakol et al., 1994; Moskowitz et al., 1998).

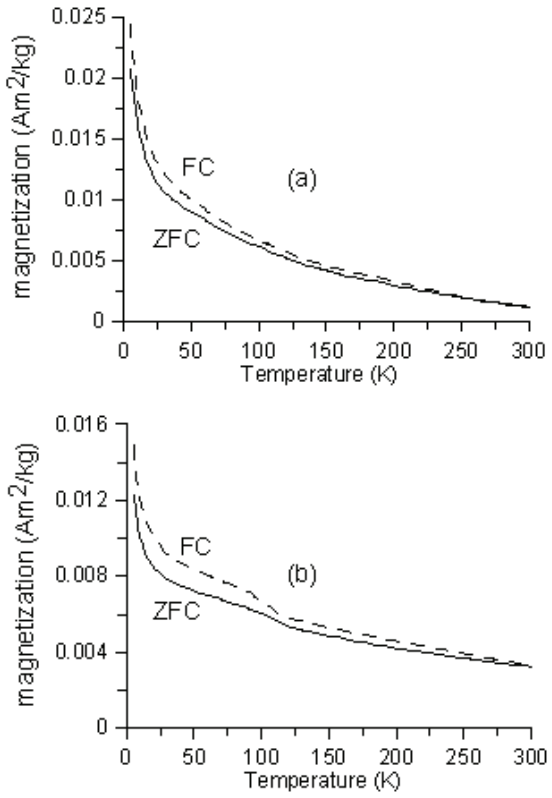

Fig. 4. Zero-field-cooled and field-cooled warming curves. (a) glacial and (b) interglacial. Both show a sharp drop in remanence below ~30 K reflecting the presence of SP particles and/or paramagnetic minerals. The glacial sample continues to decay gently to minimum values at room temperature whereas the interglacial sample shows a second sharp drop between 100 and 120 K that represent the verwey transition of non stoichiometric magnetite.

AC susceptibility: The behaviour of the susceptibility at low temperature and its frequency dependence is illustrated in Figure 5. There is a notable difference between interglacial and glacial samples: The interglacial sediments (Fig. 5b) show just the inverse temperature dependence characteristic of a dominant paramagnetic behaviour. As anticipated AC susceptibility is highest at lowest temperature (5 K) and drops sharply to ~ 25 K after which the decay with increasing temperature levels off. It is approximately constant between 120 and 300 K.

In glacial intervals, sediments show both temperature and frequency dependence (Fig. 5a). From 5 K, the susceptibility drops to a minimum at ~ 25 K from where it abruptly rises to maximum at 50 K. This drops significantly to 100 K where the decrease levels off slightly. A second drop occurs at ~125 K from where the susceptibility continues to decrease slightly to a minimum at around 170 K. From ~ 190 K, there is a general trend of gradual increase in the susceptibility up to room temperature. The frequency dependence increases significantly as

we move towards room temperature, with lower frequencies producing high susceptibility values.

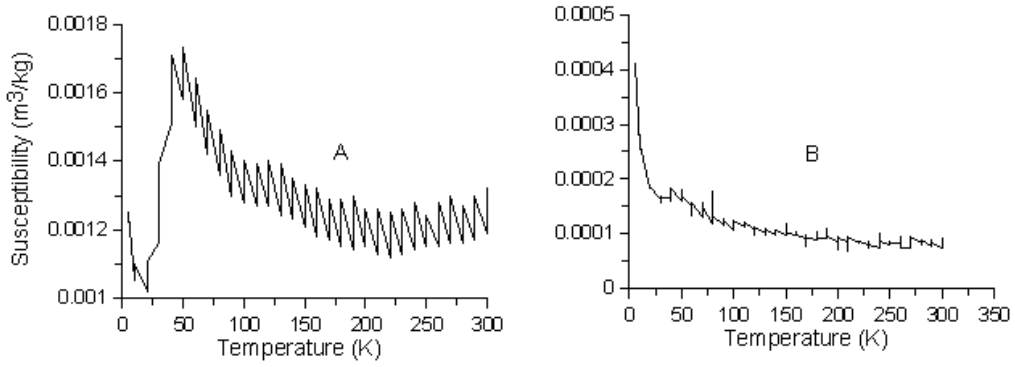

Fig.5. Temperature and frequence dependence of AC susceptibility. Glacial samples show both frequency and temperature dependence while only temperature dependence for interglacial. Frequency of measurement are 1, 10, 100 and 1000 Hz.

The shape of the susceptibility curve between 5 and 100 K is similar to that obtained by Moskowitz et al. (1998) for titanomagnetite bearing samples of basaltic material from the Hawaiian deep drill hole (SOH1). They suggested it to be as a consequence of the superposition of paramagnetic, antiferromagnetic and ferromagnetic susceptibilities from different iron phases. In our case, we consider paramagnetic and/or ferromagnetic susceptibilities as the likely causes for the observed variations.

4.3.1.4 High temperature magnetic measurements

The two representative bulk samples show distinct signatures during high temperature cycling of magnetization (Fig. 6). On heating from 25 to 700 °C, the glacial sample (inset in Fig. 6a) shows a continuous, gentle drop in magnetization up to about 500 °C where a change to a steeper slope is observed to ~ 600 °C. Above this temperature, it remains fairly constant although there is a tiny drop at ~670 °C, a minute hint to the presence of hematite. The cooling curve is reversible up to 680 °C (because this part is paramagnetic) and then steadily increases, though with a smaller magnetization compared to the initial heating curve.

The interglacial sample shows a markedly different response in the high temperature measurements (inset in Fig. 6b). The heating curve shows a gentle decrease in magnetization from room temperature up to 360 °C where it rises abruptly to values closer to the starting

magnetization value. This increase in the magnetization maintains a broad peak between 420 and 475 °C that slightly dips towards higher temperatures, culminating in a sharp drop between 475 and ~600 °C. From 600 to 700 °C, the drop is gentle, consistent with that osberved at temperatures < 360 °C. The cooling curve is non-reversible and has a magnetization lower than that of the heating curve. The observed jump at 360 °C is consistent with high temperature oxidation of non magnetic iron phases into magnetic phases. This thermomagnetic behaviour is virtually the same as that observed for sapropel S1 in the Mediterranean by Passier et al. (2001) who identified two types of pyrite through their oxidation behaviour. They reported that framboidal pyrite of 5-10 um size range was easily oxidized at lower temperatures (starting at ~360°C) because of their large reactive surface area. Euhedral pyrite was oxidized at temperatures starting at ~420 °C.

We identify the non magnetic Fe bearing mineral pyrite from electron microscopy, while the non magnetic Fe-bearing clay mineral nontronite was identified from the XRD analysis (data not shown). We therefore believe either one of these or both are responsible for the transformation observed. Thermal treatment of nontronite (Moskowitz and Hargraves, 1984) reveals that paramagnetic behaviour remains above 700 °C which rules out its contribution to the thermal behaviour of our sample.

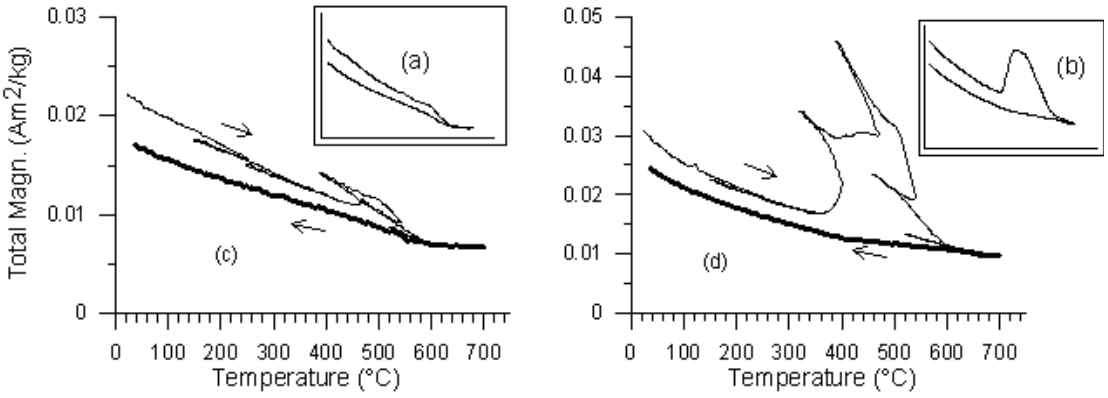

Fig.6. Thermomagnetic runs measured on a translation type Curie balance in air. The insert are single runs from room temperature to 700 T and back. The other two curves are incremental runs performed to determine thermal transformation. Incremental runs were performed at maximum temperatures of 250, 350, 400, 470, 540, 620 and 700 °C.

Here, pyrite which makes up over 50 % of the Fe bearing component of the magnetic extract (see section 4.3.2.3 on the electron microscope observations) is also the phase that is oxidized via magnetite and maghemite to ultimately hematite. The pyrite becomes oxidized at

360 °C and exhibits a broad peak in the magneetization between 420 and 475 °C, similar to the curves depicted in Passier et al. (2001). The broadness of this oxidation peak shows that the different types of pyrite (i.e. framboids and euhedral pyrite) jointly occur in these sediments as will be seen in the SEM.

To document the alteration in greater detail we performed so called incremental thermomagnetic runs as well (Figs 6a, 6b). They show indeed the alteration and the occurrence of minute pyrite in the glacial sample as well. Its presence could only be vaguely surmized from the single segment thermomagnetic run. It is evident that the magnetite formed oxidizes rapidly to hematite (the magnetization tail at temperatures to 600-620°C is barely noticeable). Importantly, in both glacial and interglacial samples there is a small decrease in magnetization from 250°C upward. This could be due to the presence of maghemitized coatings on magnetite particles (glacial samples) or possibly due to the presence of intermediate monosulphides (primarily greigite) that are chemically removed at that temperature range (interglacial samples).

4.3.2 Scanning electron microscopy (SEM)

SEM analysis was performed on magnetic extracts and HLS. A wide range of iron-bearing mineral phases was observed with a significant distinction between glacial and interglacial sediments. They include pure iron oxides, titanium bearing iron oxides, and iron sulphides. These particles occur in a broad grain size range, varying from a few hundreds of nm to tens of microns, reflecting the complex sedimentary environment that is composed of several sources for the origin of the magnetic assemblage.

4.3.2.1 Iron oxides

The pure iron oxides constitute a large fraction of the extracts, approximately 30% in the glacial sample and ~20 % at the interglacial stage. They vary both in size and shape, with the dominant shapes being spherules and irregular shaped grains. A greater proportion of the iron oxides are made up of irregularly shaped rounded grains ranging in size from a few μm to ~ 30 μm make up the majority of the iron oxides.

Magnetic spherules with different surface features, comprising well rounded, smooth as well as rough exteriors were observed (Fig. 7). The general composition ranges from pure iron oxides, iron oxides with Al and Si inclusions, as well as Fe-Ti oxides. Spherules deposited at interglacial where fewer are smoother and entirely composed of Fe and O (Fig 7f). The glacial level is shown in Fig. 7a-e and the interglacial level (Fig. 7f).

Fig. 7a and b are composed of iron and oxygen with small inclusions of Al and SI as was observed from the energy dispersive x-ray analysis (EDS) (see appendix). We classify these as magnetite spherules based on previous studies that have identified similar particles (Suk et al., 1990; Sun and Jackson, 1994; Franke et al., 2007).

Fig. 7c shows a broken spherule demonstrating its internal framework while Fig. 7d is a chunk of some of the building blocks that has disintegrated from the broken spherule. The internal morphology shows well-developed dendritic structures which indicate rapid crystallization from a high temperature melt. Iron, oxygen and bromine are the three chemical components identified with EDS. We believe the Br observed is probably the L line for Al which has the same energy position as the K line for Br.

The partially disintegrated framboid in Fig. 7e is composed of small euhedral particles measuring ~ 600 nm in a very regular array. In some EDS spectra only Fe was detected and in others, both Fe and O. Although no traces of sulphur were identified, the morphology and arrangement of the microcrystals point towards a pyrite origin. McCabe et al. (1987) and Suk et al. (1990) amongst others have reported the occurrence of such oxidized framboids and classify them as of secondary origin formed by the transformation of framboidal pyrite. Such framboids could consist of diagenetic magnetite, hematite or goethite formed by the oxidation of pyrite.

Magnetic spherules in marine environments may originate from a number of sources i.e. cosmic, diagenetic, anthropogenic and volcanic sources, each with distinctive characteristics that can be used to distinguish them from each other. The presence of nickel is a strong indicator for cosmic origin (Fredriksson and Martin, 1963; El Goresy, 1968; Parkin et al., 1980). None of the identified grains showed traces of Ni. However, Ni is readily depleted in the crust of the spherules during ablation processes implying only a detailed analysis of a broken or cut (and polished) particle (or thin section) can provide a genuine conclusion about its origin. This shows an iron oxide rich composition without nickel. This evidence rules out cosmic origin for the particles. Anthropogenic origin is also not a candidate because the sediments date over 15 ka, a time when there was no human influence. Spherules of diagenetic origin produced from framboidal pyrite oxidation (Suk et al., 1990) are available and easy to identify because of their perculiar shape (Fig. 7e). The presence of Ti is diagnostic of volcanic spherules (Fredriksson and Martin 1963; Freeman, 1986, Franke 2007b).

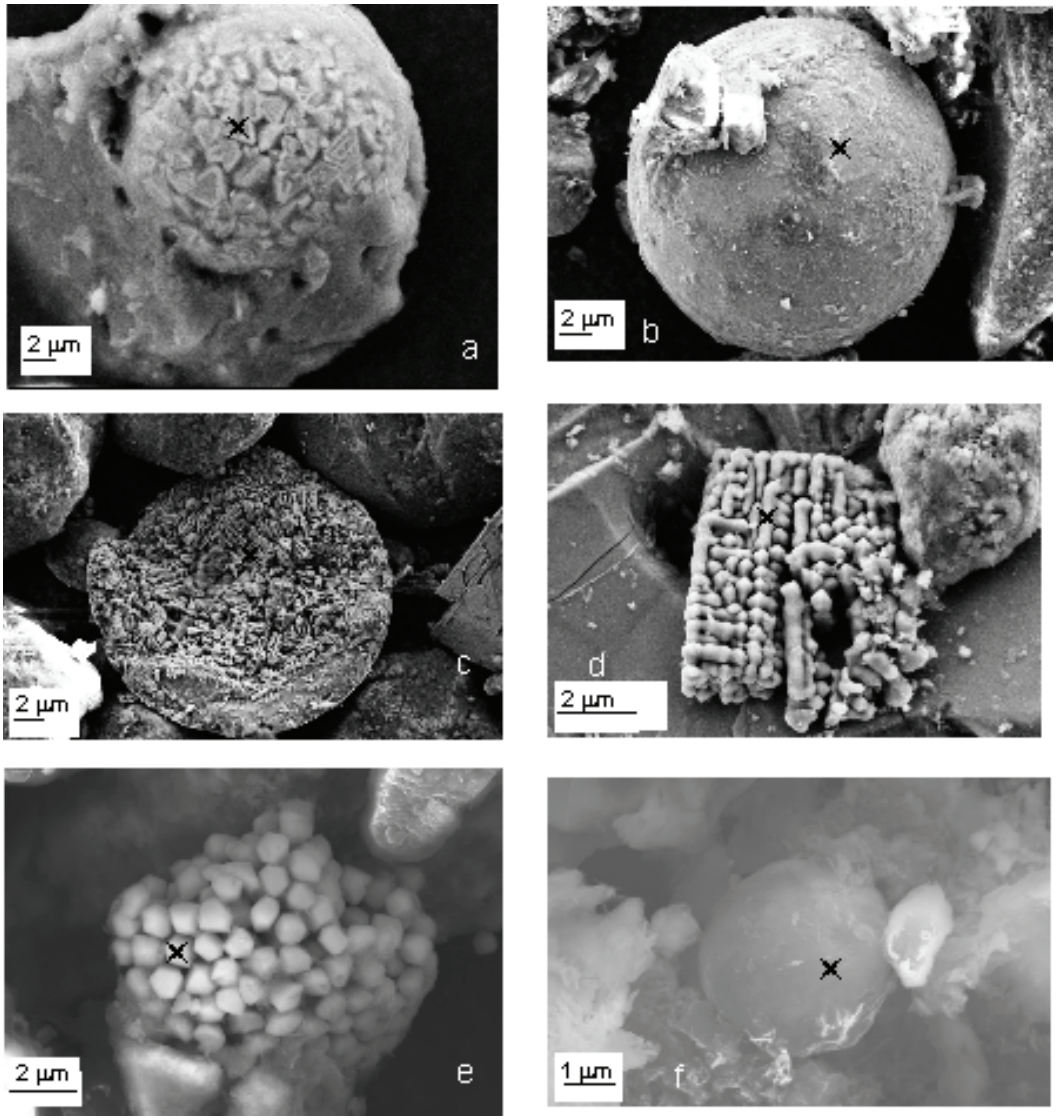

Fig. 7. SEM micrographs of iron oxides obtained in SE mode. The X symbol indicates spots from where EDS (see Appendix) were obtained. (a-e) are from glacial samples while (f) is from interglacial. (a) Magnetic spherule with interlocking triangular crystals. (b) Spherule with smooth surface. (c) Internal framework of a broken spherule displaying dendritic structures. (d) Further displays some of the building blocks of the spherule. (e) Magnetite framboids resulting from the oxidation of pyrite. (f) Typical spherule with smooth surface observed in interglacial sediments.

The broken spherule observed in our sediments made it possible to measure the internal composition. The lack of an interlocking crystal surface and imperfect spherical forms are attributed to volcanic origin. The interlocking triangular crystals observed in Fig. 7a might suggest an extraterrestrial source. However, the presence of Al and Si in its spectra rules out this source. As with many of the observed magnetic spherules which show Ti enrichment and perfectly spherical shapes, we attribute them to volcanic source, originating from the near by African continent (e.g., Franke et al., 2007).

4.3.2.2 Fe-Ti oxides

About 60 percent of the magnetic particles in the glacial sample and 25 % in the interglacial sample consist of Ti bearing iron oxides. The degree of substitution varies significantly, with some grains containing more Ti than Fe. Their shapes and grain sizes also vary, with typical size range of between 1 and 30 μm. Most of the grains are irregularly shaped with rounded features,

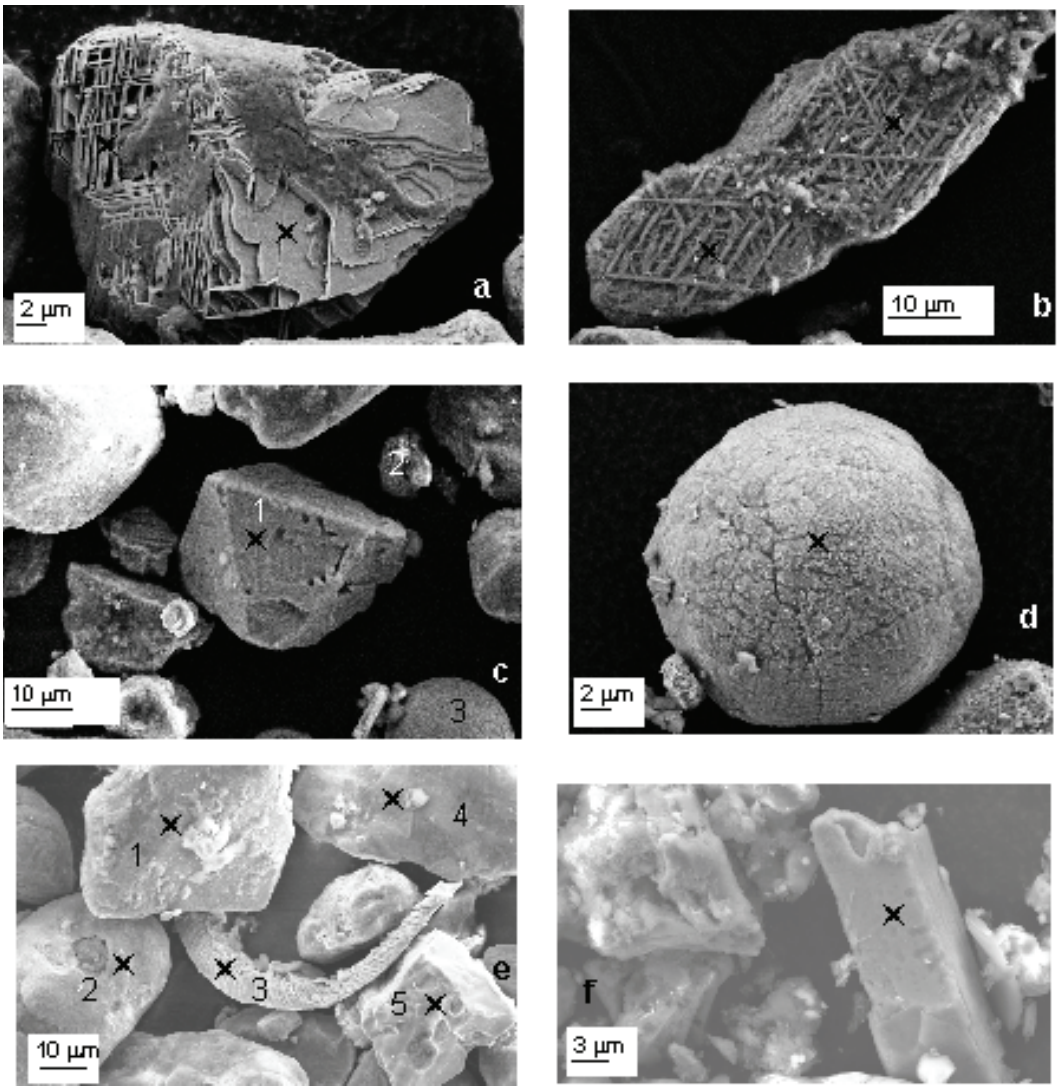

Fig. 8. SEM micrographs of iron titanium oxides obtained in SE mode. The X symbol indicates spots from where EDS (see Appendix) were obtained. (a-e) are from glacial samples while (f) is from interglacial. (a) and (b) show (hemo) ilmenite lamellae after the titanomagnetite intergrowths have been preferentially dissolved. (c) Octahedral titanomagnetite grain with sharp edges and displaying dissolution marks (1). Magnetite framboid (2) and spherule (3) are also identified. (d) Titanium rich spherule of volcanic origin with mild dissolution features. (e) Amorphous grains with an unidentified magnetic structure of possibly organic origin. (f) Titanomagnetite grains showing severe dissolution.

The Ti bearing particles in the glacial samples (Fig. 8a-e) show a wide range of features prominent amongst which are the titanohematite lamellae intergrown with titanomagnetite (TM) (Fig. 8a & b). Freeman (1986), von Dobeneck et al. (1987), and Garming et al. (2005, 2007) and several others have described such intergrowths to be products of high temperature oxidation of titanomagnetite. An example is Fig. 8a which shows exsolution texture of the Fe-Ti-O with the preferential dissolution of the TM intergrowth that left behind the more resistant titanohematite or ilmenite lamellae. Freeman (1986) used the exsolution features of such minerals and the Ti content to suggest a basic magma source. We therefore attribute this particle to a magmatic source. The shrinkage cracks observed in indicate low temperature oxidation (Petersen and Vali, 1987). Fig 8c shows an octahedral titanium bearing particle (titanomagnetite) with sharp edges and dissolution marks which suggest possible aeolian transport. The inclusion of Ti and the large grain size rules out biomineralization as the source.

Fig. 8d shows a Ti-rich spherule with a rough surface morphology that may be attributed to dissolution (Franke et al., 2007).

Interglacial samples showed lower concentration of these particles, with strong dissolution features (Fig. 8f). Typical grain sizes range between 1 and 10 μm.

4.3.2.3 Iron sulphides

Although iron sulphides were previously believed to be of little significance to the magnetic properties, recent studies have emphasized their relevance to paleomagnetism, post-depositional and environmental reconstruction. Indeed, we document their occurrence also in our samples. The iron sulphides were observed in the heavy fraction extracted by heavy liquid separation and not by the magnetic extraction. This implies a non magnetic iron sulphide, (almost) all pyrite when expressed on a molar basis.

The occurrence of iron sulphides in glacial sediment was very limited, making up less than 2 percent of the extract. The presence of minute quantity of pyrite was also confirmed by the thermomagnetic run (Fig. 6a).

Typical micographs of the iron sulphides are illustrated in Fig. 9a & b. They are the dominant Fe bearing minerals in interglacial sediments, making up over 50 % of the iron bearing component. They occur as framboids with a fairly wide range of sizes (between 6 to 14 μm), the framboids consist of euhedral microcrystals measuring between 0.1 and 1μm in diameter with different crystal shapes. Framboids also occur in large clusters which can reach

dimensions of ~ 250 by 480 μm (Fig 9a). The octahedron and truncated octahedron shapes are depicted in Fig. 9b.

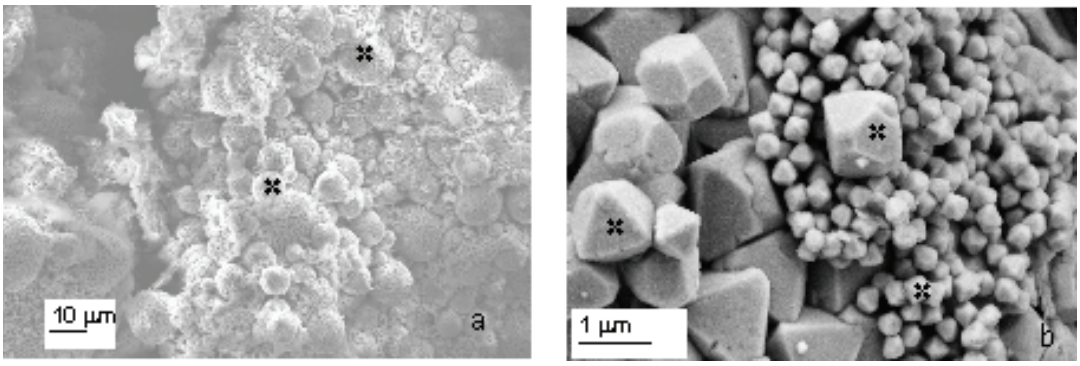

Fig. 9. Typical SEM micrographs of iron sulphides obtained in SE mode. The X symbol indicates spots from where EDS (see Appendix) were obtained. (a) Cluster of numerous pyrite framboids, with varying sizes. (b) Euhedral pyrite microcrystals of two sizes. Also note the crystal shapes (octahedron and truncated octahedron).

Fig. 10 is a cluster of irregularly shaped magnetic grains composed of iron and oxygen (EDS, see Appendix) which was uncovered from the glacial sample which based on its composition could be interpreted as oxidized pyrrhotite. Freeman (1986) reported a similar grain cluster of iron and sulphur composition which they classify as pyrrhotite crystals held together by magnetic attraction.

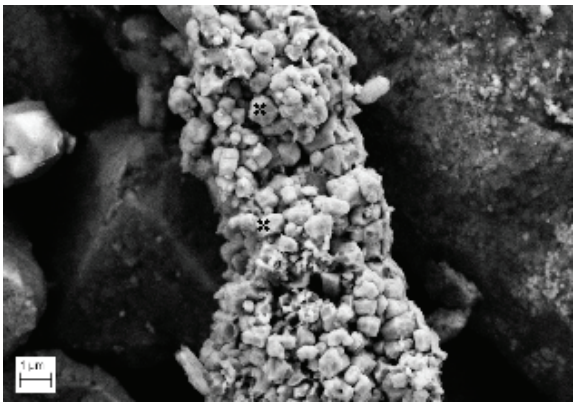

Fig. 10. SEM micrographs obtained in SE mode. The X symbol indicates spots from where EDS (see Appendix) were obtained. Clusters of small magnetic grains.

Pyrrhotite can be formed diagenetically under very reducing conditions with abundant pyrite. However, it has been shown (Schoonen & Barnes 1991; Lennie et al., 1995) that the low temperatures do not favour pyrrhotite formation. Metamorphic rocks are potential sources of detrital pyrrhotite in sediments (Horng & Roberts, 2006). Since pyrite and goethite occur extensively in such sediments and can also oxidize, they cannot be rule out as the origin of the observed particle.

4.4 Discussion

The low and high temperature experiments, FORC analysis, and SEM observations provide diagnostic features that can be used to identify and characterize the magnetic mineral content of these sediments. Here we put all information into a larger paleoenvironmental, paleoclimatic and diagenetic context.

4.4.1 Magnetic transitions

Several reasons have been proposed to explain the rapid decrease in the remanence at low temperature between 5 and 30 K. These include contributions from superparamagnetic particles, the occurrence of paramagnetic materials that become ordered at very low temperature (carbonates, silicates, phosphates), as well as ferromagnetic hemoilmenite. Also frozen spin glass as coatings can occur. Here, all three contributions are possible. FORC measurements have revealed the presence of SP particles in the glacial samples. The magnetic phase contributing to this phase is still not well documented. However, we suggest high coercivity hematite and/goethite coatings on quartz grains as the probable source. Kosterov (2001) proposed hemoilmenite with 8–10 mole % of hematite as a possible low temperature superparamagnetic phase in subaerial basalts. This solid solution series was also identified in SEM of the glacial sediments. However, despite the fact that the interglacial sample showed no presence of SP particles and hemoilmenite, their remanences also responded similarly during low temperature measurements. We attribute this to paramagnetic clay minerals contained in both samples and derived from the African continent by both eolian and fluvial pathways.

The presence of magnetite has been confirmed by the Verwey transition observed in the interglacial sediments between 100 and 120 K. Based on the energy dispersive x-ray analysis,

we attribute the cause of the observed shift in the position from the stoichiometric value of 120 K to Ti substitution (See appendix). Titanomagnetites are amongst the dominant minerals analysed with EDS. For titanomagnetite $Fe_{3-x}Ti_xO_4$ with $0<x<1$, it has been shown (Kakol et al., 1994) that the Verwey transition is suppressed for $x > 0.04$. Since the EDS is semi-quantitative, we cannot determine the value for x. Moskowitz et al. (1998) demonstrated the effects of Ti substitution in the low temperature characteristics of magnetite. They observed that the transition temperature T_v decreases with increasing Ti substitution. The absence of the Verwey transition in glacial sediments can also be attributed to patial oxidation of the magnetite. This assertion is drawn from the higher DP of magnetite in the IRM component analysis. The soft component in the interglacial sample may be related to core/shell situation where mild reduction has dissolved the shell of the particles leading to reduction of the DP and introduces a Verwey transition and skew the coercivity distribution to the left.

Although Itambi et al. (in revision) observed evidence for the presence of hematite/goethite in these sediments, no low temperature transitions were observed to support these results. However, the lack of the Morin transition (T_m) does not imply the absence of hematite. It has been shown that T_m can be reduced or even suppressed by small amounts of isomorphous substitution of Ti or Al (Morin, 1950; Creer, 1962; Besser et al., 1967; Morrish, 1994) and small particle sizes (Bando et al., 1965). Hematite and/or goethite have been suggested to occur as ultrafine coatings on quartz grains from the Saharan desert deposited in Atlantic Ocean (Balsam et al., 1995). These could not be extracted by both magnetic separation methods used and as stated above. The presence of the high coercivity minerals is therefore confirmed by the continual IRM acquisition up to 7 Tesla. From the IRM component analysis, goethite was detected as the dominant high coercivity mineral which contributes about 42 % of the remanence in glacial samples whereas the hematite fraction which was also identified was significantly less, contributing only 8 % to the glacial sample, and about 5 % during interglacial.

4.4.2 Diagenetic sulphidization

Reductive dissolution of magnetic particles in sediments has been widely documented (Canfield and Berner, 1987; Karlin, 1990). This may result in the loss of the primary NRM signal via the formation of new iron phases. Sulphidization has been used to reconstruct past environmental conditions at depositional sites. High productivity and availability of organic matter provides a thriving environment for microphylic bacteria which produces H_2S (Froehlich et al., 1979). The H_2S reacts with dissolved ferrous iron forming greigite which

will subsequently react to the more stable pyrite if the sulphide content is high (Sweeney and Kaplan, 1973; Berner, 1984).

The abundance of pyrite framboids in our sediments, especially during interglacial times, suggests that reducing conditions persisted, aided by high marine productivity. However, marine productivity in this region is enhanced also during glacial periods by upwelling driven by stronger NE trades. Using the diagenetic parameter $Fe/\kappa_{nd,}$ where κ_{nd} is the non diamagnetic susceptibility (Funk et al., 2004) Itambi et al. (in revision) were unable to detect diagenesis. The ARM and IRM were also high, compared with other cores which showed evidence for dissolution. This might suggest that bottom water conditions were not sufficiently reducing to be able to significantly dissolve the magnetic particles. However, productivity driven diagensis is highly favoured and it is not ruled out.

Another suggestion which is strongly favoured is a different source for Fe. The Senegal and Gambia Rivers have been documented as pathways through which a significant amount of dissolved Fe and suspended particles are transported to this location (Gac and Kane, 1986a, 1986b). Some of the dissolved iron is precipitated at the mixing zone between fresh and sea water, producing magnetic phases such as goethite (Odin 1975). These secondary minerals and dissolved Fe in the pore water may provide reactive substances for reaction with sulphur. In this scenario, the detrital magnetic particles will remain unaffected by dissolution provided there is sufficient reactive iron available. In the Arabian Sea, reductive diagenesis has been credited with the preservation of the primary signals (deMenocal et al., 1991; Bloemendal et al., 1993). Fine grained magnetite produced in situ by magnetotactic bacteria is preferentially dissolved during oxidation of organic matter, and the primary magnetic particles that represent climate variations remain (largely) unaffected.

Several formation pathways for pyrite framboids have been proposed, but none seems to be generally accepted. Some authors (Sweeney and Kaplan, 1973; Wilkin and Barnes, 1997) have suggested greigite as a prerequisite for framboid formation whereas more recent studies (Butler and Rickard, 2000) have disputed such claims, demonstrating that they could be formed by the oxidation of ferrous iron monosulphide by hydrogen sulphide. Taylor (1982) showed that framboid formation could take place in free suspension by the coagulation of iron sulphide gel particles which in a marine environment could be the result of biogenic bisulphide ions reacting with Fe^{2+}. Framboids formation is rapid, resulting from aqueous solutions highly saturated with iron monosulphide and pyrite. Euhedral textures on the other hand form slowly in less saturated environments (Sweeney and Kaplan, 1973; Goldhaber and Kaplan, 1974). Low concentration (<2%) of euhedral pyrite in the glacial therefore suggests

minimal diagenesis. The presence of both textures at the interglacial suggests that secondary pyrite formation occurred at slow rates after burial, yielding euhedral particles. This resulted because most of the reactive iron had been reduced during early diagenesis and sulphate reduction rates were much lower comparable to recently deposited organic matter (Passier et al., 1999).

4.5 Conclusions

The characterization of the magnetic mineral assempblages reveals that the Senegal continental margin is a complex sedimentary setting for the magnetic mineralogy. Detrital magnetic mineral fluxes tend to be controlled by fluvial and aeolian transport pathways which are modulated by humid and arid climate (respectively) over northwest Africa. Larger grain sizes observed for the glacial sediments together with higher goethite and hematite contributions reflects stronger wind strengths and aridity over North Africa where by dust was mobilized and transported into the ocean. In contrast, interglacials are dominated by finer magnetic particles which is a reflection of fluvial transport resulting from intense precipitation.

Superparamagnetic particles also contribute to the glacial signals as revealed in the FORC measurements and AC susceptibility, with evidence pointing to hematite or goethite as the carrier.

Thermal transformation occurring between 350 and 500 °C revealed by Curie balance measurement and SEM suggest that both framboidal and euhedral pyrite dominate the iron phases at interglacial intervals. Pyrite domination is evidence for the post-depositional alteration of the magnetic minerals. The occurrence at all interglacial intervals studied (only one shown here) suggest that diagenesis was climate driven, possible stimulated by high productivity.

The occurrence of secondary magnetite points to the remagnetization of these sediments, imparting a chemical remanence that might mask the primary signals (Sun and Jackson, 1994; Suk et al., 1990; Rowan and Robert, 2006). However the degree to which this secondary magnetization has affected the primary signal over northwest Africa is quite minimal as very few of such particles were observed. This is also true for non climate related magnetic spherules that also occur in the sediments in low concentrations.

Acknowledgments: We thank Petra Witte for her support with the electron microscopy and the members of the Paleomagnetic Laboratory at Utrecht University (where part of this work was done) for their support. We also acknowledge Christine Franke for carrying out some of the Curie balance measurements and providing helpful suggestions. This work was supported by the German Research Foundation (DFG) through the European graduate collage EUROPROX (University of Bremen).

5. A multi-proxy study of late Quaternary sediments from the Gulf of Guinea indicating millennial-scale precipitation changes over central Africa

Itambi[1] A. C., von Dobeneck[1, 2] T and Adegbie[3] A. T.

1) Geosciences Department, University of Bremen, Klagenfurter Strasse, D-28359 Bremen, Germany
2) Research Center Ocean Margins, University of Bremen, Leobener Strasse, D-28359 Bremen, Germany
3) Nigerian Institute for Oceanography and Marine Research (NIOMR), P.M.B. 80108, Victoria Island, Lagos, Nigeria

Abstract

We combine environmental magnetism, geochemical measurements and color reflectance to study sediment cores from two latitudinal positions within the Gulf of Guinea. This area is suitable in investigating climate change over Central and West Africa because of its potential to record high influx of aeolian and fluvial sediments. Three zones representing the degree of alteration of the primary signal were identified from cross plots of magnetic parameters and show a strong primary signal, with some intervals severely affected by diagenesis. The magnetic signature is dominated by fine-grained magnetite while residual hematite prevails in the reduced intervals.

The records show millennial-scale changes in climate during the last glacial and interglacial cycles. At the northern location, the past 5.5 kyr are marked by high frequency oscillations corresponding to high Ti, which suggests aeolian input and hence aridity. The southern location remains under the influence of the ITCZ and thus could not register aeolian signals. The last African Humid Period is characterized by high fluvial input and low productivity. The millennial-scale climatic signals indicate that drier and/or colder conditions persisted during the late Holocene.

This manuscript has been submitted to the Journal of Quaternary Science.

5.1 Introduction

Many studies have demonstrated that Quaternary climate variations in equatorial and subtropical Africa is primarily controlled by 19 and 23 kyr orbital precession cycles which regulate summer insolation and thus the strength of the West African monsoon. The monsoon controls the amount of precipitation on the West African continent which determines the influx of terrigenous materials into the Atlantic Ocean. DeMenocal et al. (2000a & b) Sarnthein (1978), Ruddiman and Janecek (1989) and Kutzbach and Street-Perrott (1985) investigated climate variability within the African continent using different proxies and related it to the African monsoon. Quite recently attention is being focused on the climatic and environmental change during the Holocene following observations of rapid climatic events during the last glacial in high latitude climate archieves (O'Brien et al., 1995; Bond et al., 1997). Ice core records from Mt Kilimanjaro have provided some evidence for the Holocene climate variability in tropical east Africa (Thompson et al., 2002). In addition, numerous studies on lake sediments revealed significant variability in African climate during the Holocene (e.g., Talbot et al., 1984; Street-Perrott and Perrot, 1990; 1996; Gasse, 2000; Giresse et al., 2005 and Shanahan et al., 2006). These studies link changes in lake levels to fluctuation in precipitation.

This study is aimed at further investigating the paleo-climatic and environmental evolution in the Central African region with special attention focused on millennial-scale precipitation variations during the Holocene, using marine sediments recovered in the Gulf of Guinea from off-shore Cameroon and Gabon,. We combine high resolution rock magnetic parameters, elemental abundances and color reflectance to reconstruct the regional climate history in the Late Pleistocene. Previous studies in this area were mostly based on geochemical and palynological proxies (e.g., Gasse and van Campo 1994; Barker et al., 2001; and Schefuß et al., 2005).

Rock magnetic properties can trace contents and characteristics of environmentally sensitive magnetic minerals in rocks and sediments even at very low concentrations and have evolved into recognized tools in paleoclimatic and environmental studies since their inception over two decades ago (Thompson et al., 1980; Thompson and Oldfield, 1986), being. Amongst many others, works of Bloemendal et al. (1992), Verosub and Roberts (1995), Frederichs et al. (1999), Peters and Dekkers (2003) have demonstrated the potential of environmental magnetism to discriminate sediments by lithology, origin, depositional and post-depositional processes from their magnetic mineral mineralogy and grain size. Dekkers

et al. (1994), Vigliotti et al. (1999) and Funk et al. (2004)showed that a combined magnetic and geochemical analysis can identify diagenetic alterations.

Elemental abundances from high resolution XRF scanning provide ratios representing climatically driven flux variations of terrigenous and biogenic sources (Arz et al., 1998; Jansen et al., 1998). High resolution color reflectance data have been used successfully in paleoclimatic studies to unravel millennial-scale changes e.g. in the Cariaco basin (Peterson et al., 2000). In this paleoclimatic study, we therefore combine these three methods and their potentials to draw conclusions on provenance and transport issues.

5.1.1 Study area

Our study area is the easternmost Equatorial Atlantic within the confines of the Gulf of Guinea which runs from the west coast of Ivory Coast to the Gabon estuary (Fig. 1). Seasonal insolation changes result in two prominent seasons i.e., dry and rainy seasons. Variation in the West African monsoon over this region is known to produce significant changes in the atmospheric circulation controlling annual rainfall, moisture, temperature and wind (Baldi et al., 2003). Strong solar radiation in boreal summer heats the landmass creating a region of low pressure; the Intertropical Convergence Zone (ITCZ), where water-vapor rich air flows in from the surrounding ocean contributing to the monsoon rainfall (Ruddiman, 2001). Its location varies seasonally and determines the latitudinal distribution of moisture and rainfall. Strong SE trade winds during boreal summer move the ITCZ to about 18° to 20°N and strong NE trades push the northern limit close to the equator (3°-5°N) in winter. Over land the ITCZ extends farther north or south than over the oceans due to the seasonal variation in land temperatures. The strength of the monsoon has been related to periodic orbital changes in summer insolation (Kutzbach, 1981) as well as vegetation cover (Kutzbach, 1996 and Brovkin et al., 1998).

The Gulf of Guinea deposits composed of a 4000 m thick sequence of Cretaceous, Tertiary and Quaternary sediments deposited via eolian and riverine pathways. Strong Harmattan surface winds (NE trades) transport Saharan dust rich in organic and clastic sediments into the ocean (Westerhausen et al., 1993; Romero et al., 1999). A recent study by Stuut et al. (2005) traced aeolian dust deposition rich in iron, aluminum, smectite and titanium from the Sahara desert to the eastern equatorial Atlantic. Within the eastern Gulf of Guinea, these dust particles range in size between 10 and 40µm. The dust is washed out by enhanced precipitation within and slightly below the ITCZ.

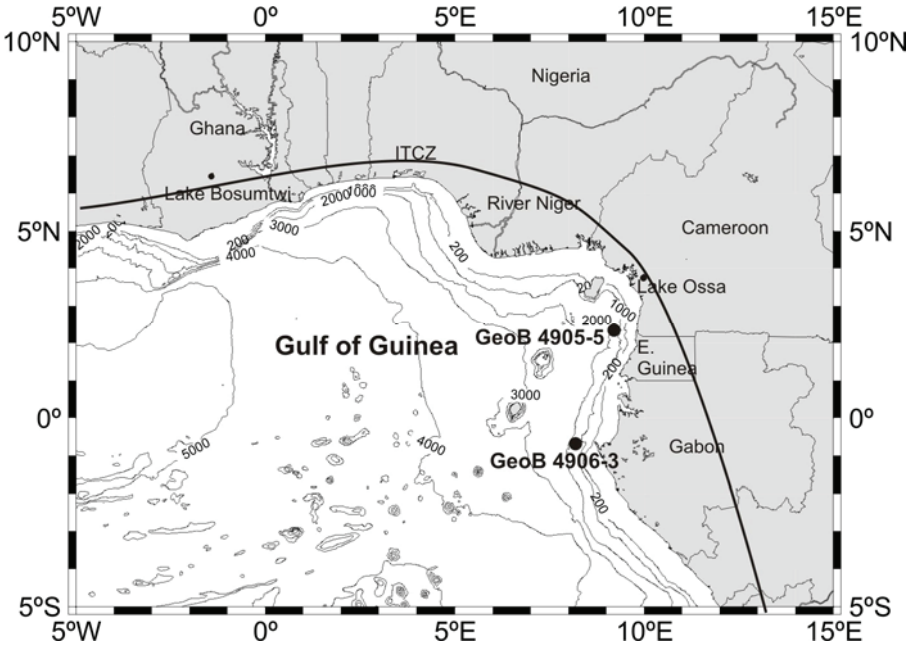

Figure 1. Location map showing the position of the two investigated cores and the northern winter boundary of the ITCZ

Numerous rivers such as the Volta, Niger and Congo Rivers discharge into the gulf bringing along vast amounts of terrigenous sediments. The Congo River is the second most voluminous river in the world, discharging about 1.5 million cubic feet of water per second and 40 Mt/yr of terrigenous materials into the ocean (Gaillardet et al., 1999). The Niger River also has a large watershed (~2.3 million km^2) draining regions with vastly different climatic conditions. Westerhausen et al. (1993) estimated that >60% of the total organic carbon accumulated on the shelf off eastern Liberia, Ivory Coast and Gabon is of terrigenous origin. Upwelling regions along the west coast of Africa and Equatorial Atlantic as well as influx of nutrient-rich fresh water boost productivity (Binet and Marchal, 1993) increasing the deposition of biogenic matter.

The surface and subsurface hydrography of the South Atlantic has been comprehensively described by Peterson and Stramma (1991). The hydrographic regime of the Gulf of Guinea is dominated by the westward flowing North and South Equatorial Currents (NEC, SEC respectively) and the South Equatorial Countercurrent (SECC) flowing eastward between 3°N and 2°S at a depth of 100 m.

5.2 Materials

Two gravity cores recovered along an N-S transect on the eastern Gulf of Guinea during RV Meteor cruise M41/1 (Schulz et al., 1998b) are investigated here: GeoB 4905-4 off Cameroon (2°30.0'N, 9°23.4'E, water depth 1328 m, length 12.18 m) and GeoB 4906-3 off Gabon (0°44.4'S, 08°22.6'E, water depth 1274 m, length 12.36 m) (Fig. 1). The cores consist of diatom and nannofossil oozes with silica-bearing nannofossil ooze predominant in the northern while diatom ooze dominates the southern location. Bioturbation at a varying degree is indicated by worm borrows filled with fecal pellets visible in some layers.

5.3 Methods

5.3.1 Rock magnetism

Low field magnetic susceptibility (κ) was measured on archive halves of the sediment cores at a resolution of 1 cm using an automatic core scanner with a *Bartington Instruments* MS2F spot sensor, which allow us to measure background values after each point measurement to correct for instrumental drifts. This parameter measures primarily magnetite concentration (Thompson et al., 1980; Verosub and Roberts, 1995).

A range of more specialized rock magnetic measurements were performed on discrete samples taken at 5 cm intervals for GeoB 4906-3 and 10 cm for GeoB 4905-4 in 6.2 cm^3 cubes. Dual frequency (470 Hz and 4700 Hz) susceptibility measurements with a *Bartington Instruments* MS2B unit was used to infer the contribution of ultra-fine superparamagnetic (SP) particles to the susceptibility signal using the diagnostic frequency dependent susceptibility $\kappa_{fd\%}$ (Dearing et al., 1996).

Isothermal Remanent Magnetization (IRM) was imparted at 23 incremental steps up to a 700 mT field in an automated pass-through *2G Enterprises* cryogenic rock magnetometer 755 R.. The IRM at this maximum field was considered as the saturation remanent Magnetization (SIRM) and together with 300 mT IRM used in calculating the S ratio given by the equation (King and Channel, 1991; Bloemendal et al., 1992; Maher and Thompson, 1999)

$$S_{0.3T} = \frac{IRM_{0.3T}}{SIRM}$$

This index reflects the relative proportion of the high-coercivity minerals (antiferro-magnets hematite and goethite) mainly to low-coercive (Ti-) magnetite. However, only the hematite and magnetite fraction could be inferred in this study due to the limitation of the

saturation field used. Ferrimagnetic minerals have a $S_{-0.3\ T}$ close to 1; the ratio decreases with an increasing antiferromagnetic content.

Using the same instrument, Anhysteretic Remanent Magnetization (ARM) was imparted in the laboratory by a 100 mT alternating peak field and a 40 μT DC biasing field. The ARM was subsequently AF demagnetized at increments of 5 mT from 5-50 mT, and increments of 10 mT from 60-100 mT. Anhysteretic susceptibility (κ_{arm}) was generated by normalizing the ARM with the DC biasing field. ARM is used as grain size and concentration indicator of sub-micron magnetite (Thomson and Oldfield, 1986; King et al., 1982; Oldfield and Yu, 1994).

5.3.2 X-ray fluorescence

Relative elemental abundances for elements from potassium to strontium were obtained at 2 cm resolution using a *CORTEX* X-ray flourescence (XRF) scanner at the ODP core repository center in Bremen. The acquired data were processed using the Kevex software giving element concentrations as counts per second (cps). Jansen et al. (1998) and Röhl and Abrams (2000) provide a detailed description of the instrument and measurement.

5.3.3 Color Spectroscopy

The *Geotek Multi Sensor Core Logger* (MSCL) mounted with a digital *Geoscan II* camera was used for acquiring color reflectance for the split cores. The cores were cleaned to smooth the surface and remove any oxidized layer before measurement. Line scanning was performed at a high resolution (1 mm) and averaged over 1 cm intervals. Sediment color reflectance is closely correlated with pigmented antiferromagnetic minerals hematite and goethite which are typically contained in dust and give sediments a reddish-brown appearance (Deaton and Balsam, 1991; Balsam et al., 1995). The reflectance is also affected by carbonate and organic matter contents. High carbonate content results in higher reflectance whereas organic contents lower the reflectance (e.g. Mix et al., 1995; Balsam et al., 1999).

5.3.4 Chronostratigraphy

Adegbie et al. (2003) established an age model for the adjacent core GeoB 4905-4 using ^{14}C ages and correlation of $\delta^{18}O$ record to the GISP2 record. This chronology was used to construct an age-depth relationship for GeoB 4906-3 by direct correlation of both Ca records (Fig. 2). Intermediate ages where generated by linear interpolation between tie points. Other independently correlating parameters (ARM, IRM, and porosity) acted as checks on these points by going through each parameter after assigning a tie point.

The chronology of our sediment cores provide a 45 ka record (GeoB 4906-3) and 52 ka (GeoB 4905-4, Adegbie et al., 2003) spanning the last glacial and interglacial events ie., marine isotope stages (MIS1) 1, 2 and late 3. The average sedimentation rate at this location was 28 cm/kyr.

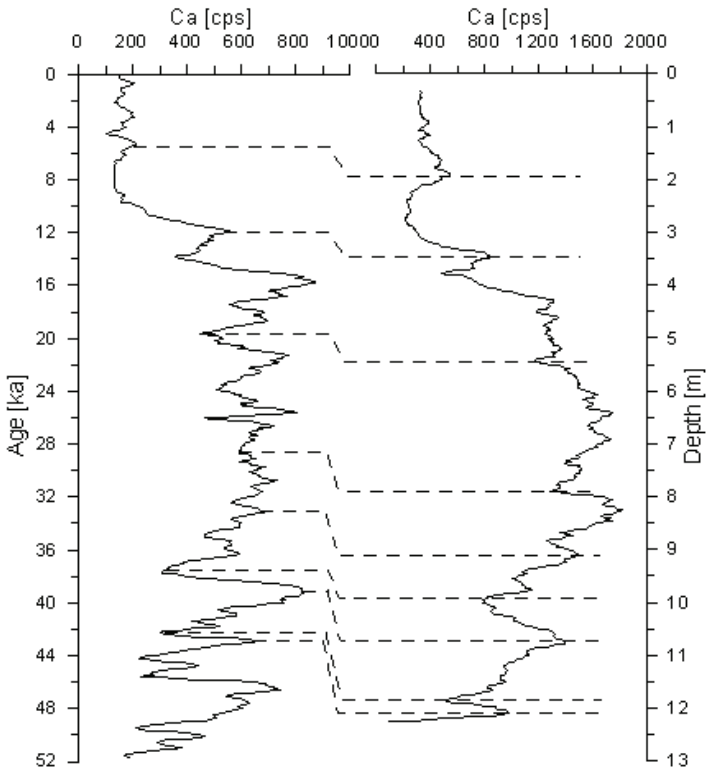

Figure 2. Correlation tie points of Ca records used to transfer the age model of core GeoB 4905-5 established by Adegbie et al. (2003) to core GeoB 4906-3.

5.4 Results and Discussion

5.4.1 Environmental magnetism

5.4.1.1 Primary and secondary signals

Secondary signals resulting from post depositional dia- and authigenesis can seriously compromise the paleoenvironmental interpretation of rock magnetic signals (e.g., Karlin et al., 1987). In order to discriminate between pristine and overprinted record sections, biplots of the magnetic parameters κ_{arm} vs. κ (King et al., 1982) and $S_{-0.3\ T}$ vs. κ_{arm}/κ are examined, which both mark a relative depletion of the diagenesis sensitive fine-grained magnetite fraction and are therefore indicative of post-depositional alteration.

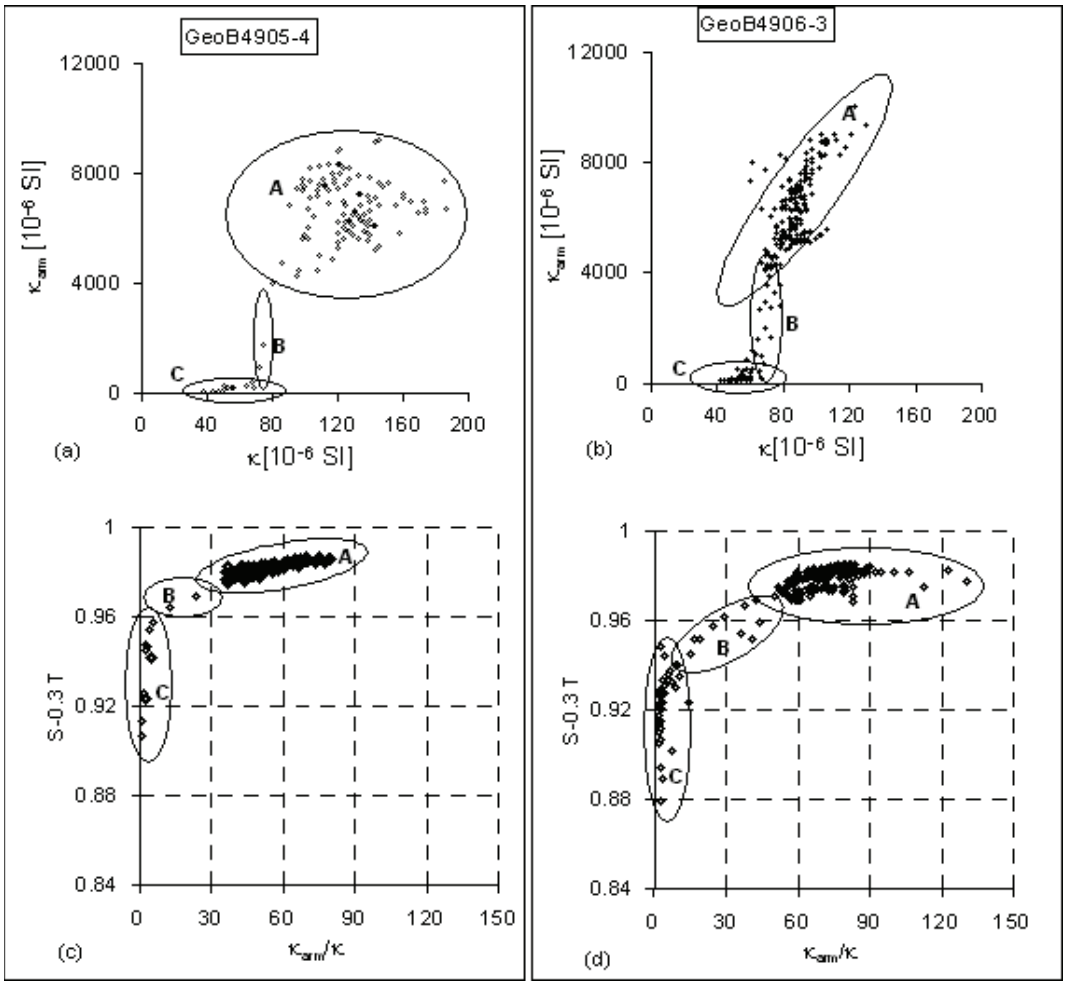

Figure 3. Diagnostic biplots of magnetic parameters indicating diagenetic iron reduction. Cluster A represents pristine conditions, cluster B a transition zone with partially reduced magnetite and cluster C pervasive magnetite dissolution.

κ_{arm} vs. κ (Fig. 3a&b) shows the dependence of magnetite concentration and grain size. Grain size variations are indicated by changes in slope while a change along a line of constant slope is indicative of varying magnetite concentrations. The two plots show that all the samples can be grouped into three well defined zones A, B and C (Fig. 3). The concentration of fine-grained single domain (SD) magnetite is highest in the first group of samples (A) with κ and κ_{arm} values greater than $80x10^{-6}$ SI and 4000xμSI respectively.

The susceptibility values are more constant in group B while the κ_{arm} varies. Group C is characterized by very low susceptibility and remanence approaching zero. At site GeoB 4905-4 (Fig. 3a), zone A is characterized by a broad dispersal of the data points without any preferential alignment along a gradient line.

In GeoB 4906-3 (Fig. 3b), there is wide variation in concentration but along the same gradient and the steep slope suggests that both parameters are strongly influenced by magnetic minerals originating from a single intermittent source and are solely dominated by SD particles while we believe that different sources are in play at the northern location. The two cores exhibit similar trends in both groups B and C.

The $S_{-0.3\ T}$ vs. κ_{arm}/κ plots combining hematite/magnetite ratio and magnetite grain size (Fig. 3c and d) also separates into three similar groups. Zone A represents areas where fine-grained magnetite strongly contributes to the signals. In core GeoB 4905-4, this zone is less extensive in the grain size parameter. The wider distribution in GeoB 4906-3 (κ_{arm}/κ between 50 and 150 units, Fig. 3d) indicates larger magnetite grain size variations.

Studies such as Karlin and Levi (1983) and Leslie et al. (1990) have shown that primary iron oxides can be dissolved through reductive diagenesis. In a reducing, typically sulfidic environment the fine grained magnetite is preferentially dissolved leaving behind the more resistant coarser fraction. Hematite and goethite are more resistant to reductive dissolution and therefore less depleted in diagenetically affected sediments (e.g. Bloemendal et al., 1992). High hematite and goethite (lower $S_{-0.3\ T}$), low susceptibility, coarsening of magnetite and low remanence therefore indicates diagenesis. From our cross plots (Fig. 3), we can identify such intervals by very low κ and κ_{arm} in the κ_{arm} vs. κ plot. Coinciding low $S_{-0.3\ T}$, κ, and coarser grain size (low κ_{arm}/κ) in the $S_{-0.3\ T}$ vs. κ_{arm}/κ plot confirm magnetite dissolution (Bloemendal et al., 1992). We therefore suggest that zone A represents primary signal of detrital magnetite input. Zone B is a zone of partial depletion while zone C is fully depleted.

Further confirmation of post-depositional modification of the sediment composition was derived using the diagenetic proxy parameter Fe/κ (Funk et al., 2004). Our observations point to a significant degree of magnetite alteration at the grey shaded bands identified in the

magnetic parameters (Fig. 4a and b) characterized by lack of remanence and low susceptibility. These bands contain high Fe mineral but show no corresponding increase in the magnetic susceptibility. During reductive diagenesis fine grained magnetite is reduced leading to the precipitation of non-magnetic iron phases such as pyrite. The lack of remanence at these intervals is therefore an indicator for post-depositional dissolution of magnetite. At both locations, diagenesis effects are detected between 38 and 44 ka, coinciding with peaks in productivity. Other diagenetic layers in GeoB 4906-3 are not as clearly related to climate. All concerned intervals are marked in Fig. 4 and all succeeding graphics.

5.4.1.2 Magnetic fluxes

Variations in concentration, mineralogy and grain-sizes of the magnetic minerals are shown in Fig. 4. Magnetic mineral concentrations at site GeoB 4905-4 are higher with magnetic susceptibility ranging between 40 and $200x10^{-6}$ SI (Fig. 4a) and between 40 and $120x10^{-6}$ SI at site GeoB 4906-3 (Fig. 4b). Three prominent intervals showing minima in magnetic mineral concentrations occur. These intervals correspond to the B and C clusters on the bivariate plots of Fig. 3 that were shown to be affected by reductive diagenesis. Magnetite is dominant the magnetic signature as indicated by high $S_{-0.3\ T}$ values generally above 0.98. However, the presence of residual hematite is confirmed at the intervals with $S_{-0.3\ T}$ <0.98 due to the preferential depletion of magnetite.

Magnetite grain-size (κ_{arm}/κ) follows a similar trend as $S_{0.3\ T}$. Its down-hole variation is more pronounced, showing a coarser assemblage at the northern location especially during the last glacial (MIS 2). We attribute this to a larger Saharan dust component, while the terrigenous input at the southern location is mostly fluvial.

Most of the samples fall within the SD threshold suggesting that the sediments were deposited in a low energy environment. Although the study area lies in close proximity to the volcanic chain of islands along the Cameroon volcanic line, no significant evidence was seen that suggest accumulation of volcanic material here over the last 52 ka. This is either because these islands might have stopped erupting before 52 ka BP or the volcano-clastic materials were being deposited in another region.

Apart from the intervals with magnetite dissolution, the most significant changes in the magnetic mineral fluxes are observed during the last 16 kyr where a slight but significant shift in the magnetic profiles occurs. There is a slight increase during colder periods as evident

during the Younger Dryas. However, since the middle Holocene detrital input of magnetite has steadily increased.

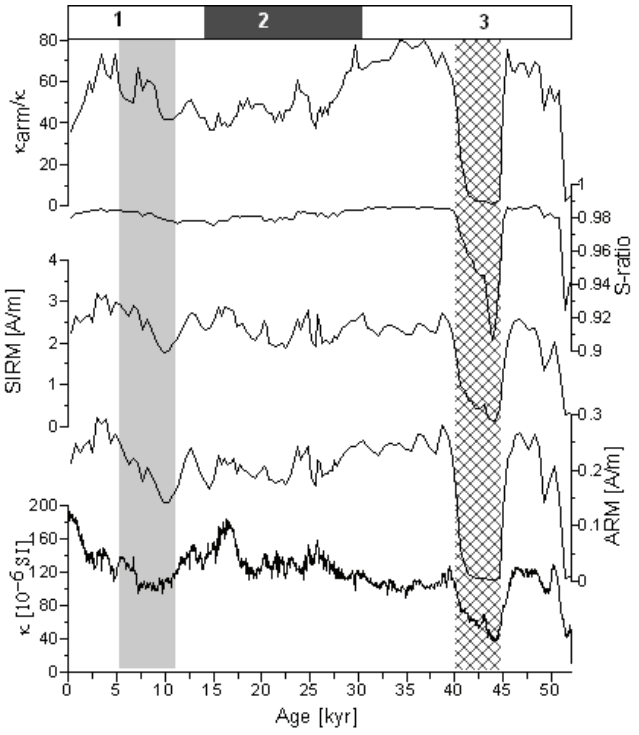

(4a)

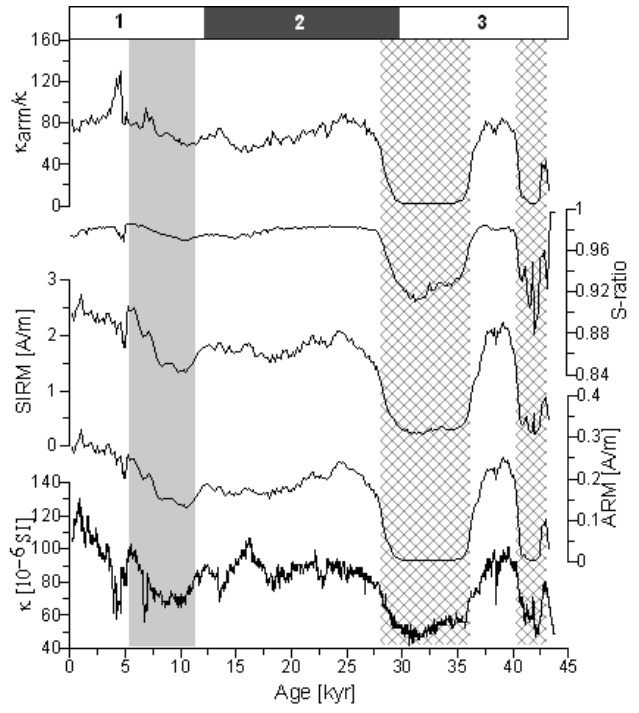

(4b)

Figure 4. Compilation of environmental magnetic records of cores **(a)** GeoB 4905-5 and **(b)** GeoB 4906-3. The grey band represents the AHP while the cross hatch shows intervals severely affected by reductive diagenesis of iron oxides.

5.4.2 Elemental abundances and color reflectance

Profiles of elemental abundances and color reflectance (Fig. 5a and b) show significant variation in sediment fluxes. Fe and Ti are proxies of terrigenous input while Ca represents carbonate content (Adegbie et al., 2001; Zabel et al., 2001).

The variability with respect to amplitude and abundance differs between both locations (Fig. 5a). Fe and Ti correlate positively and are frequently, but not systematically opposed to Ca intensity. Zabel et al. (2001) and Adegbie et al. (2003) have interpreted these signals by mutual dilution of terrigenous and marine input. During the late MIS 3, there was a gradual decrease in Fe and Ti and with lower amplitudes variations. High amplitude oscillations seen in GeoB 4905-4 occur more frequently during the last glacial. A pronounced decrease in Ca deposition at the onset of the last deglaciation probably indicates a drop in marine productivity which remains very low during the Holocene. This drop is observed in both cores. The terrigenous signals remain relatively higher especially in GeoB 4906-3 (Fig. 5b) where Fe increases significantly except for intervals of low Fe between 4-6 and 11.5-14 ka. Fe is higher during the glacial period in the northern location (GeoB 4905-4). Marine productivity in this region is stimulated by upwelling driven by stronger NE trades. Ca content is therefore substantially higher during the last glacial. At the southern location upwelling is generally more intense and Ca intensities double the signal level of the northern location.

Color Reflectance varies between 38-62% in GeoB 4905-4 and 28-46% in GeoB 4906-3 implying that the northern-most core is more enriched in pigmented minerals whereas the low reflectance in the southern core has higher organic matter content.

5.4.2.1 Terrestrial vs. marine fluxes

The variation in terrigenous vs. biogenic accumulation is depicted by the Fe/Ca ratio (Fig. 6a) where high values signify enhanced terrigenous sedimentation. This ratio shows a very high degree of variability in terrigenous input especially at the interglacial periods MIS1 and 3. These signatures are closely correlated to northern hemisphere ice core record (GISP). At about 15 ka the terrigenous content begins to increase, marking the onset of the last African Humid Period (AHP). This is consistent with other records

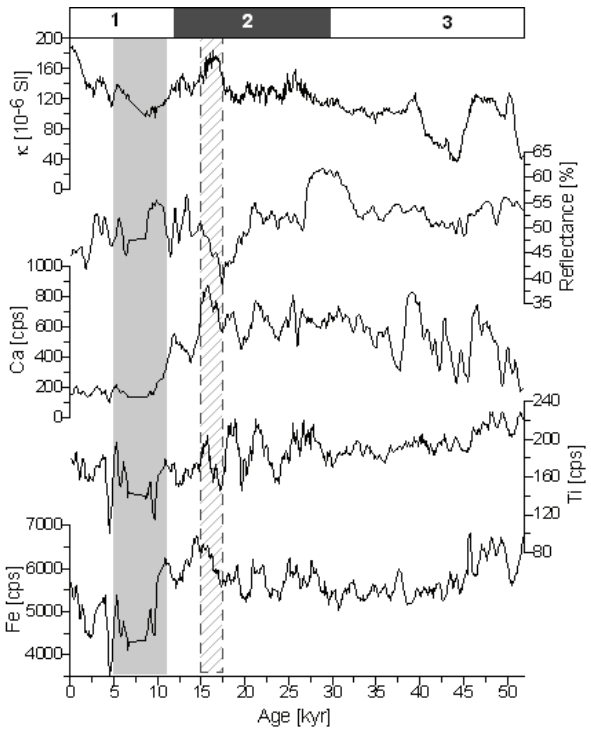

(5a)

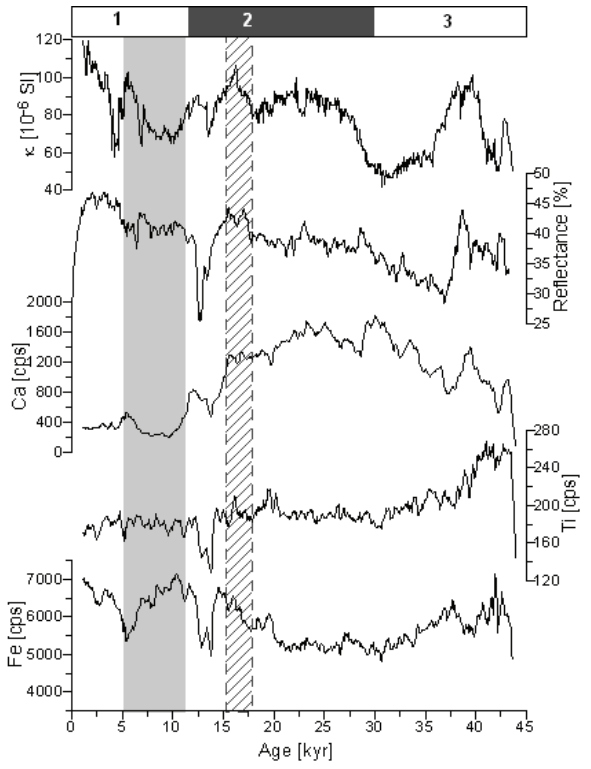

(5b)

Figure 5. Compilation of element and color reflectance records of cores **(a)** GeoB 4905-5 and **(b)** GeoB 4906-3. The grey band is the AHP while the shade shows transition from glacial to interglacial conditions.

e.g., by Maley and Brenac (1998) and deMenocal et al. (2000) identifying the onset of humid conditions at this time. Terrigenous sedimentation was lowered during the Younger Dryas

between 11 and 13 ka followed by a huge and abrupt jump marking the onset of the Holocene (e.g. Garcin et al., 2007 and Weldeab et al., 2007).

The African Humid Period between 12 and 5 ka is a product of the orbital precessional cycles controlling tropical African climate (Kutzbach, 1981; deMenocal et al., 1993, 2000). Summer insolation intensifies at precession maxima strengthening the African monsoon and resulting in intense precipitation and increase vegetation cover over most of North Africa. Model studies by Prell and Kutzbach (1987) show that a summer insolation 8% greater than today results in a 40% increase in precipitation. The last insolation maximum occurred between 9-10 ka and had its impact well imprinted in the sediments from the eastern Equatorial Atlantic (Fig. 6); the period is marked by high terrigenous input (Fe/Ca) and low Ca within the Gulf of Guinea. During this period, most of the Sahara desert was covered by vegetation and contained numerous small and large lakes (Sarnthein, 1978; COHMAP, 1988) strictly limiting aeolian fluxes as a result. The high terrigenous content must therefore be due to precipitation enhanced weathering as a result of greater monsoon strength and higher runoff. The onset and termination of the humid period and the pattern is very similar to that observed by deMenocal et al. (2000a, b) in sediments from the northwest African continental margin.

In contrast, the glacial situations (MIS 2) with lower Fe/Ca ratios are associated with stronger NE trades (Verardo and McIntyre, 1994) stimulating upwelling and marine productivity. Sea level lowstands during glacial periods exposed the shelves of the West African continental margin leading to sediment erosion and export into the ocean (e.g. Bleil and von Dobeneck 2003). At the same time, stronger winds and dryer conditions prevailed, eroding, transporting and depositing aeolian dust into the ocean. We believe these factors to be responsible for the higher fluctuation in terrigenous input at site GeoB 4905-4 situated closer to the southern boundary of the Sahara dust plume. This higher terrigenous flux is however overcompensated by much higher marine productivity during the glacial.

Fe/Ti ratio is an indicator for fluvial vs. aeolian sediment input where low, Ti-rich values are indicative of a higher eolian contribution. Aeolian sediments seem to contribute significantly at the northern location (GeoB 4905-4) with high amplitude oscillations wjich is discussed below.

5.4.2.2 Millennial-scale climate variability during the late Holocene

Unlike the ice core records from the northern hemisphere which show little variability during the Holocene, sediments originating from the central African region document a

significant degree of climate variability during this period. The Holocene record is characterized by millennial to sub-millennial scale climate oscillations that range from hundreds of years to a few thousands of years (Fig. 7a and b). Our sampling resolution corresponds to 40 years for color intensity and 80 years for element data resolving also sub-millennial climate changes. In core GeoB 4905-4 the last ~5.5 kyr are characterized by high amplitude decadal to millennial scale climate changes in reflectance and Fe/Ti. Ti is a good indicator for Saharan dust (Zabel et al., 2001) enriched in the pigmented (reddish-brown) iron minerals hematite and goethite (Balsam et al., 1995, Itambi et al., in revision). The strong positive correlation observed in the reflectance and Fe/Ti (Fig. 7) further confirms that there is a strong aeolian signature indicating drought or reduce precipitation. These occur at the intervals 6.6-5.7, 5.5-4.6, 4.2-3.5, 2.4-1.5 ka.

Similar short term changes in hydrology during the last 16 kyr have been reported from several African lacustrine sediment records: Lake Bosumtwi in West Africa (e.g., Talbot et al., 1984; Street-Perrott and Perrot, 1990; Shanahan et al., 2006), lakes Barombi Mbo, Bambili and Ossa in Cameroon, Central Africa (respectively from Giresse et al., 2005; Stager and Anfang-Sutter, 1999) and Eastern Africa (Barker et al., 2001; Gasse, 2000).

At lake Bosumtwi, lake level fluctuations representing decrease in precipitation have been identified at <13, 11.2-10.10, 8.2-7.1, 4.2-3 and <1 ka. In Eastern Africa these occur at <12 ka, 10.4-9.8, 7.8-7.2, 5.9, 4.5-2.5 and 2-1 ka. Pollen records from Lake Ossa (Giresse et al., 2005) show drying at the intervals 4-3.4, 2.8-2.1 and 1.8-0.5 ka. The two marine records presented here therefore seem to register similar periodic changes in precipitation over central Africa.

The Fe/Ti and reflectance records show that the northern core GeoB 4905-4 is most suitable to register short changes in precipitation over central Africa. Seasonality changes (dry and rainy seasons) are much stronger to the north of central Africa. The dry season becomes lengthy northward whereas the rainy season becomes more dominant to the south. Because the northern boundary of the winter position of the ITCZ and the southern limit of aeolian dust deposition are in proximity, this core is well positioned to register dust and precipitation changes.

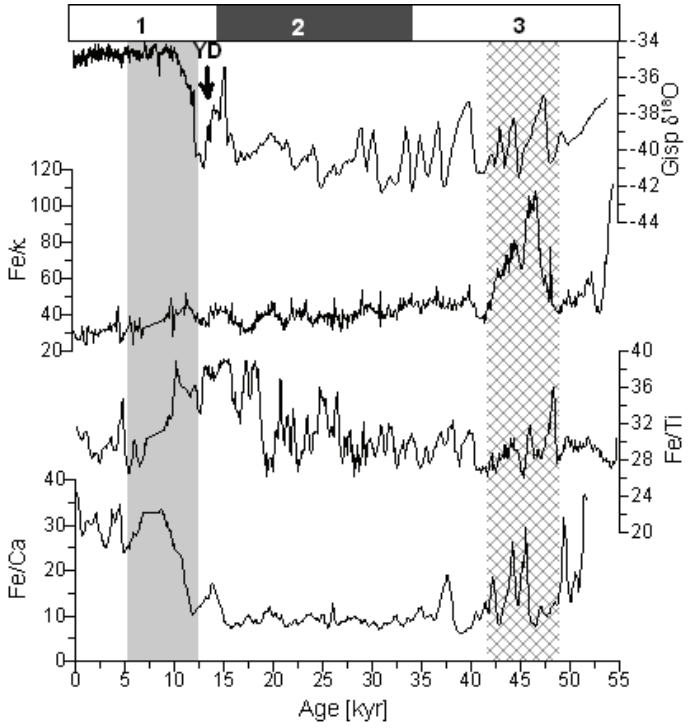

(6a)

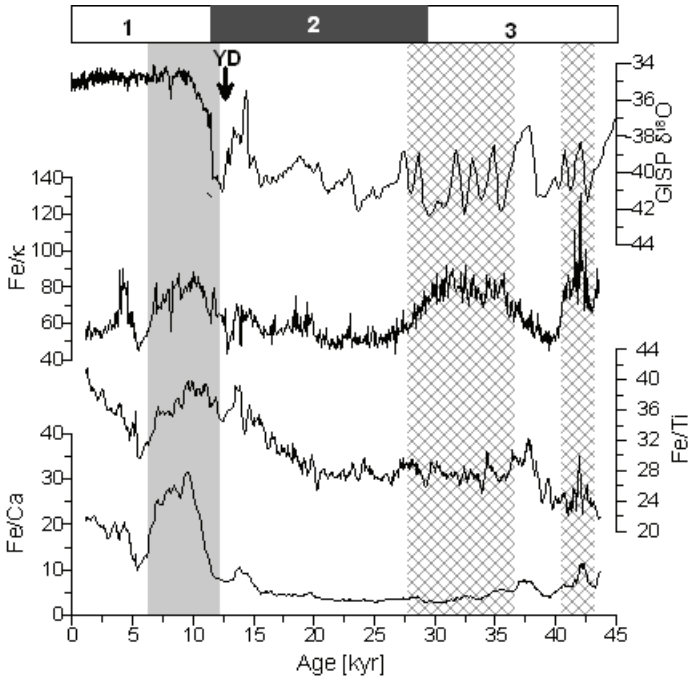

(6b)

Figure 6. Diagnostic ratios of environmental conditions: Fe/Ca indicates the variation in terrigenous vs. biogenic fraction. Fe/Ti is a proxy for determining Saharan dust fluxes with lower values (high Ti) being indicative of higher aeolian input. Fe/K is a diagenesis proxy. Reflectance can also be used to trace Saharan dust. (6a) is GeoB 4905-4, (6b) GeoB 4906-3.

The southern core GeoB 4906-3 receives terrigenous sediments from forested regions with significant rainfall throughout the year, maintaining more humid conditions even during dry periods.

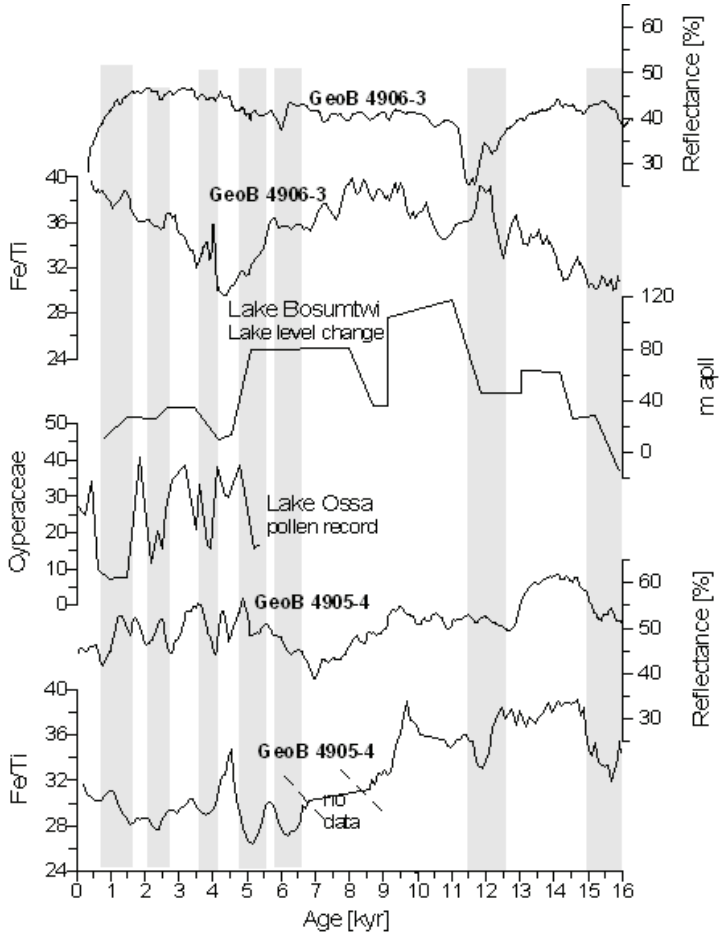

Figure 7. LGM to Holocene section of reflectance and Fe/Ti data. 7 indicate the prominence in both cores and their correlation to lake records from the African continent which indicates changes in aridity during the late Holocene Girresse et al., 2005; Shannahan et al., 2006). Note the high variability at the northern location

The occurrence of humidity oscillations superimposed on the AHP rules out precessional changes in solar insolation as the sole driving force behind precipitation changes over central Africa. Previous studies such as Broeker et al. (1994 2003), Ganopolski and Rahmstorf (2001) and Hemming (2004) have shown that millennial-scale climate changes can be related to the shut down of the deep water circulation during pulses of fresh water input into the north Atlantic. However, this does not explain the significant variations observed in our records during the last 5.5 kyr as sea level hasn't changed much during this period (Fairbanks, 1989 and Perrott and Perrott, 1990). We therefore believe that the Holocene climate variability in central Africa is rather driven by regionally acting mechanisms which are not imprinted in the high latitude records. This assertion is supported by Schefuß et al. (2005) who attributed the SST gradient in tropical and subtropical south Atlantic to precipitation changes over central Africa.

5.5 Conclusions

Combining high-resolution rock magnetic, element and reflectance measurements has been an effective strategy to reconstruct the paleoclimate and sedimentary environment of the Gulf of Guinea, deciphering in detail the depositional and post-depositional processes of the last 52 ka. The record of the Fe/κ_{nd} and magnetic parameters shows that the sediments of this region have been affected by iron diagenesis at varying intensities, depending on the organic carbon supply and bottom-water oxygenation. Our results demonstrate that the African climate varied during the Holocene with several intervals of aridity, consistent with on-shore lake records. Variability during the AHP demonstrates and supports the argument that the African climate variability is controlled both by orbital forcing as well as monsoonal precipitation.

6. Conclusion and recommendations

6.1 Conclusion

The multi proxy approach employed in this study proved to be valuable as was demonstrated in Chapter 2 where magnetic parameters were able to distinguish the low resolution Heinrich signals. A combination with the geochemical proxies was able to reveal millennial scale oscillations in the southern-most core. We have therefore been able to determine the true complexity of these records by integrating the various techniques

This study was able to identify the variation of northwest African climate which shows variations at two time scales synchrounous with North Atlantic Heinrich Events and Dansgaard-Oeschger cycles. Drier conditions persisted over northwestern Africa, at Heinrich events, generating stronger winds which eroded and deposited Saharan dust into the ocean. Model results show that the weakening of the Atlantic meridional overturning circulation (AMOC) is directly linked to such climatic changes over Africa. Future projections show that weakening of AMOC by anthropogenic induced warming. The northwest African climate will therefore be severely impacted by human activities should the current trends in global warming persist.

Dansgaard-Oeschger cycles on the other hand are more prominent and are the dominant signatures in the southern-most location at 12°N. This location which showed little fluctuation in wind speeds is more susceptible to precipitation changes resulting from weakening of the West African monsoon. Occurrence of the signals south of 13 °N therefore suggests that aridity occurs further south of the Sahel at shorter times-scales than previously recognized.

The latitudinal dependence of the climatic signals suggests that a climatic boundary existed between 12 and 13°N during the last glacial period. This implies the northern summer boundary of the ITCZ shifted to the south.

The Holocene period was also quite unstable. Unlike previous believes that tropical African climate was entirely controlled by orbital forcing, recent studies supported by this work shows that a second climate forcing that result in millennial-scale oscillation in climate in this regions exists. The last 5.5 kyr saw many periods of reduced rainfall over central Africa which also relate to the weakening of the West African monsoon.

Detailed characterizations of the magnetic mineral assemblages revealed that non climate related sources have little impact on the magnetic signals. Glacial sediments are composed of primary minerals of detrital origin that have undergone minimal post depositional alteration. Magnetic minerals of volcanic origin and secondary minerals were

observed that do not significantly contribute to the primary signals. The interglacial samples showed strong evidence for reductive diagenesis. The wide spread of the dissolution at all the interglacial intervals of several depths studied suggests that this post-depositional process was climate related, probably linked to high productivity during these climatic periods.

6.2 Recommendations

The study has shed more light into climate variability over northwest Africa, and the factors that drive such change in climate as well as environmental factors that may mask or destroy the primary magnetic signals that are climate related. However, a number of questions were raised in the course of the research that need to be further investigated.

The African humid period (AHP) represent an important climatic period over north Africa that has been well documented, displaying abrupt onset and termination at 12.8 and 5.5 kyr respectively (deMenocal et al., 2000a; Adkins et al., 2006). The findings in this thesis suggest termination at 3 kyr. The 3 kyr termination is far later than was reported at 20°N by deMenocal et al. (2000a). Although some African lakes show termination around 3 ka, terrigenous flux in marine sediment has only been reported between 5 and 6 kyr. Since the top 15 kyr were data by linear interpolation, the observed discrepancy might be as a result of the dating. It is therefore suggested that a more constrained age model be developed for the top 15 kyr for these cores. If the 3 kyr observed in our records are correct, this will represent a significant latitudinal difference in climate during the Holocene.

Although the superparamagnetic particles have been shown to be present in this area (Itambi et al. (2008), and this study), the magnetic phase has still not been confirmed. Because the scanning electron microscope is not able to resolve such ultra fine particles, further work should be done using transmission electron microscope. Bacterial magnetite of ultra fine grain has been widely reported in marine sediments and can significantly affect the climatic signals. It is therefore important to identify this fraction.

References

Adamec, D., J. J. O'Brien (1978), The seasonal upwelling in the Gulf of Guinea due to remote forcing. *J. Phys. Oceanogr,* 8: 1050-1060.

Abreu, L. de., N. J. Shackleton, J. Schönfeld, M. Hall, and M. Chapman (2003), Millennial-scale oceanic climate variability off the Western Iberian margin during the last two glacial periods, *Mar. Geol.*, 196, 1-20.

Adegbie, A. T. (2001), Reconstruction of paleoenvironmental conditions in Equatorial Atlantic and the Gulf of Guinea basins for the last 245,000 years. *Berichte*, Fachbereich Geowissenschaften Universität Bremen, Bremen. 178p.

Adegbie, A. T., R. R. Schneider, U. Röhl, G. Wefer (2003), Glacial millennial-scale fluctuations in central African precipitation recorded in terrigenous sediment supply and freshwater signals offshore Cameroon, *Palaeogeo. Palaeocli. Palaeoeco*., 197, 323-333.

Adkins, J., P. deMenocal, G. Eshel (2006), The "African Humid Period" and the record of marine upwelling from excess 230^{Th} in Ocean Drilling Program Hole 658C, *Paleoceanography,* 21, 4203.

Arimoto, R. (1995), Trace elements in the atmosphere over the North Atlantic, *J. Geophys. Res*., 100, 1199-1213.

Arz, H. W., J. Pätzold, and G. Wefer (1998), Correlated millennial-scale changes in surface hydrography and terrigenous sediment yield inferred from last-glacial marine deposits off northeastern Brazil, *Quaternary Research,* 50, 157-166.

Baldi, M. F. Meneguzzo, A. D. Giovanni, G. Maracchi, M. Pasqui, V. Capecchi, A. Crisci, F. Piani (2003), Guinea Gulf SST and Mediterrenian summer climate: analysis of interannual variability. Proceedings of the Sixth European Conference on Applications of Meteorology, Rome, 15-19 September 2003.

Balsam, W. L., and B. C. Deaton (1991), Sediment dispersal in the Atlantic Ocean: evaluation by visible light spectra, *Rev. Aquat. Sci.,* 4, 411-447.

Balsam, W. L., B. L. Otto-Bliesner, and B. C. Deaton (1995), Modern and last glacial maximum aeolian sedimentation patterns in the Atlantic Ocean interpreted from sediment iron oxide content, *Paleoceanography,* 10, 493-507.

Balsam, W. L., B. C. Deaton and J. E. Damusth (1999), Evaluating the optical lightness as a proxy for carbonate content in marine sediment cores: implication for marine sedimentation, *Mar Geol* 161: 141–153.

Bando, Y., M. Kiyama, N. Yamamoto, T. Takada, T. Shinjo and H. Takaki (1965), The magnetic properties of α-Fe_2O_3 fine particles, *J. Phys. Soc. Jpn.* 20 2086.

Bard, E., F. Rostek, J. -L. Turon, and S. Gendreau (2000), Hydrological impact of Heinrich Events in the subtropical northeast Atlantic, *Science,* 289, 1321-1324.

Barker, P. A., F. A. Street-Perrott, M. J. Leng, P. B. Greenwood, D. L. Swain, R. A. Perrott, R. J. Telford and K. J. Ficken (2001), A 14,000-year oxygen isotope record from diatom silica in two alpine lakes on Mt. Kenya. *Science* 292: 2307-2310.

Berner, R. A. (1980), *Early Diagenesis, A Theoretical Approach*, Princeton University Press.

Besser, P. J., A. H.Morrish and C. W. Searle (1967), Magnetocrystalline anisotropy of pure and doped hematite, *Phys. Rev.* 153, 632-640.

Beveridge, A. A. S., H. Elderfield and N. J. Shackleton (1995), Deep thermohaline circulation in the low-latitude Atlantic during the last glacial, *Paleoceanography* 10, 643–660.

Bickert, T. and G. Wefer (1996), Late Quaternary deep-water circulation in the South Atlantic: Reconstruction from carbonate dissolution and benthic stable isotopes, In W. H. Berger, G. Wefer, G. Siedler "The South Atlantic: Present and past circulation". Springer, 599-620.

Binet, D., E. Marchal (1993), The Large Marine Ecosystem of Shelf Areas in the Gulf of Guinea: Long-Term Variability Induced by Climatic Changes. In *Large Marine Ecosystems - Stress Mitigation and Sustainability*, K. Sherman, L. M. Alexander, B. Gold, Eds. American Association for the Advancement of Science, Washington; 104-118.

Bleil, U., T. von Dobeneck (1999), Geomagnetic events and relative paleointensity records - clues to high resolution paleomagnetic chronostratigraphies of late Quaternary marine sediments, In G. Fischer, G. Wefer, (eds) *Use of Proxies in* Paleoceanography, Examples from the South Atlantic. *Springer*, Berlin; 635-654.

Bloemendal, J., B. Lamb and J. King (1988), Paleoenvironmental implications of rock-magnetic properties of late Quaternary sediment cores from the eastern Equatorial Atlantic, *Paleoceanography,* 3, 61-87.

Bloemendal, J., J. W. King, F. R. Hall and S. J. Doh (1992), Rock magnetism of Late Neogene and Pleistocene deep sediments: relationship to sediment source, diagenetic processes and sediment lithology, *J. Geophys. Res.,* 97, 4361-4375.

Bloemendal, J., J. W. King, A. Hunt, P. B. deMenocal, A. Hayashida (1993), Origin of the sedimentary magnetic record at Ocean Drilling Program sites on the Owen Ridge, western Arabian Sea. *J. Geophys. Res.,* 98, 4199-4219.

Bonan, G. B., et al. (2002), The land surface climatology of the community land model coupled to the NCAR community climate model, *J. Clim.*, 15, 3123-3149.

Bond, G., H. Heinrich, W. Broecker, L. Labeyrie, L. McManus, J. Andrews, S. Huon, R. Jantschik, S. Clasen, C. Simet, K. Tedesco, M. Klas, G. Bonani, and S. Ivy (1992), Evidence for massive discharges into the North-Atlantic Ocean during the last glacial period, *Nature.*, 360, 245-249.

Bond, G. C., W. S. Broecker, S. Johnsen, J. F. McManus, L. Labeyrie, J. Jouzel, and G. Bonani (1993), Correlation between climate records from North Atlantic sediments and Greenland ice, *Nature,* 365, 143-147.

Bond, G. C., and R. Lotti (1995), Iceberg discharges into the North Atlantic on millennial time scales during the last glaciation, *Science,* 267, 1005-1010.

Bond, G., W. Showers, M. Cheseby, R. Lotti, P. Almasi, P. deMenocal, P. Priore, H. Cullen, I. Hajdas and G. Bonani (1997), A pervasive millennial scale cycle in North Atlantic Holocene and glacial climates, *Science* 278:1257-1266.

Braconnot, P., et al. (2007), Results of PMIP2 coupled simulations of the Mid-Holocene and Last Glacial Maximum – Part 2: feedbacks with emphasis on the location of the ITCZ and mid- and high latitudes heat budget, *Clim. Past*, 3, 279-296.

Broecker, W. S. (1994), Massive iceberg discharges as triggers for global climate change, *Nature*, 372, 421-424.

Broecker, W. S. (2000), Abrupt climate change: Causal constraints provided by the paleoclimate record, *Earth Sci. Rev*., 51, 137-154.

Broecker, W. S. (2003), Does the trigger for abrupt climate change reside in the ocean or in the atmosphere, *Science,* 300, 1519-1522.

Brovkin, V., M. Claussen, V. Petoukhov and A. Ganopolski (1998), On the stability of the atmosphere-vegetation system in the Sahel and Sahara region. *J. Geophys. Res.* 103 (D4): 31613-31624.

Brownlee, D. E. (1981), Extraterrestrial components, in The Sea, vol. 7, 733–762, edited by C. Emiliani, John Wiley, New York.

Brownlow, A., E. W. Hunter and D. W. Parkin (1966), Cosmic spherules in a Pacific core, Geophys. J. R. Astron. Soc., 12, 1–12.

Butler, R. F., S. K Banerjee (1975), Single-domain grain size limits for metallic iron. *J. Geophys. Res.* 80: 252-259.

Butler, I. B. and Rickard (2000),Framboidal pyrite formation via the oxidation of iron (II) monosulphide by hydrogen sulphide, *Geochimica et Cosmochimica Acta* 64 2665-2672.

Cacho, I., J. O. Grimalt, C. Pelejero, M. Canals, F. J. Sierro, J. A. Flores, and N. Shackleton (1999), Dansgaard-Oeschger and Heinrich event imprints in Alboran Sea paleotemperatures, Paleoceanography, 14(6), 698-705.

Cane, M. and A. C. Clement (1999), in *Mechanisms of Global Climate Change at Millennial Time Scales*, P. U. Clark, R. S. Webb, L. D. Keigwin, Eds. *Geophysical Monograph 112, American Geophysical Union, Washington, DC*, 373-383.

Canfield, D. E. and R. A. Berner (1987), Dissolution and pyritization of magnetite in anoxic marine sediments, *Geochim. Cosmochim. Acta., 51*, 645-659.

Charney, J. G. (1975), Dynamics of Deserts and Drought in Sahel, *Q. J. Roy. Meteor. Soc.*, 101, 193-202.

Chiang, J. C. H., and A. Koutavas (2004), Climate change- Tropical flip-flop connections, *Nature, 432*, 684-685.

Citeau, J., et al. (1989), Questions relative to ITCZ migrations over the tropical Atlantic Ocean, sea surface temperature and Senegal River runoff, *Meteorol. Atmos. Phys.* , 41, 181-190.

Coey, J. M. D. (1988), Magnetic properties of iron in soil iron oxides and clay fractions. In: Stucki JW et al (eds) Iron in soils and clay minerals, Reidel, Dordrecht, 397-466.

COHMAP members. 1988. Climatic changes of the last 18,000 years: Observations and model simulations. *Science* 241: 1043-1052.

Cook, K. H., and E. K. Vizy (2006), Coupled model simulations of the west African monsoon system: Twentieth- and Twenty-First-century simulations, *J. Clim.,* 19, 3681-3703.

Cornell, R. M. and U. Schwertmann (1996), The Iron Oxides: Structure, Properties, Reactions, Occurrence and Uses, VCH.

Curry, W. B. and G. P. Lohmann (1986), Late quaternary carbonate sedimentation at the Sierra Leone Rise (Eastern Equatorial Atlantic Ocean). *Mar. Geo*. 70, 223–250.

Curry, W. B. and G. P. Lohman (1990), Reconstructing past particle fluxes in the tropical Atlantic Ocean. *Paleoceanography* 5, 487–505.

Dahl, K., et al. (2005), Assessing the role of North Atlantic freshwater forcing in millennial scale climate variability: a tropical Atlantic perspective, *Clim. Dyn.,* 24, 325-346.

Dansgaard, W., S. J. Johnson, H. B. Claussen, D. Dahl-Jensen, N. S. Gundestrup, C. U. Hammer, C. S. Hvidberg, J. P. Steffensen, A. E. Sveinbjörndottir, J. Jouzel, and G. Bond (1993), Evidence for general instability of past climate from a 250-kyr ice core record, *Nature*, 364, 218-220.

Dearing, J. A., R. J. L. Dann, K. Hay, J. A. Lees, P. J. Loveland, B. A. Maher, and K. O'Grady (1996), Frequency-dependent susceptibility measurements of environmental materials, *Geophys. J. Int*., 124, 228-240.

Dekkers, M. J. (1997), Environmental magnetism: an introduction, *Geol. Mijnbouw,* 76, 163-182

Dekkers, M. J. (2007). Magnetic proxy parameters, *In:* D. Gubbins and E. Herrero-Bervera (eds.), *Encyclopedia of Geomagnetism and Palaeomagnetism*. Springer, 525-534.

Dekkers, M. J., J. L. Mattéi, G. Fillion and P. Rochette (1989), Grain size dependence of the magnetic behaviour of pyrrhotite during its low temperature transition at 34 K, *Geophys. Res. Lett.,* 16, 855–858.

deMenocal, P. B., W. F. Ruddiman, and E. M. Pokras (1993), Influence of high- and lowlatitude on African terrestrial climate; Pleistocene aeolian records from equatorial Atlantic Ocean Drilling Program Site 663, *Paleoceanography,* 8, 209-242.

deMenocal, P. B. (1995), Plio-Pleistocene African climate, *Science*, 270, 53-59.

deMenocal, P. B., J. Adkins, J. Ortiz, and T. Guilderson (2000), Millennial-Scale Sea-Surface Temperature Variability During The Last Interglacial and its Abrupt Termination, Eos Trans. AGU, 81 (48), Fall Meet. Suppl.

deMenocal, P. J. Ortiz, T. Guilderson, J. Adkins, M. Sarnthein, L. Baker and M. Yarusinsky (2000a), Abrupt onset and termination of the African Humid Period: rapid climate responses to gradual insolation forcing, *Quat. Sci. Rev.,* 19, 347-361.

deMenocal, P. J., T. Guilderson, and M. Sarnthein (2000b), Coherent High- and Low-Latitude Climate Variability During the Holocene Warm Period, *Science.,* 288, 2198-2202.

deMenocal, P., J. Bloemendal, and J. King (1991), A rock-magnetic record of monsoonal dust deposition to the Arabian Sea: evidence for a shift in the mode of deposition at 2.4 Ma. *In* Prell, W. L., Niitsuma, N., et al., *Proc. ODP, Sci. Results,* 117: College Station, TX (Ocean Drilling Program), 389-407.

Douville, H., et al. (2006), On the tropical origin of uncertainties in the global land precipitation response to global warming, *Clim. Dyn.*, 26, 367-385.

Duplessy, J. C., N. J.Shackleton, R. G. Fairbanks, L. Labeyrie, D. Oppo, N. Kallel (1988), Deep water source variations during the last climatic cycle and their impact on the global deep water circulation. *Paleoceanography* 3, 343–360.

Dupont, L. M., et al. (2008), Thirty thousand years of vegetation development and climate change in Angola (Ocean Drilling Program Site 1078), *Clim. Past Discuss.*, *4*, 111-147.

Dunlop, D. J. and Ö. Özdemir (1997), *Rock Magnetism: Fundamentals and Frontiers. Cambridge Studies in Magnetism,* Cambridge University Press.

El Goresy, A. (1968), Electron microprobe analysis and Ore microscopic study of magnetic spherules and grains collected from the Greenland Ice, *Beitr. Min. und Petr.* 17, 331-346.

EPICA Project-Members (2006), One-to-one coupling of glacial climate variability in Greenland and Antarctica, *Nature*, 444, 195-198.

Evans, M., and F. Heller (2003), Environmental Magnetism: Principles and Applications of Enviromagnetics, *Academic Press*. 293p.

Fairbanks, R. G. (1989), A 17,000-year glacio-eustatic sea level record: influence of glacial melting rates on the Younger Dryas event and deep-ocean circulation. *Nature* 342: 637-642.

Fairbanks, R. G., et al. (2005), Radiocarbon calibration curve spanning 0 to 50,000 years BP based on paired 230Th/234U/238U and 14C dates on pristine corals, *Quat. Sci. Rev.*, 24, 1781-1796.

Fang X-M, Y. Ono, H. Fukusawa, P. Bao-Tian, J. J. Li, G. Dong-Hong, K. Oi, S. Tsukamoto, M. Torii and T. Mishima (1999), Asian summer monsoon instability during the past 60,000 years: magnetic susceptibility and pedogenic evidence from the western Chinese Loess Plateau. *Earth Planet Sci Lett* 168, 219–232.

France, D. E. and F. Oldfield (2000), Identifying goethite and hematite from rock magnetic measurements of soils and sediments, *J. of Geophys. Res.* 105, 2781-99.

Franke, C., T. Frederichs and M. J. Dekkers (2007a), Efficiency of heavy liquid separation to concentrate magnetic particles, *Geophys. J. Int.,* 170, 1053-1066.

Franke, C., T. von Dobeneck, M. R. Drury, J.D. Meeldijk and, M. J. Dekkers (2007b), Magnetic Petrology of Equatorial Atlantic Sediments: Electron Microscopic Results and their Environmental Magnetic Implications, *Paleoceanography*, 22, 4207.

Frederichs, T., U. Bleil, K. Däumler, T. von Dobeneck, and A. M. Schmidt (1999), The magnetic view on the marine paleoenvironment: Parameters, Techniques and Potentials of rock magnetic studies as a key to paleoclimatic and paleoceanographic changes. In G. Fischer and G. Wefer (eds), Use of proxies in paleoceanography: Examples from the South Atlantic. *Springer*, 575-599.

Fredriksson, K. and L. R. Martin (1963), The origin of black spherules found in the Pacific islands, deep-sea sediments, and Antarctic ice, *Geoch. Cosm. Acta* 27, 245-248.

Freeman, R. (1986), Magnetic mineralogy of pelagic limestones, *Geophys. J. R. astr. Soc.,* 85, 433-452.

Froelich, P. N., G. P. Klinkhammer, M. L. Bender, N. A. Luedtke, G. R. Heath, D. Cullen, P. Dauphin, D. Hammond, B. Hartman and V. Maynard (1979), Early diagenesis of organic matter in pelagic sediments of the eastern equatorial Atlantic: suboxic diagenesis, *Geochimica et Cosmochimica Acta* 43 1075-1090.

Fischer, G., B. Donner, V. Ratmeyer, R. Davenport, and G. Wefer (1996), Distinct year-to-year particle flux variations off Cape Blanc during 1988-1991: relation to d18O-deduced sea-surface temperatures and trade winds, *J. Mar. Res., 54*, 73-98.

Folland, C. K., et al. (1986), Sahel rainfall and worldwide sea temperatures, 1901-85, *Nature*, 320, 602-607.

Funk, J. A., T. von Dobeneck, and A. Reitz (2004), Integrated rock magnetic and geochemical quantification of redoxomorphic iron mineral diagenesis in Late Quaternary sediments from the Equatorial Atlantic. In G. Wefer, S. Mulitza and V. Ratmeyer (eds) The South Atlantic in the Late Quaternary: Reconstruction of Material Budget and Current Systems. *Berlin, Springer-Verlag*: 237-260.

Funk, J. A., T. von Dobeneck, T. Wagner and S. Kasten (2004b), Late quaternary sedimentation and early diagenesis in the Equatorial Atlantic Ocean: patterns, trends and processes deduces from rock magnetic and geochemical records, In The South Atlantic in the Late Quaternary: Reconstruction of Material Budgets and Current Systems, pp. 461–497, eds Wefer, G., Mulitza, S. & Ratmeyer, V., Springer-Verlag, Berlin.

Gac, J. Y., and A. Kane (1986a), Le fleuve Sénégal. I- Bilan hydrologique et flux continentaux de matières particulaires à l'embouchure, *Sci. Geol. Bull.,* 39(1*),* 99-130.

Gac, J. Y., and A. Kane (1986b), Le fleuve Sénégal II- Flux continentaux de matières dissoutes a I'embouchure, *Sci. Geol. Bull.,* 39(2), 151-72.

Gaillardet, J., B. Dupre, P. Louvat, and C. J. Alle`gre (1999), Global silicate weathering and CO2 consumption rates deduced from the chemistry of large rivers. *Chem. Geo.* 159: 3–30.

Garcin, Y., A. Vincens, D. Williamson, G. Buchet, J. Guiot (2007), Abrupt resumption of the African monsoon at the Younger Dryas-Holocene climatic transition. *Quat. Sci. Rev.* 26: 690–704.

Garming, J. F. L., U. Bleil and N. Riedinger (2005), Alteration of magneticmineralogy at the sulfate methane transition: analysis of sediments from the argentine continental slope, *Phys. Earth Planet. Inter.,* 151, 290–308.

Garming, J. F. L., U. Bleil, C. Franke and T. von Dobeneck (2007), Low-temperature partial magnetic self-reversal in marine sediments by magnetostatic interaction of titanomagnetite and titanohematite intergrowths, *Geophys. J. Int.,* 170 (3), 1067-1075.

Gasse, F. (2000), Hydrological changes in the African tropics since the Last Glacial Maximum. Quat. Sci. Rev. 19: 189-211.

Gasse, F, E. van Campo (1994), Abrupt post-glacial climate events in West Asia and North Africa monsoon domains. *Earth and Planet. Sci. Rev.* 1256: 435–456.

Ganopolski, A. and S. Rahmstorf (2001), Rapid changes of glacial climate simulated in a coupled climate model, *Nature,* 409, 153-158.

Giresse, P., J. Maley and A. Kossoni (2005), Sedimentary environmental changes and millennial climatic variability in a tropical shallow lake (Lake Ossa, Cameroon) during the Holocene, *Palaeogeo., Palaeocli.Palaeoeco.* 218: 257–285.

Glaccum, R. A. (1978), The mineralogical and elemental composition of mineral aerosols over the tropical North Atlantic; the influence of Saharan dust, Master's thesis, University of Miami. Coral Gables, FL, 161 p.

Goldhaber, M. B. and I. R. Kaplan (1974), *The Sulfur Cycle*. In: E.D. Goldberg, Editor, *The Sea* **vol. 5**, Wiley-Interscience, New York pp. 569–655.

Govindaraju, K. (1994), compilation of working values and descriptions for 383 geostandards, *Geostandard. Newslett.,* 18, 1–158.

Grousset, F. E., et al. (1998), Saharan wind regimes traced by the Sr-Nd isotopic composition of subtropical Atlantic sediments: Last Glacial Maximum vs today, *Quat. Sci. Rev*, 17, 395-409.

Hagen, E. (2001), Northwest African upwelling scenario, *Oceanol. Acta., 24*, 113-128.

Hagen, E., and R. Schemainda (1984), Der Guineadom im ostatlantischen Stromsystem, *Beitr. Meereskunde,* 51, 5-27.

Hales, K., et al. (2006), Interaction of vegetation and atmospheric dynamical mechanisms in the mid-holocene African monsoon, *J. Clim.*, 19, 4105-4120.

Heinrich, H. (1988), Origin and consequences of cyclic ice rafting in Northeast Atlantic Ocean during the past 130000 years, *Quat. Res.*, 29, 142-152.

Hemming, S. R. (2004), Heinrich events: Massive late pleistocene detritus layers of the North Atlantic and their global climate imprint, *Rev. of Geophys.*, 42, RG1005.

Heslop, D. and M. Dillon (2007), Unmixing magnetic remanence curves without a priori knowledge, *Geophys. J. Int.* 170(2), 556-566.

Heslop, D., T. von Dobeneck, and M. Höcker (2007), Using non-negative matrix factorization in the unmixing of diffuse reflectance spectra, *Mar. Geol.,* 241, 63-78.

Holz, C., J. B. W. Stuut and R. Henrich (2004), Terrigenous sedimentation processes along the continental margin off NW Africa: implications from grain-size analysis of seabed sediments, *Sedimentology,* 51, 1145-1154.

Horng, C. -S. and A. P. Roberts (2006), Authigenic or detrital origin of pyrrhotite in sediments?: Resolving a paleomagnetic conundrum, *Earth Planet. Sci. Lett.*, 241, 750-762.

Jacobs, I. S. (1963), Metamagnetism of siderite ($FeCO_3$). *J. Appl. Phys.* 34, 1106–1107.

Kakol, Z., J. Sabol, J. Strickler, A. Kozlowsiki and J. M. Honig (1994), Influence of titanium doping on the magnetocrystalline anisotropy of magnetite, *Phys. Rev. B.,* 49, 12767-12772.

Imbrie, J., J. D. Hays, D. G. Martinson, A. McIntyre, A. C. Mix, J. J. Morley, N. G. Pisias, W. L. Prell, and N. J. Shackleton (1984), The orbital theory of Pleistocene climate: Support from a revised chronology of the marine $\delta^{18}O$ record. In: Berger, A. und J. Imbrie (eds.), Milankovitch and Climate. D. Reidel, *Norwell, Mass*., 269-305.

Itambi, A. C., T. von Dobeneck, S. Mulitza, T. Bickert and D. Heslop (*2008*) Millennial-scale North West African droughts relates to H Events and D-O Cycles: Evidence in marine sediments from off-shore Senegal, *Paleoceanography*.

Jansen, J. H. F., S. J. Van der Gaast, B. Koster, and A. J. Vaars (1998), CORTEX, a shipboard XRF-scanner for element analyses in split sediment cores, *Mar. Geol.,* 151, 143-153.

Jullien, E., et al. (2007), Low-latitude "dusty events" vs. high-latitude "icy Heinrich events", *Quat. Res.*, 68, 379-386.

Kalnay, E., et al. (1996), The NCEP/NCAR 40-year reanalysis project, *B. Am. Meteorol. Soc.*, 77, 437-471.

Kattan, Z., J. Y. Gac, and J. L. Probst (1987), Suspended sediment load and mechanical erosion in the Senegal Basin, Estimation of the surface runoff concentration and relative contributions of channel and slope erosion, *J. Hydrol., 92*, 59-76.

Karlin, R., and S. Levi (1983), Diagenesis of magnetic minerals in recent hemipelagic sediments, *Nature,* 303, 327-330.

Karlin, R., M. Lyle, and G. R. Heath (1987), Authigenic magnetite formation in sub-oxic marine sediments, Nature*,* 326, 490-493.

Kennett, J. P., and B. L. Ingram (1995), A 20,000-year record of ocean circulation and climate change from the Santa Barbara Basin, *Nature,* 377*,* 510-514.

King, J., S. K. Banerjee, J. Marvin and O. Ozdemir (1982), A comparison of different magnetic methods for determining the relative grain-size of magnetite in natural materials: some results from lake sediments, *Earth Planet. Sci. Lett.,* 59*,* 404-419.

King, J. W., J. E. T. Channel (1991), Sedimentary magnetism, environmental magnetism, and magnetostratigraphy.*Rev. Geophys. Suppl. (IUGG Report-Contributions in Geomagnetism and Paleomagnetism),* 29: 358–370.

Kruiver, P. P., M. J. Dekkers and D. Heslop (2001), Quantification of magnetic coercivity components by the analysis of acquisition curves of isothermal remanent magnetisation, *Earth Planet. Sci. Lett.* 189, 269– 276.

Kutzbach, J. E. (1981), Monsoon climate of the early Holocene: climate experiment with the earth's orbital parameters for 9000 years ago, *Science,* 214, 59-61.

Kutzbach, J. E, F. A. Street-Perrott (1985), Milankovitch forcing of fluctuations in the level of tropical lakes from 18 to 0 kyr BP. *Nature* 317: 130-134.

Kutzbach, J. E. (1996), Vegetation and soil feedbacks on the response of the African monsoon to orbital forcing in the early to middle Holocene. *Nature* 384: 623-62.

Koopmann, B. (1981), Sedimentation von Saharastaub im subtropischen Nordatlantik während der letzten 25.000 Jahre, *Meteor Forsch.,* 35, 23-59.

Lamb, P. J. (1978), Large-Scale Tropical Atlantic Surface Circulation Patterns Associated with Sub-Saharan Weather Anomalies, *Tellus*, 30, 240-251.

Larrasoaña, J. C., A. P. Roberts, E. J. Rohling, M. Winklhofer and R. Wehausen (2003), Three million years of monsoon variability over the northern Sahara, *Clim. Dyn*., 21, 689-698.

Lee, D. D., and H. S. Seung (1999), Learning the parts of objects by non-negative matrix factorization, *Nature,* 401, 788-791.

Legates, D. R., and C. J. Willmott (1990), Mean Seasonal and Spatial Variability in Gauge-Corrected, Global Precipitation, *Int. J. Clim.*, 10, 111-127.

Lennie, A. R., K. E. R. England and D. J. Vaughan (1995), Transformation of synthetic mackinawite to hexagonal pyrrhotite: a kinetic study, *Am. Mineral.* 80, 960–967.

Leslie, B. W., D. E. Hammond, W. M. Berelson, S. P. Lund (1990), Diagenesis in anoxic sediments from the California borderland and its influence on iron, sulfur and magnetite behavior. *J. Geophys. Res.* 95: 4453-4470.

Levis, S., et al. (2004), Soil feedback drives the mid-Holocene North African monsoon northward in fully coupled CCSM2 simulations with a dynamic vegetation model, *Clim. Dyn.*, 23, 791-802.

Liu, Z., et al. (2007), Simulating the transient evolution and abrupt change of Northern Africa atmosphere-ocean-terrestrial ecosystem in the Holocene, *Quat. Sci. Rev.*, 26, 1818-1837.

Liu, Z. Y., et al. (2006), On the cause of abrupt vegetation collapse in North Africa during the Holocene: Climate variability vs. vegetation feedback, *Geophys. Res. Lett.*, *33*, L22709, doi:10.1029/2006GL028062.

McCabe, C., R. Sassen and B. Saffer (1987), Occurrence of secondary magnetite within biodegraded crude oil, *Geology* 15, 7–10.

Maher, B. A. (1988), Magnetic properties of some synthetic sub-micron magnetites, *Geophys. J.,* 94, 83-96.

Maher, B. A., R. Thompson (1999), Paleomonsoons: I. The magnetic record of paleoclimate in the terrestrial loess and paleosol sequence. In: B.A. Maher and R. Thompson, Editors, *Quaternary climates, environments, and magnetism*, University Press, Cambridge 81–125.

Maley, J., P. Brenac (1998), Vegetation dynamics, palaeoenvironments and climatic changes in the forests of western Cameroon during the last 28,000 years B.P, *Review of Palaeobotany and Palynology* 99: 157–187.

Martin, W. R. and F. L. Sayles (1996), $CaCO_3$ dissolution in sediments of the Ceara Rise, western equatorial Atlantic *Geochim. Cosmochim. Acta*, 60, 243-263.

McManus, J. F., et al. (2004), Collapse and rapid resumption of Atlantic meridional circulation linked to deglacial climate changes, *Nature*, 834-837.

Meybeck, M., H. M. Lô, G. Cauwet, and J. Y. Gac (1987), Geochemistry of the sahelian Gambia river during the 1983 high-water stage. Mitteilungen Geologisches Paläontologisches Institut Universität Hamburg, 64, 461-473.

Mienert, J., R. Stein, P. Schultheiss, and Shipboard Scientific Party (1988), Relationship between grain density and biogenic opal in sediments from Sites 658 and 660, In: Ruddiman, W., Sarnthein, M., et al., *Proc. ODP, Init. Repts.,* 108, Sect. 2: College Station, TX (Ocean Drilling Program), 1047-1053.

Middleton, N. J., (1985), Effect of drought on dust production in the Sahel, *Nature*, 316, 431-434.

Michel, P. (1973), *Les Bassins des fleuves Sénégal et Gambie. Étude Géomorphologique*, ORSTOM, Paris.

Mix, A. C., S. E. Harris and T. R. Janecek (1995), Estimating lithology from nonintrusive reflectance spectra: Leg 138, In Pisias, N.G., Mayer, L.A., Janecek, T.R., Palmer-Julson, A., and van Andel, T.H. (Eds.), *Proc. ODP, Sci. Results,* 138: College Station, TX (Ocean Drilling Program), 413-427.

Morin, J. (1950), Magnetic susceptibility of α-Fe_2O_3 and Fe_2O_3 with added titanium. *Phys. Rev.* 78, 819–820.

Morrish, A. H. (1994), *Canted antiferromagnetism: hematite.* World Scientific Publishing Company, Singapore.

Moskowitz, B. M. and R. B. Hargraves (1984), Magnetic cristobalite: a possible new magnetic phase produced by the thermal decomposition of nontronite. *Science* 225, 1152-1154.

Moskowitz, B. M., M. Jackson and C. Kissel (1998), Low-temperature magnetic behaviour of titanomagnetites, *Earth Planet. Sci. Lett.* 157, 141–149.

Mulitza, S., and C. Rühlemann (2000), African monsoonal precipitaion modulated by interhemispheric temperature gradients, *Quat. Res.*, 53, 270-274.

Mulitza, S., and cruise participants (2006), Report and preliminary results of METEOR Cruise M65/1, Dakar-Dakar, 11.06-1.07.2005. Berichte, Fachbereich Geowissenschaften, Universität Bremen, No. 252, 151 pages, Bremen.

Mulitza, S., M. Prange, J. -B. Stuut, M. Zabel, T. v. Dobeneck, C. A. Itambi, J. Nizou, and M. Schulz (2008), Sahel megadroughts triggered by glacial slowdowns of Atlantic meridional overturning, *paleoceanography*

Mullender, T. A. T., van A. J. Velzen and M. J. Dekkers (1993), Continuous drift correction and separate identification of ferromagnetic and paramagnetic contributions in thermomagnetic runs, *Geophys. J. Int.,* 114, 663-672.

Newell, R. E., and J. Hsiung (1987), Factors controlling free air and ocean temperature of the last 30 years and extrapolation to the past, in *Abrupt climatic change; evidence and implications*, edited by W. H. Berger and L. D. Labeyrie, pp. 67-87.

Nicholson, S. E. (2000), The nature of rainfall variability over Africa on time scales of decades to millenia, *Global Planet. Change*, 26, 137-158.

Nicholson, S. E., and J. P. Grist (2003), The seasonal evolution of the atmospheric circulation over West Africa and equatorial Africa, *J. Clim.*, 16, 1013-1030.

O'Brien, S. R., P. A. Mayewski, L. D. Meeker, D. A. Meese, M. S. Twickler and S. I. Whitlow 1995. Complexity of Holocene Climate as Reconstructed from a Greenland Ice Core. *Science* 270: 1962-1964.

Odin, G. S. (1975), Migration du fer des eaux continentales jusqu'aux eaux océaniques profondes. *C. R. Hedb. Seances Acad. Sci., Ser. D,* 28, 1665-1668.

Oldfield, F., and L. Yu (1994), The influence of particle size variations on the magnetic properties of sediments from the north-eastern Irish Sea, *Sedimentology.,* 41, 1093-1108.

Oleson, K. W., et al. (2004), Technical description of the Community Land Model (CLM), 174 pp, NCAR.

Orange, D., et al. (1993), Geochemical assessment of atmospheric deposition including Harmattan dust in continental West Africa, in *Tracers in Hydrology*, edited by N. E. Peters, et al., pp. 303-312.

Özdemir, Ö., D. J. Dunlop and B. M. Moskowitz (1993), The effect of oxidation on the Verwey transition in magnetite, *Geophys. Res. Lett.* 20, 1671–1674.

Passier, H. F., Böttcher, M. E., and G. J. de Lange (1999), Sulphur enrichment in organic matter of Eastern Mediterranean sapropels; a study of sulphur isotope partitioning. *Aquat. Geochem.,* 5:99–118.

Peck, J. A., et al. (2004), A magnetic mineral record of Late Quaternary tropical climate variability from Lake Bosumtwi, Ghana, *Palaeogeogr. Palaeoclimatol. Palaeoecol.*, *215*, 37-57.

Peters, C., and M. J. Dekkers (2003), Selected room temperature of magnetic parameters as a function of mineralogy, concentration and grain-size, *Phys. Chemist. Earth,* 28, 659-667.

Petersen N. and H. Vali (1987), Observation of shrinkage cracks in ocean floor titanomagnetite, *Phys. Earth Planet. Inter.,* 46, 197-205.

Petersen, N., T. von Dobeneck, H. Vali (1986), Fossil bacterial magnetite in deep-sea sediments from the South Atlantic Ocean, *Nature* 320, 611–615.

Peterson, R. G. and L. Stramma (1991), Upper-level circulation in the South Atlantic Ocean. *Progr. in Oceanogr.* 26: 1-73.

Peterson, L. C., G. H. Haug, K. A. Hughen and U. Röhl (2000), Rapid changes in the hydrologic cycle of the tropical Atlantic during the last glacial. *Science* 290: 1947–1951.

Pike, C. R., A. P. Roberts and K. L. Verosub (1999), Characterizing interactions in fine magnetic particle systems using first order reversal curves, *J. Appl. Phys.* 85, 6660–6667.

Pike, C. R., A. P. Roberts, M. J. Dekkers, and K. L. Verosub (2001), An investigation of multi-domain hysteresis mechanisms using FORC diagrams, *Phys. Earth Planet. Inter.,* 126, 11–25.

Prange, M. (2008), The low-resolution CCSM2 revisited: new adjustments and a present-day control run, *Ocean Science*, in press.

Prell, W. L. and J. E. Kutzbach (1987), Monsoon variability over the last 150000 years. *J. Geophys. Res.* 92: 8411–8425.

Prospero, J. M., and T. N. Carlson (1981), Saharan Air Outbreaks over the Tropical North-Atlantic, *Pure and Applied Geophysics*, *119*, 677-691.

Prospero, J. M., and R. T. Nees (1977), Dust Concentration in the Atmosphere of the Equatorial North Atlantic: Possible Relationship to the Sahelian Drought, *Science,* 196, 1196-1198.

Prospero, J. M., R. A. Glaccum, and R. T. Nees (1981), Atmospheric transport of dust from Africa to South America, *Nature,* 289, 570-572.

Prospero, J. M., and P. J. Lamb (2003), African droughts and dust transport to the Caribbean: Climate change implications, *Science,* 302, 1024-1027.

Roberts, A. P., C. R. Pike and K. L. Verosub (2000), FORC diagrams: A new tool for characterizing the magnetic properties of natural samples, *J. Geophys. Res.* 105, 28461–28475.

Rochette, P., G. Fillion, J. -L. Mattéi and M. J. Dekkers (1990), Magnetic transition at 30–40 Kelvin in pyrrhotite: Insight into a widespread occurrence of this mineral in rocks, *Earth Planet. Sci. Lett.* 98, 319–328.

Robinson, S. G. (1984), The late Pleistocene paleoclimatic record of North Atlantic deep-sea sediments revealed by mineral magnetic measurements, *Phys. Earth Planet. Inter.,* 42, 22-47.

Rohling, E. J., P. A. Mayewski, and P. Challenor (2003), On the timing and mechanism of millennial-scale climate variability during the last glacial cycle. *Climate Dynamics* 20, 257-267.

Röhl, U., and L. J. Abrams (2000), High resolution, down-hole and non destructive core measurements from sites 999 and 1001 in the Caribbean Sea: application to the Late Paleocene thermal maximum, *Proc. ODP Sci. Results,* 165, 191-203.

Romero, O. E., C. B. Lange, R. J. Swap and G. Wefer (1999), Eolian-transported freshwater diatoms and phytoliths across the equatorial Atlantic record temporal changes in Saharan dust transport patterns. *J. Geophys. Res*. 104: 3211–3222.

Ruddiman, W. F. and T. P. Janecek (1989), Pliocene-Pleistocene biogenic and terrigenous fluxes at equatorial Atlantic sites 662, 663 and 664. *Proc. ODP Sci. Results,* 108.

Ruddiman, W. F. (2001), *Earth's Climate: Past and Future*, WH Freeman and Co.

Sarnthein, M. (1978), Sand deserts during glacial maximum and climatic optimum. *Nature* 272: 43-46.

Sarnthein, M., and B. Koopmann (1980), Late Quaternary deep sea record on Northwest African dust supply and wind circulation, *Palaeoecol. Africa, 12*, 239-253.

Sarnthein, M., G. Tetzlaff, B. Koopmann, K. Wolter, and U. Pflaumann (1981), Glacial and interglacial wind regimes over the eastern subtropical Atlantic and Northwest Africa, *Nature*, 293, 193-196.

Sarnthein, M., J. Thiede, U. Pflaumann, H. Erlenkeuser, D. Fiitterer, B. Koopmann, H. Lange, and E. Seibold (1982), Atmospheric and oceanic circulation patterns off northwest Africa during the past 25 million years. In: U. von Rad, K. Hinz, M. Sarnthein, and E. Seibold, (eds.), *Geology of Northwest African Continental Margin,* Berlin- Heidelberg-New York (*Springer-Verlag*), 545-604.

Sarnthein, M., K. Winn, S. J. A. Jung, J. C. Duplessy, L. Labeyrie, H. Erlenkeuser, G Ganssen (1994), *Changes in east Atlantic deepwater circulation over the last 30,000 years: Eight time slice reconstructions, Paleoceanography,* 9, 209-267

Sarnthein, M., et al. (2000), Fundamental modes and abrupt changes in North Atlantic circulation and climate over the last 60 ky – Concepts, reconstruction and numerical modeling, in *The Northern North Atlantic: A Changing Environment*, edited by P. Schäfer, et al., pp. 365–410, Springer, Berlin.

Schefuß, E., et al. (2005), Climatic controls on central African hydrology during the past 20,000 years, *Nature*, 437, 1003-1006.

Schoonen, M. A. A. and H. L. Barnes (1991), Mechanisms of pyrite and marcasite formation from solution: III. Hydrothermal processes, *Geochim. Cosmochim. Acta* 55, 3491– 3504.

Schwertmann, U. (1985), Properties of goethites of varying crystallinity. *Clays Clay Miner.* 33, 369–378.

Schwertmann, U. (1988), Occurrence and formation of iron oxides in various pedo-environments. In: J. W. Stucki, Editor, Iron in Soils and Clay Minerals, *Reidel Dordrecht,* 267–308.

Schramm, R., and J. Heckel (1998), Fast analysis of traces and major elements with ED(P)XRF using polarized X-rays: TURBOQUANT, *J. Phys. IV*, 8, 335–342.

Schulz, H., R. -U. von Rad and H. Erlenkeuser (1998), Correlation between Arabian Sea and Greenland climate oscillations of the past 110000 years, *Nature*, 393, 54-57.

Schulz, H. D. and cruise participants. (1998), *Report and preliminary results of METEOR-Cruise M 41/1, Malaga to Libreville*. Berichte, Fachbereich Geowissenschaften, Universität Bremen, Bremen.

Schütz, L. and K. A. Rahn (1982), Trace element concentrations in erodible soil, *Atmospheric Environment*, 16, 171-176.

Shackleton, N. J., et al. (2004), Absolute calibration of the Greenland time scale: implications for Antarctic time scales and for d14C, *Quat. Sci. Rev.*, 23, 1513-1522.

Shackleton, N. J., et al. (2000), Phase relationships between millennial-scale events 64,000-24,000 years ago, *Paleoceanography*, 15, 565-569.

Shanahan, T. M., J. T. Overpeck, C. W. Wheeler, J. W. Beck, J. S. Pigati, M. R.Talbot, C. A. Scholz, J. Peck and J. W. King (2006), Paleoclimatic variations in West Africa from a record of the late Pleistocene and Holcene lake level stands of Lake Bosumtwi, Ghana, *Palaeogeo. Palaeocli. Palaeoeco.* 242: 287–302.

Shackleton, N. J., H. R. G. Fairbanks, T. Chiu, and F. Parrenin (2004), Absolute calibration of the Greenland time scale: implications for Antarctic time scales and for $\delta^{14}C$, *Quat. Sci. Rev*., 23, 1513-1522.

Smirnov, A. A. and J. A. Tarduno (2005), Thermochemical remanent magnetization in Precambrian rocks: Are we sure the geomagnetic field was weak?, *J. Geophys. Res.*, 110, B06103, doi:10.1029/2004JB003445.

Solomon, S., et al. (Eds.) (2007), *IPCC, 2007: Climate Change 2007: The Physical Science Basis. Contribution of Working Group I to the Fourth Assessment Report of the Intergovernmental Panel on Climate Change*, 996 pp., Cambridge University Press, Cambridge, United Kingdom and New York, NY, USA.

Stager, J. C. and R.Anfang-Sutter (1999), Preliminary evidence of environmental changes at Lake Bambili (Cameroon, West Africa) since 24,000 years BP, *Journal of Paleolimnology* 22: 319–330.

Street-Perrott, F. A., and R. A. Perrott (1990), Abrupt climate fluctuations in the tropics: the influence of Atlantic Ocean circulation, *Nature,* 343, 607-612.

Stuut, J. B., M. Zabel, V. Ratmeyer, P. Helmke, E. Schefuß, G. Lavik, and R. Schneider (2005), Provenance of present-day aeolian dust collected off NW Africa, *J. Geophys. Res*., 110.

Suk, D., D. R. Peacor and R. Van Der Voo (1990), Replacement of pyrite framboids by magnetite in limestone and implications for paleomagnetism, *Nature* 345, 611-613.

Sweeney, R. E. and I. R. Kaplan (1973), Pyrite framboid formation: laboratory synthesis and marine sediments. *Econ. Geol.* 68, **618–634.**

Tada, R., T. Irino and I.Koizumi (1999), Land-ocean linkage over orbital and millennial timescales recorded in late Quaternary sediments of the Japan Sea. *Paleoceanography **14**,* 236–247.

Talbot, M. R., D. A. Livingstone, P. A. Palmer, J. Maley, J. M. Melack, G. Delibrias and S. Gulliksen (1984), Preliminary results from sediment cores from lake Bosumtwi, Ghana, In: J.A. Coetzee, S.R. Van Zinderen and E.M. Bakker, Editors, *Palaeocology of Africa and the Surrounding Islands*, Balkema, Rotterdam 173–192.

Thiede, J., E. Suess, and P. Mueller (1982), Late Quaternary fluxes of major sediment components to the sea floor at the Northwest African continental slope: In von Rad, U., K. Hinz, M. Sarnthein, and E. Seibold, (eds.), *Geology of the Northwest African Continental Margin:* Berlin (Springer Verlag), 605-631.

Thompson, R., R. W. Battarbee, P. E. O'Sullivan and F. Oldfield (1975), Magnetic susceptibility of lake sediments, *Liminology and Oceanography* 20, 687–698.

Thompson, R., J. Bloemendal, J. A. Dearing, F. Oldfield, T. A. Rummery, J. C. Stober and G. M. Turner (1980), Environmental applications of magnetic measurements, *Science,* 207, 481-486.

Thompson, L. G., E. Mosley-Thompson, M. E. Davis, K. A. Henderson, H. H. Brecher, V. S. Zagorodnov, T. A. Mashiotta, P. Lin, V. Mikhalendo, D. R. Hardy and J. Beer (2002), Kilimanjaro ice core records: evidence of Holocene climate change in tropical Africa, *Science* 298: 589–593.

Thompson, R. and F. Oldfield (1986), *Environmental Magnetism*, *Allen Unwin*, London.

Thorpe, A. N., J. A. Minkin, F. E. Senftle, C. Alexander, C. Briggs, H. T. Evans, Jr., and G. L. Nord, Jr. (1977), Cell dimensions and antiferromagnetism of lunar and terrestrial ilmenite single crystals, *J. Phys. Chem. Solids*, 38, 115–123.

Tiedemann, R., M. Sarnthein, and N. J. Shackleton (1994), Astronomic timescale for the Pliocene Atlantic $\delta^{18}O$, and dust flux records of Ocean Drilling Program Site 659, *Paleoceanography,* 9, 619-638.

Van Velzen, A. J. and M. J. Dekkers (1999), Low-temperature oxidation of magnetite in loess-paleosol sequences: a correction of rock magnetic parameters, *Studia Geophysia et Geodaetica,* 43, 4, 357-375

Verardo, D. J. and A. McIntyr (1994), Production and destruction: Control of biogeneous sedimentation in the tropical Atlantic 0 to 300,000 years B.P. *Paleoceanography 9*: 63-86.

Verosub, K. L., and A. P. Robert (1995), Environmental magnetism: past, present, and future, *J. Geophys. Res.,* 100, 2175-2192.

Verstraete, J. M. (1992), The seasonal upwellings in the Gulf of Guinea. *Progr. in Oceanogr.* 29: 1-60.

Vigliotti, L., L. Capotondi and M. Torii (1999), Magnetic properties of sediments deposited in suboxic-anoxic environments: relationships with biological and geochemical proxies, In *Paleomagnetism and Diagenesis in Sediments,* edited by D. H. Tarling and P. Turner, *Geol. Soc. Lond*. Spec. Publ. 151: 71–83.

Von Dobeneck, T., N. Petersen and H. Vali (1987), Bakterale Magnetofossilien. *Geowiss. in unserer Zeit,* 1, 27-35.

Wang, Y. J., H. Cheng, R. L. Edwards, Z. S. An, J. Y. Wu, C. –C. Shen and J. A. Dorale (2001), A High-Resolution Absolute-Dated Late Pleistocene Monsoon Record from Hulu Cave, China, *Science,* 294, 2345.

Wang, Y., et al. (2008), Detecting vegetation-precipitation feedbacks in mid-Holocene North Africa from two climate models, *Clim. Past*, 4, 59-67.

Weldeab, S., W. D. Lea, R. R. Schneider, and N. Andersen (2007), 155,000 Years of West African Monsoon and ocean thermal evolution, *Science,* 316 1303-1307.

Westerhausen, L., J. Poynter, G. Eglinton, H. Erlenkeuser and M. Sarnthein (1993), Marine and terrigenous origin of organic matter in modern sediments of the equatorial East Atlantic: the $\delta^{13}C$ and molecular record. *Deep Sea Research Part I: Oceanogr. Res. Papers* 40(5): 1087-1121.

Wien, K., et al. (2005), Fast application of X-ray fluorescence spectrometry aboard ship: how good is the new portable Spectro Xepos analyser?, *Geo-Mar. Lett.*, 25, 248–264.

Yoshioka, M., et al. (2007), Impact of desert dust radiative forcing on Sahel precipitation: Relative importance of dust compared to sea surface temperature variations, vegetation changes, and greenhouse gas warming, *J. Clim.*, 20, 1445-1467.

Zeng, N., et al. (1999), Enhancement of interdecadal climate variability in the Sahel by vegetation interaction, *Science*, 286, 1537-1540.

Zabel, M., R. Schneider, T. Wagner, A. T. Adegbie, U. de Vries and S. Kolonic (2001), Late Quaternary climate changes in Central Africa as inferred from terrigenous input to the Niger Fan. *Quat. Res*. 56: 207-217.

ACKNOWLEDGMENTS

I wouldn't have been able to complete this work without the unselfish support of many people. First of all, I am grateful to my promoter Prof. Tilo von Dobeneck for his relentless support since my arrival to the University of Bremen, guiding me through my studies, providing insightful suggestions and discussions while always being concern about the welfare of my family. Your immense support has made possible for me to succeed today and remain indebted to you.
Further more, I am grateful to my co-promoter Dr Mark Dekkers of the Paleomagnetism Group at Fort Hoofddijk, Utrecht University for the helpful helpful discussions and constructive comments.
Thanks also go to Dr Torsten Bickert who obtained funding for this project from the DFG under the EUROPROX graduate collage, and to Dr Stefan Mulitza for the invaluable support.

I thank my colleagues (former and present) of the Marine Geophysics research group at the University of Bremen for their invaluable support. I thank Prof. Ulrich Bleil, PD Dr Dave Heslop, Dr Thomas Frederichs, Dr Linda Garming, Dr Christine Franke, Dr Frank Schmieder, Dr Cecile Blanchet, Dr Mellanie Dillon, Liane Brück, Heindrik Müller, Christian Hilgenfeldt, Cornelia Köhler, Yanzhe Fu, Heike Piero, and Marion Milling-Goldbach.

I also thank all the members of the Paleomagnetism Group at Fort Hoofddijk, Utrecht University for the immense support they gave me during my brief stay in Utrecht. Special thanks to Prof. Cor Langereis, Silja Huesing, Tom Mullender, Drs Iuliana Vasiliev and Andy Biggin.

My colleagues of the European graduate collage under which this project was carried out are acknowledged for their support and discussions especially during the coffee and science meetings. Thanks to Prof. Helmut Willems, the chairman of this collage for making it possible.

My journey to Germany wouldn't have been possible without the support of my family. I am grateful to my mother Mrs Itambi Esther for determination to see us through. My brothers and sisters (Gaius, Maurine, Maroline, Jessy, Delphine and Asaah) have been very supportive through out the years. Special thank to my wife Lucie Asong and son Itambi Asaah Gyam Emanuel for their love, encouragements and for coping with the long absence.
To my friends Ilham Bouimetarhan, Ding Feng, Chegnui Bekeny, Tuijah Divine, Njabon Lilian, I say thank you very much for your support and encouragements, and to all whose names have not been mentioned here, I do appreciate all your support in making me successful.

Appendix

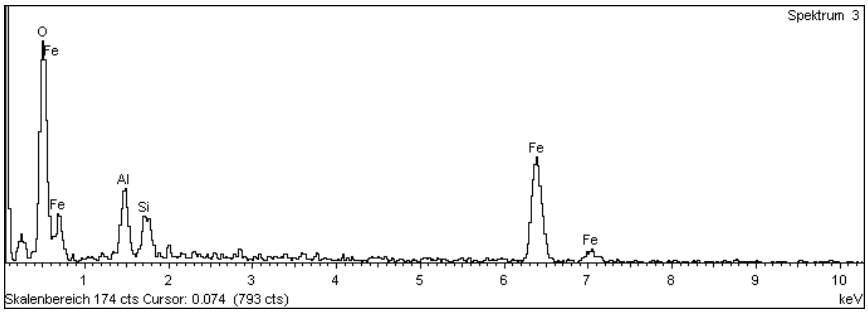

Fig 7a

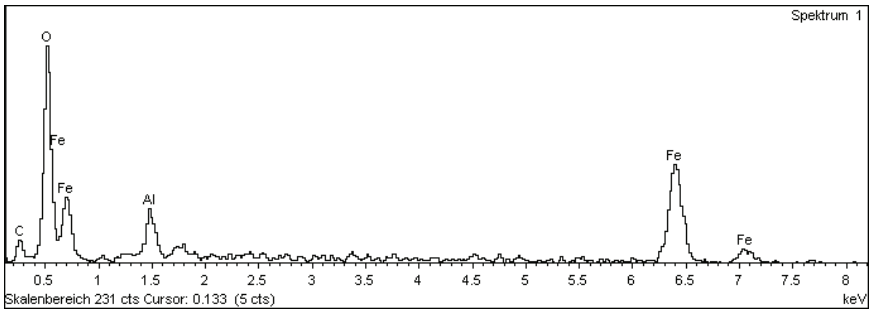

Fig 7b

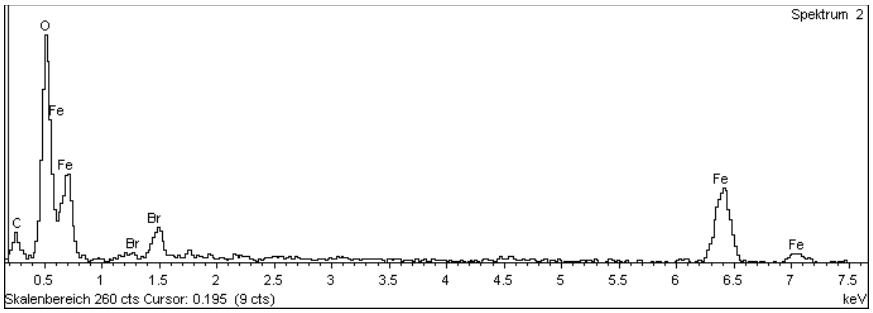

Fig 7c and d

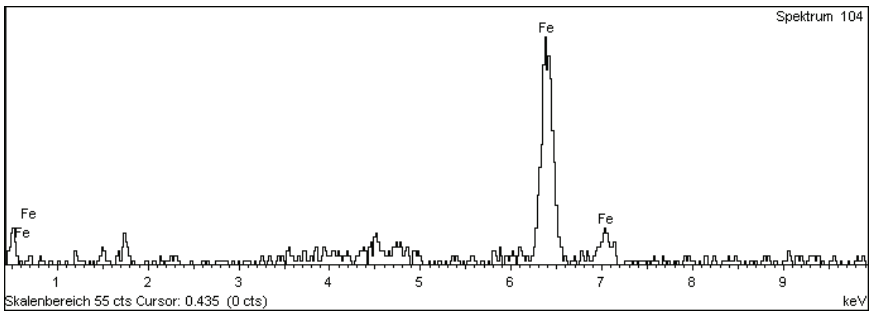

Fig 7e

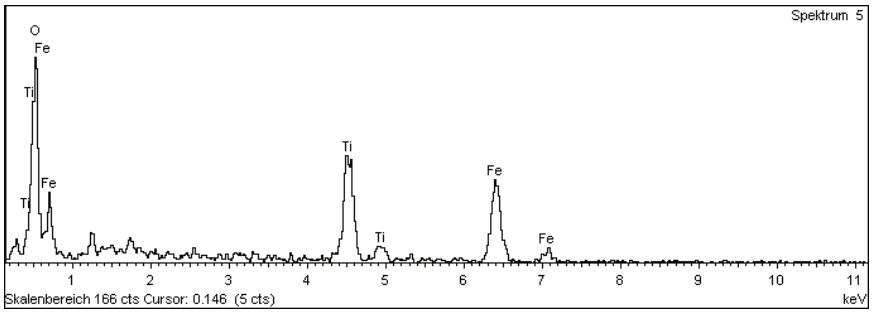

Fig. 8a

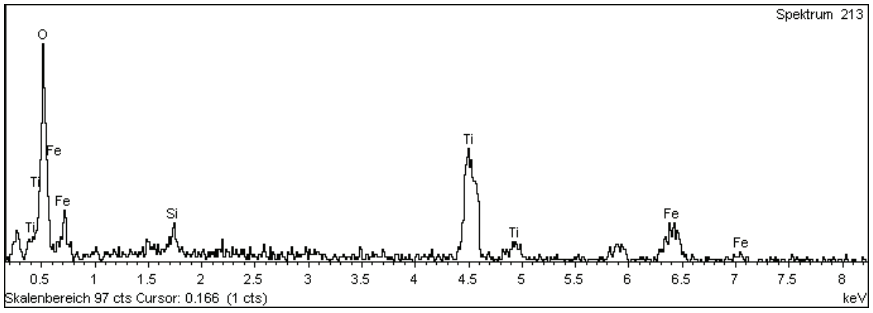

Fig 8 c (1)

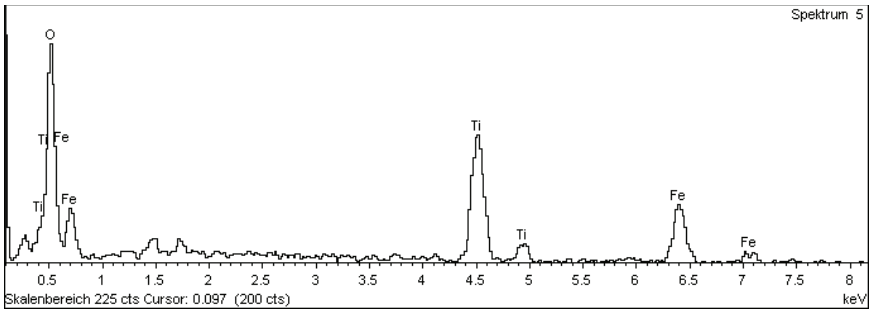

Fig 8d

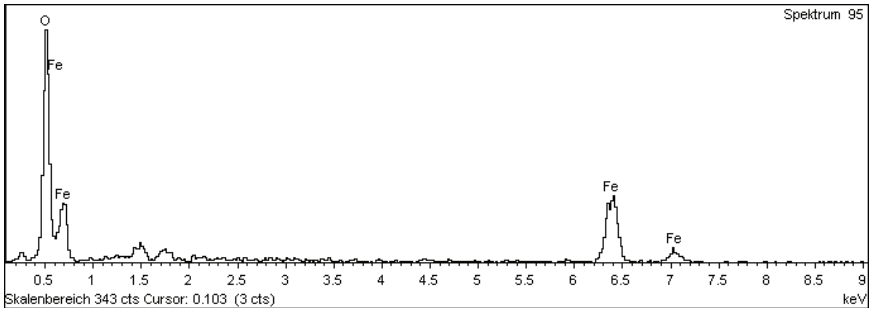

Fig 8 e (3)

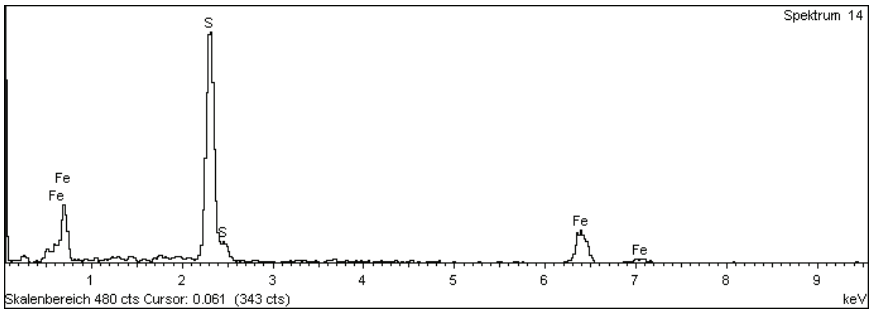

Fig 9b

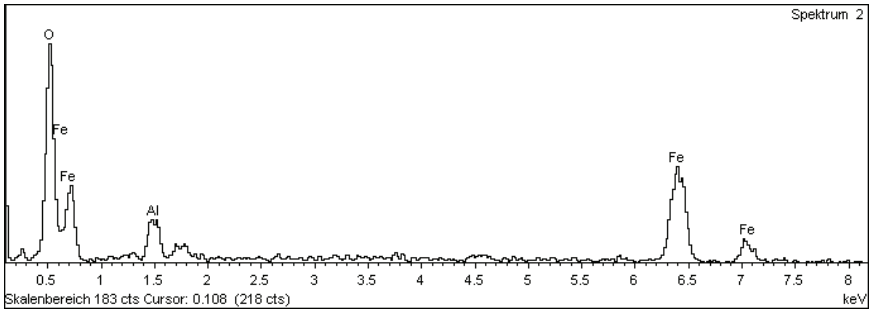

Fig 10

The above EDS spectra are taken from the listed figure number.